NASW-2106

(NASA-CR-128318) EXPERIMENTAL INVESTIGATION OF COMBUSTOR EFFECTS ON ROCKET THRUST CHAMBER PERFORMANCE Interim Report (Rocketdyne) Jun. 1972 118 p CSCL 21H G3/28

N72-33738

Unclas 16385

Rocketdyne
North American Rockwell

R-8903

EXPERIMENTAL INVESTIGATION OF COMBUSTOR EFFECTS ON ROCKET THRUST CHAMBER PERFORMANCE INTERIM REPORT

June 1972

Contract NASw-2106

W. H. Nurick
Member of Technical Staff
Advanced Programs

APPROVED BY

F. E. Campagna
Program Manager, Advanced Programs

Rocketdyne
North American Rockwell

6633 Canoga Avenue,
Canoga Park, California 91304

FOREWORD

This interim report was prepared for the NASA Manned Spacecraft Center, Houston, Texas, by Rocketdyne, a Division of North American Rockwell Corporation. The study was conducted in accordance with contract NASw-2106 under Rocketdyne General Order 9308.

ABSTRACT

This interim report presents the results of the first-year efforts of a design and experimental program to develop special instrumentation systems, design engine hardware, and conduct tests using LOX/GH_2 propellants wherein the propellant flow stratification was controlled. The mixture ratio was varied from 4.6 to 6 overall. The mixture ratios in the core and outer zone were varied from 3.5 to 6 and 5 to 8, respectively. The range in boundary layer coolant was from 0 to 10 percent of the fuel. The nominal chamber pressure and thrust were 225 psia and 7000 pounds, respectively. Pressure and heat flux profiles as well as gas sampling of the exhaust products were obtained. Specific impulse efficiencies of approximately 94 percent and characteristic velocity efficiencies of approximately 97 percent were obtained during the experiments.

CONTENTS

ILLUSTRATIONS

TABLES

INTRODUCTION AND SUMMARY

The initial effort of an analytical, design, and experimental program has been conducted to document the effects of combustor flow striations on rocket thrust chamber performance. The overall program is designed to complement several analytical programs now in progress all in support of the goals of the JANNAF sub-committee on Liquid Rocket Thrust Chamber Performance. Analytical techniques for the performance prediction of rocket engine nozzles for the case of efficient, homogeneous combustion have reached a high degree of perfection over the past several years. The JANNAF Performance Standardization Working Group has created a methodology and a group of computer programs that represent the best analytical techniques available in the industry and show encouraging results when compared with experimental data. However, many rocket engines have neither efficient combustion nor uniformly distributed combustion products. The effects of these two conditions on nozzle performance, which can total several percent, are not well documented experimentally and are only now becoming the subject of rigorous analytical studies. The objectives of this program are (1) to develop special instrumentation systems and engine hardware, and conduct tests using LOX/GH_2 propellants wherein the flow stratification is controlled, (2) obtain sufficient experimental measurements to show that the quality and completeness of experimental data are sufficient to characterize the major physical processes occurring in the rocket thrust chamber from injection to the exit plane, and (3) use the data as a check on the accuracy of JANNAF combustion models at nonhomogeneous and low performance conditions.

To meet this objective, a 16-month program, divided into the following four tasks was conducted: Task I was a design and fabrication effort to obtain an injector containing provisions for three separate flow zones and a heavily instrumented copper thrust chamber/nozzle assembly; Task II was a cold flow experimental effort to characterize the injection elements; Task III consisted of developing a gas sampling system; Task IV was to conduct hot fire experimental performance testing at altitude conditions.

In conjunction with this contract and as part of the same project, a zone radiometry system was used to analyze the thrust chamber exhaust gases. Although this work was performed under NASA Contract NAS8-21144, the two programs were conducted as parts of a single project. A complete description of the zone radiometry effort can be found in Ref. 1.

Specific impulse efficiencies of approximately 94 percent and characteristic velocity efficiencies of about 97 percent were obtained during the experiments. The mixture ratio was varied from 4.5 to 6 overall. The mixture ratios in the core and outer zone were varied from 3.5 to 6 and 5 to 8, respectively. The range in boundary layer cooling was from 0 to 10 percent of the fuel. Pressure and heat flux profiles were obtained during all data tests. The nominal operating point was:

Propellants = LOX/GH_2
Mixture Ratio = 5
BLC = 0 - 10%
Chamber Pressure = 225 psia
Thrust (ϵ_E = 25:1) = 7000 lb_f

The feasibility of all systems was demonstrated; however some modifications are required before further testing commences.

TASK I: INJECTOR AND THRUST CHAMBER DESIGN AND FABRICATION

Since the primary objective of this program was to develop the capability for acquiring high quality data, the engine design and operating parameters were selected primarily on the basis of their ability to support that goal. Thrust chamber simplicity and durability considerations also tended to exert a restraining influence on the final choice. For example, both water cooled and heat sink chamber designs were initially considered. Since accurate thrust measurements were crucial to the program objective, a water cooled design requiring a large number of water lines resulting in a large thrust bias was rejected. A heat sink design was, therefore, selected.

The heat sink thrust chamber design selected placed limits on chamber pressure and test duration. Since tests of 2-seconds duration were needed, the chamber pressure was limited to a maximum of 300 psia. Consideration of performance, heat transfer and sampling accuracy resulted in the following nominal design operating conditions for the engine.

Propellants = LOX/GH_2
Chamber pressure = 250 psia
Mixture ratio = 5
Boundary layer cooling = 0-10%
Expansion ratio = 4 and 25
Test duration = 2 seconds

INJECTOR DESIGN

In order to obtain meaningful documentation over a range of mass and mixture ratio distributions the injector was designed for precision control of the oxidizer and fuel flow in several individually supplied zones (i.e., "core", "outer ring", and "film coolant ring"). By variation of the individual mixture ratios and total flowrates within each zone, striated flows of differing mass and mixture ratio distributions could be created*. An injector assembly drawing showing the element arrangement on the face and the manifold design is shown in Fig. 1 . The major features are:

1. A 96-element injector arranged in four rings with the outer ring propellant feed controlled separately from that of the inner three rings. The element type is an impinging triplet (oxidizer/fuel/oxidizer).

2. A 96-orifice film coolant ring controlled with flow separately from the rest of the injector.

3. Manifolds with very low velocities feeding the elements to ensure uniform feed to all elements within each zone.

*Considerable emphasis was placed on designing the injector such that injection uniformity was maintained within each zone, i.e., equal fuel and oxidizer flow rates to each element and elements spaced to provide uniform flow per unit injector face area. It was recognized, however, that any real injection element produces local inhomogeneities of mass flux and mixture ratio. Therefore the Task II cold flow characterization (see later discussion) was conducted (1) to obtain element design criteria for minimizing such non-uniformities and (2) to acquire a quantitative measure of the "mixing" actually achieved.

FOLDOUT FRAME 1

FOLDOUT FRAME 2

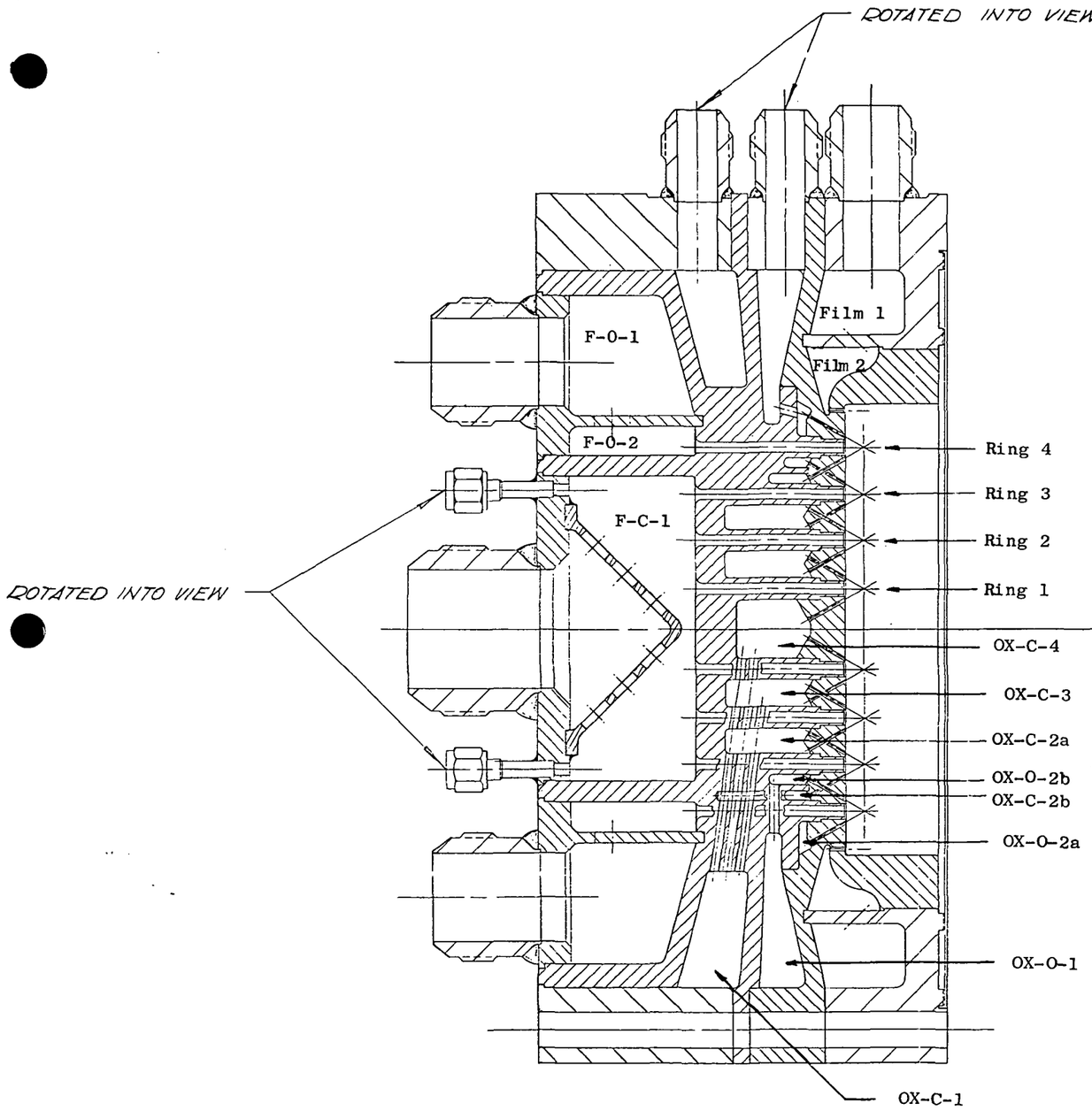

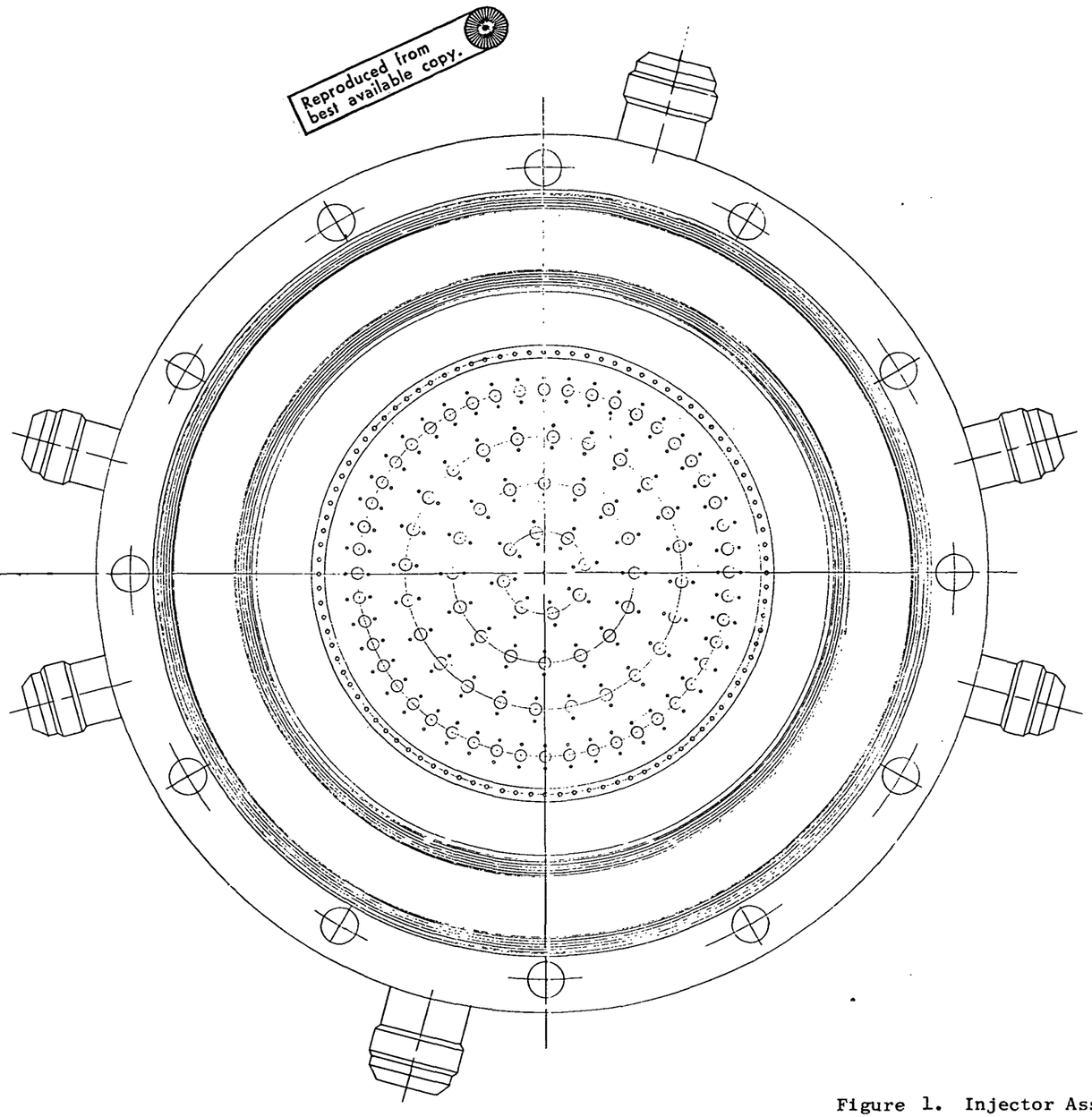

Figure 1. Injector Assembly Drawing.

4. A brazed assembly chosen to allow access to the entrances of all orifices (except the film coolant orifices) for contouring.

5. Element and row spacing selected so that if the elements of both zones are run at the same mixture ratio and element flowrate, the mass flux will be constant across the injector face.

6. The film coolant orifices spaced so that every other one is directly outboard of a corresponding outer row element.

Multiple inlets were selected for all but the core fuel to reduce the size of the manifolds. The four injector rings have numbers of elements and relative spacing designed to produce uniform mass flux across the injector face. All of the rings contain identical triplet elements which are divided 48 in the core (inner three rings) and 48 in the outer ring. When the total flows to the core and outer region are equal, the average mass flux for each ring is uniform within much less than 1% (see Table 1).

The (triplet) injector element is described in Fig. 2 and Table 2 . The centerlines of the three (coplanar) streams describe an included impingement angle of 60 degrees and their impingement point is 0.3-inch from the injector face. The orifices have length-to-diameter ratios of 14:1 and have contoured inlets. The nominal orifice flow conditions for the oxidizer and fuel are also summarized in Table 2. The orifices were sized to maintain reasonable velocities, Mach numbers, and pressure drops throughout the test range.

TABLE 1

INJECTOR NOMINAL MASS DISTRIBUTION

RING NO.	RING DIA. (in.)	RING AREA ($in.^2$)	NO. ELEMENTS	FLOW/AREA* ($lb/sec/in.^2$)
1	1.940	2.956	8	0.515
2	3.355	5.885	16	0.516
3	4.7455	8.846	24	0.516
4	6.763	18.236	48	0.518

*For equal element flow.

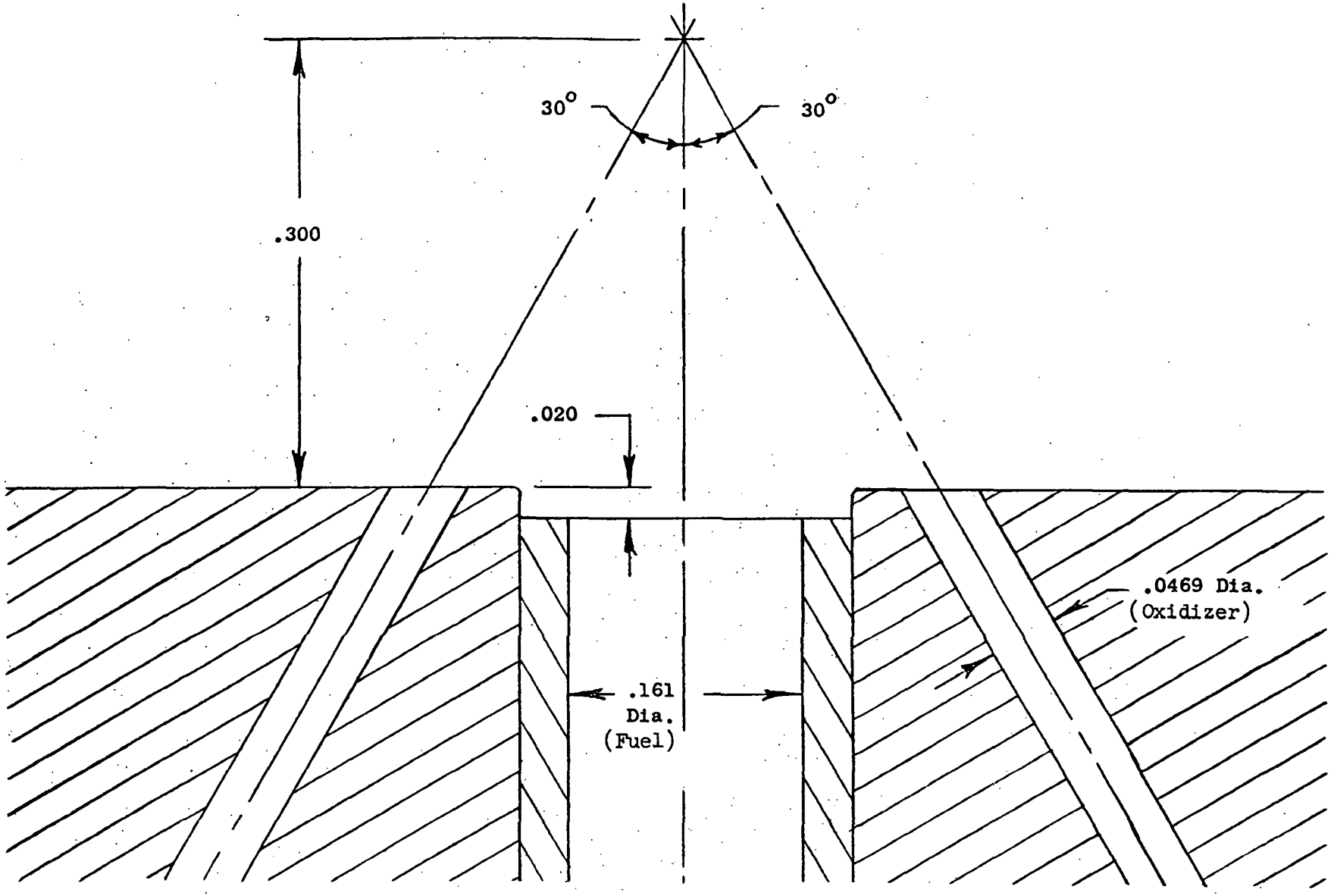

Figure 2 . Injector Element Geometry

TABLE 2

NOMINAL INJECTOR PARAMETERS

	ORIFICE DIA. in.	NO. ORIFICES	ORIFICE ΔP psi	% MASS	VELOCITY ft/sec	MACH NO.	L/D
Fuel							
Core	0.161	48	72	8.2	2690	0.620	13.6
Outer	0.161	48	72	8.2	2690	0.620	13.6
Film Coolant	0.052	96	82	1.8	2800	0.645	
Oxidizer							
Core	0.0469	96	141	40.9	126	--	13.5
Outer	0.0469	96	141	40.9	126	--	13.5

Impingement Angle	60°
Impingement Distance	0.30 in.
Chamber Diameter	6.763 in.
Mixture Ratio	
Core	5.0
Outer	5.0
Film Coolant	
% of Fuel	10.0

THRUST CHAMBER DESIGN

The thrust chamber was designed as a heat sink calorimeter unit. It contains provisions for extensive instrumentation and for cooling between tests. The combustion chamber design including the nozzle skirt is presented in Fig. 3. The chamber material is OFHC copper. The chamber is secured to the injector by 12 bolts which screw into the threaded holes: the nozzle is attached in a similar manner. The chamber L* is 20 inches and the contraction ratio is 2.0 (chamber area divided by nozzle throat area). The water cooling system, used between tests, is not shown in the figure. With low pressure water supply, the heat input to the chamber in a 2-second test can be completely removed in 15 to 20 seconds of cooling time.

The wall radius of curvature upstream of the throat was set equal to 1.5 times the throat radius. This value was selected as being representative of many engine designs and is large enough to facilitate a transonic analysis. The large radius used to form the transition from the cylindrical combustion section to the throat circlet was selected to make the turn gradual enough to prevent flow separation, while leaving enough cylindrical length to simplify the interpretation of chamber pressure measurements. The transition circlet from the throat to the conical nozzle has a radius equal to the throat radius in order to minimize the shock at the tangent point. The conical nozzle expansion angle was selected as 15 degrees to minimize contour related flow nonuniformities and to simplify interpretation of flow stratification results.

FOLDOUT FRAME 1

FOLDOUT FRAME 2

FOLDOUT FRAME 3

FOLDOUT FRAME 4

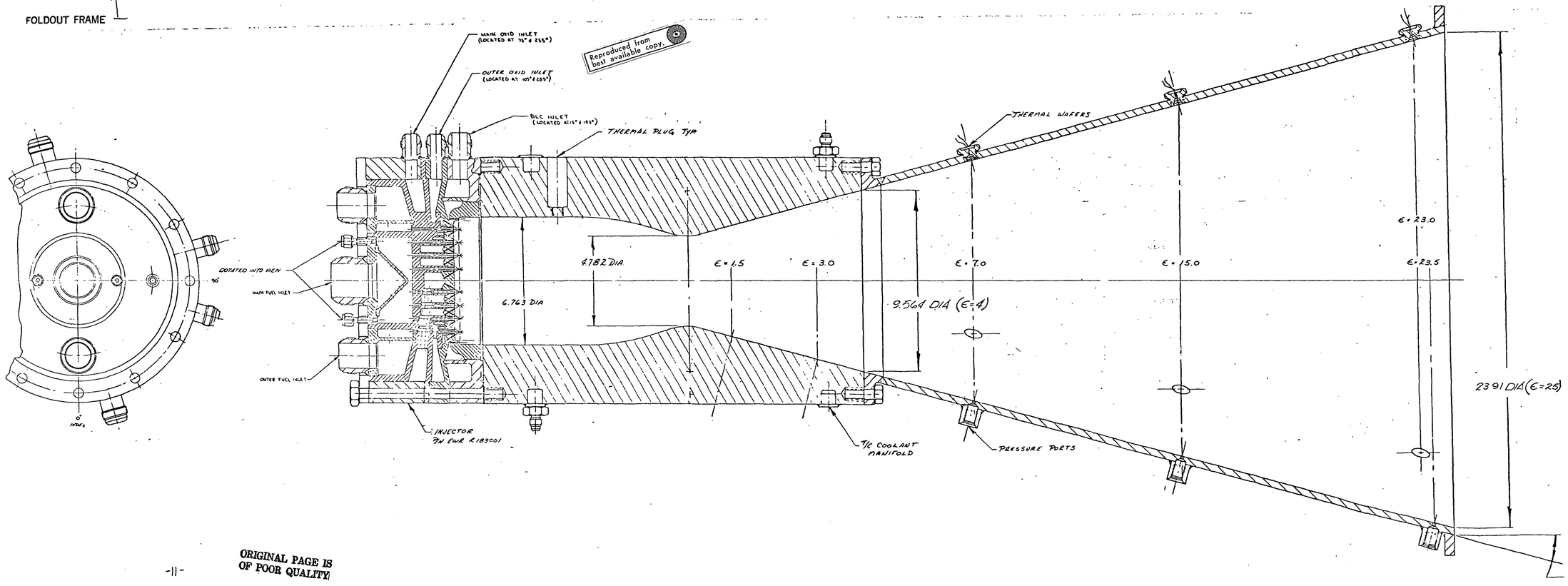

Figure 3. Overall Engine Assembly

R-8903

The nozzle extension shown in Fig. 3 is made of mild steel. The expansion is a 15-degree conical section starting at an expansion ratio of 4 and terminating at 25.

The chamber and nozzle were fully instrumented for wall pressure and temperature measurements. Tables 3 and 4 list the axial locations of all pressure taps and heat flux gages, and Fig. 4 shows the corresponding circumferential location of all measurements.

The thermal isolation plugs are incorporated into the combustion section (T_1 to T_{24}) by machining an annular groove in the bottom of a counter-based hole leaving a small supporting web at the inner surface. The groove effectively limits heat conduction to a radial path through the wall. A schematic of this type of isolation slot is shown in Fig. 5. The radial path length (t) for all of these isolation segments is 0.5 inch.

The thermal plugs shown in Fig. 5 consist of small copper disks suspended in an insulated environment resulting in fast response and reliable operation. The radial path lengths for these isolation slots are listed in Table 5. Note that the radial path length is considerably smaller for these plugs than for the isolation segments.

TABLE 3. LOCATION OF PRESSURE TAPS ON CHAMBER/NOZZLE ASSEMBLY

Pressure Tap	Axial Distance from Injector Face* (inch)	Epsilon
1	1.125	2.0 (Cylindrical)
2	"	"
3	3.30	"
4	"	"
5	5.10	"
6	"	"
7	6.85	"
8	"	"
9	14.82	1.5 (Divergent)
10	"	"
11	19.34	3.0 "
12	"	"
13	24.63	5.44 "
14	28.13	7.47 "
15	34.15	11.71 "
16	38.7	15.54 "
17	46.78	23.70 "
18	47.08	24.04 "

*Throat at 12.5 inches

TABLE 4. LOCATION OF TEMPERATURE MEASUREMENTS ON CHAMBER/NOZZLE ASSEMBLY

Temperature Measurement (Thermal Isolation Plugs)	Axial Distance from Injector Face* (inch)	Epsilon
T-1	1.125	2.0 (Cylindrical)
2	"	"
3	2.84	"
4	"	"
5	5.51	"
6	"	"
7	6.85	"
8	"	"
9	8.18	Convergent
10	"	"
11	9.52	"
12	"	"
13	10.86	"
14	"	"
15	12.19	"
16	"	"
17	"	"
18	12.8	Divergent
19	"	"
20	"	"
21	14.82	"
22	"	"
23	19.34	"
24	"	"
25+	24.6	5.44
26+	"	"
27+	34.2	11.71
28+	"	"
29+	46.8	23.70
30+	"	23.58

*Throat at 12.5 inches
+Heat flux wafers

D

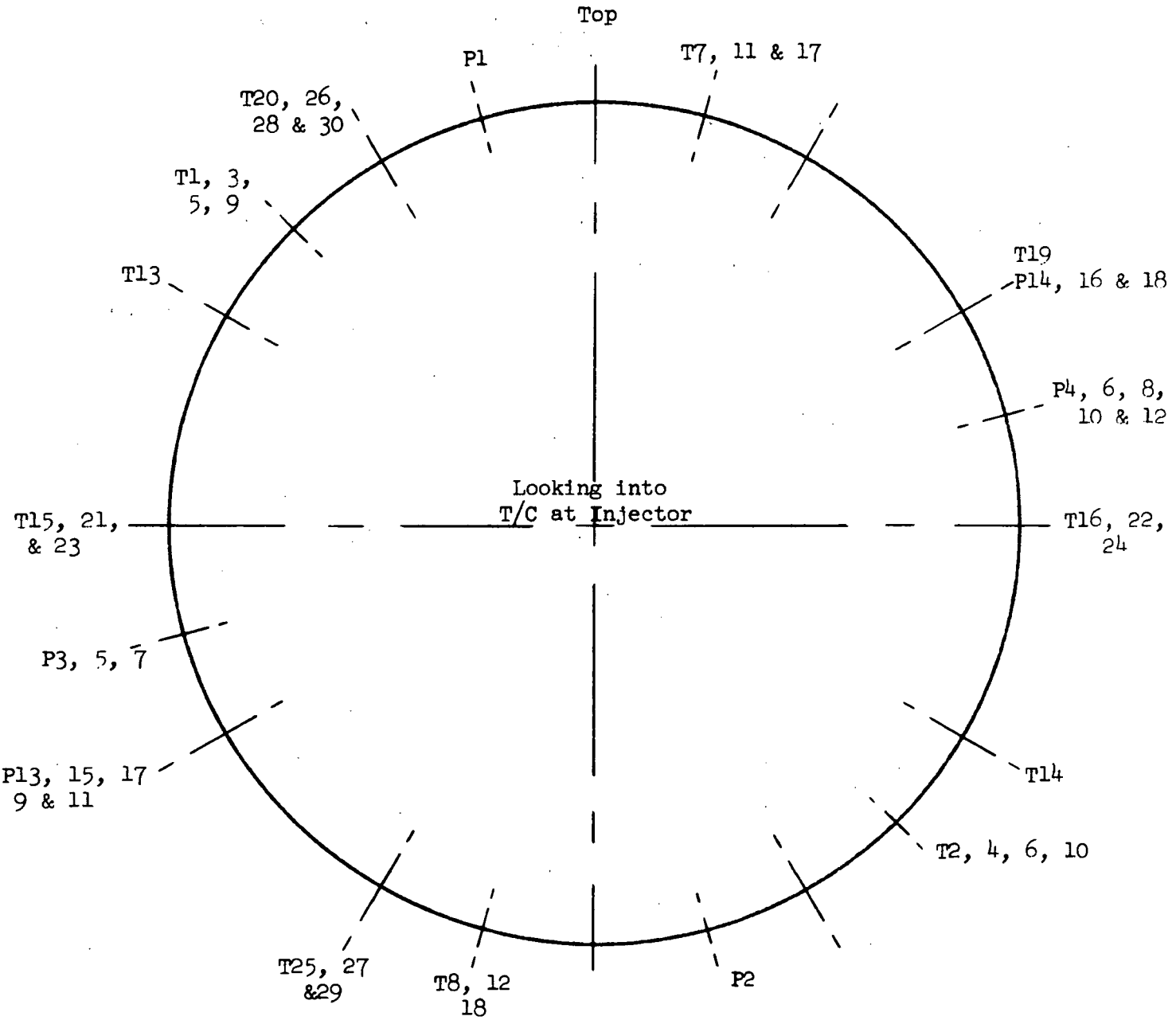

Figure 4. Circumferential Location of Pressure Ports and Temperature Isolation Slots

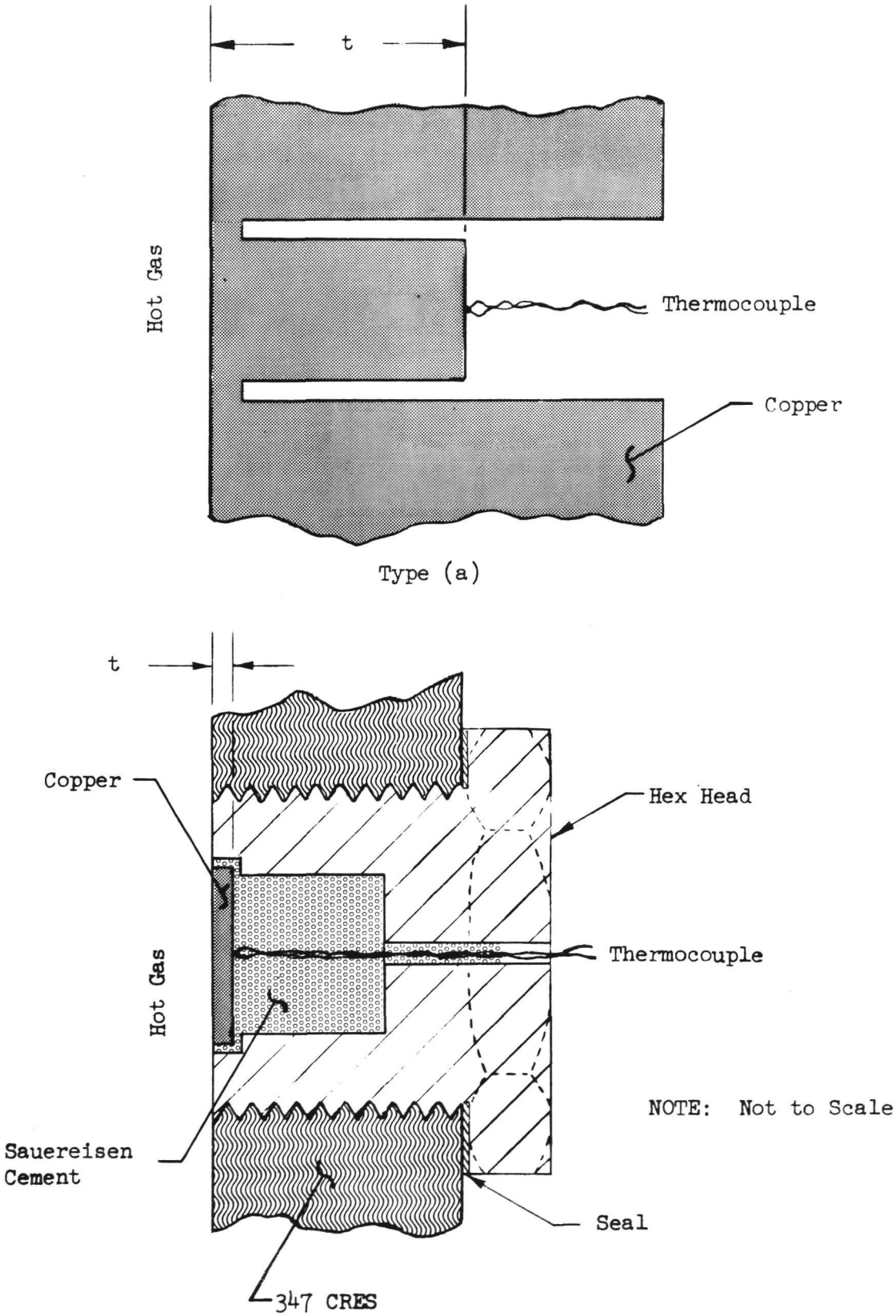

Figure 5. Schematic Cross-Sections of Heat Transfer Isolation Segments

TABLE 5 . RADIAL PATH LENGTHS FOR THERMAL PLUGS

Thermal Plug Designation*	Radial Path Length, inch
25	0.021
26	0.020
27	0.016
28	0.021
29	0.035
30	0.028

*Refer to Table 4 for the corresponding axial location of each thermal plug.

TASK II - INJECTOR COLD FLOW CHARACTERIZATION

Cold flow characterization of the injector was performed to provide an experimental description of the actual mass flux and mixture ratio distributions produced by the injector for comparison with sample and zone radiometric analysis of the exhaust. It also will serve to provide input for combustion model analyses.

Utilization of the Distributed Energy Release (DER) JANNAF combustion model computer program requires a description of the propellant mass and mixture ratio distribution, and dropsize distribution at a start plane near the injector. These can be obtained from either (1) a description of the mixing and atomization characteristics of a single injection element suitable for inclusion into the Liquid Injector Spray Pattern (LISP) sub-program, which then defines the overall distributions, or (2) definition of the overall mixing and dropsize distributions obtained from cold flow experiments using the full scale injectors. Due to facility limitations at the time of initiation of this program, testing to determine the mixing characteristics using the full scale injector was not possible.

Experimental characterization of a single element was conducted in two areas:

1. Mixing tests: to study the degree of mixing between the liquid and gas streams.
2. Atomization tests: to establish the initial droplet size distribution.

In addition, manifold flow distribution tests were made using the full scale injector to establish the degree of uniformity of flow to each element achieved with the final injector assembly.

SINGLE ELEMENT COLD FLOW TEST FACILITY

Mixing

In order to describe the flowfield produced by a given injection element the mass fraction of the total fuel and oxidizer present at each point in the flow field must be determined. A specially designed, two-phase impact probe (Fig. 6) and pressurizing facility were employed to accomplish this task. Development of the test procedure is described in Ref. 2 and the probe development is described in Ref. 3. A schematic of the overall facility is presented in Fig. 7 . Basically, the impact probe serves the function of stagnating the gas component at the probe tip while allowing the liquid droplets to proceed down the length of the probe. By measuring the stagnation pressure at the probe tip (Baratron pressure indicator) and by collecting liquid in the probe for a known interval of time, both gas and liquid flowrates can be determined at each point. An oxygen/nitrogen mixture is used to simulate the injected fuel gas while water simulates the liquid oxidizer. As the gas/liquid flow field moves through the surrounding environment on its way from the injector to the probe location, much of the gas in the environment*

*The environmental gas consists of pure nitrogen injected through a porous plate at a very low velocity base bleed around the injection element. This base bleed prevents excessive recirculation, allowing a much better simulation of the near injector region under hot firing conditions.

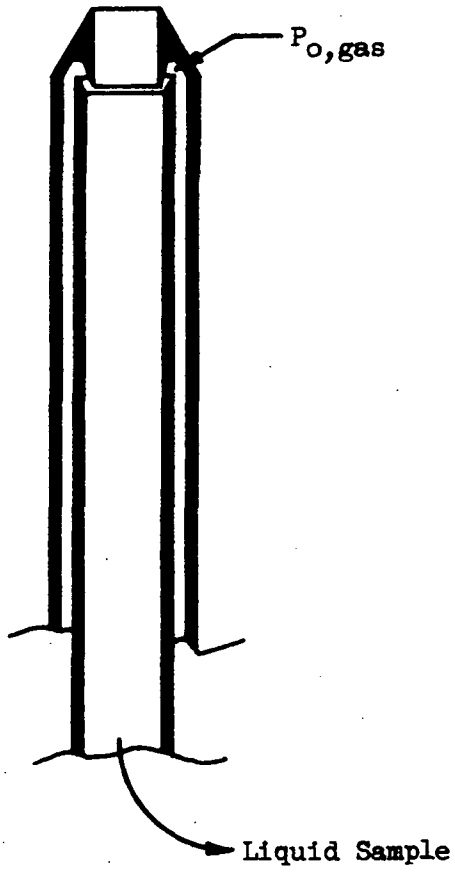

Figure 6. Schematic of Concentric Tube Two-Phase Impact Probe

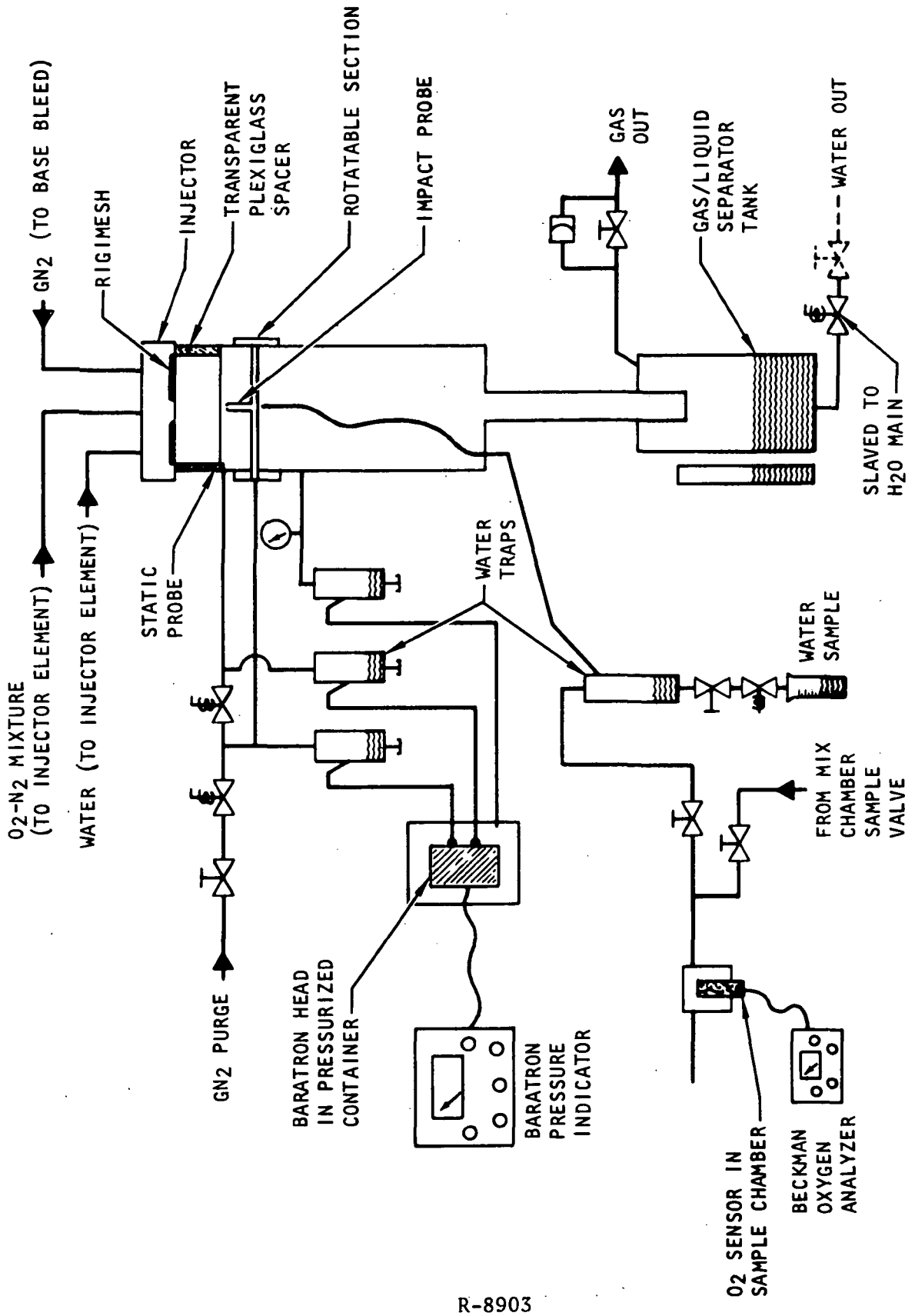

Figure 7. Cold Flow Apparatus

is ingested into the flow field. Therefore, the gas flowrate measured at the probe is composed of gas which was injected (nitrogen/oxygen mixture) and gas which was ingested (nitrogen). These two components must be segregated to determine the injected portion. To accomplish this, the gas sample which arrives at the probe is processed through an oxygen sampler. The concentration of oxygen in the sample can then be used to determine the concentration of the original injectant. Finally, to provide a constant chamber pressure, a gas/liquid separator tank (see schematic) is employed to maintain single phase gas and single phase liquid exhaust flows.

Atomization

The molten wax atomization measurement technique has been utilized and refined extensively at Rocketdyne over the past five years (see Ref. 2 for some detailed descriptions). Basically, the molten wax is injected as a simulant of a liquid propellant forming a spray which freezes as it falls to a collection surface thereby preserving its liquid dropsize distribution. The frozen wax sample is washed down with water and collected. It is vacuum dried and finally subjected to a sieve analysis determining the mass distribution as a function of droplet diameter.

Under the subject program, atomization experiments with single-element gas/liquid injector elements were performed in the apparatus shown schematically in Fig. 8 . The apparatus consists of a large (600-gallon) pressurized tank with an associated water injector which prevents hot-wax from impinging

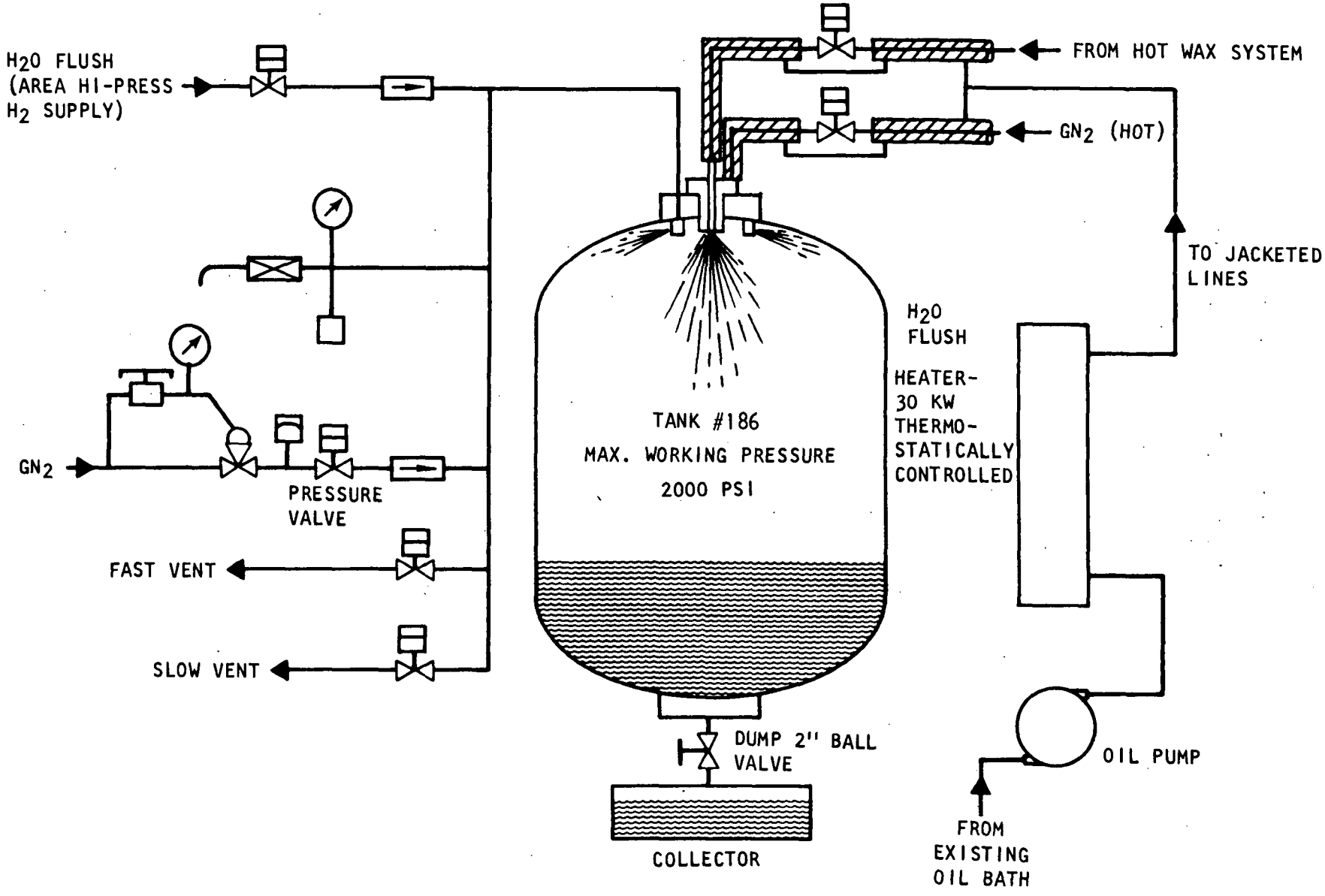

Figure 8. Pressurized Atomization Facility

on the tank walls. The single-element gas/liquid injector is mounted at the top of the tank and propellant simulants (hot wax, He or GN_2) are supplied from the hot wax supply facility. Hot wax and gas flows are made for approximately 20 seconds and the resulting wax droplets are drained and washed from the tank following tank depressurization. The droplet sample is then vacuum dried and subjected to sieve analysis in order to determine the dropsize distribution and a mass median dropsize, $\bar{D}$.

FULL SCALE INJECTOR MANIFOLD FLOW DISTRIBUTION SAMPLING FACILITY

The manifold flow distribution tests were designed to experimentally evaluate how uniformly the various fuel and oxidizer manifolds in the full scale injector distribute the propellants to each injection element. It should be noted that this is <u>not</u> the same as measuring the gas/liquid flow field produced by the full scale injector. Also, as a matter of clarification, it is pointed out that gas flow measurements were used to evaluate both fuel and oxidizer manifold flows.

A schematic of the test apparatus used to determine the gaseous flowrate through each orifice is shown in Fig. 9 . The gas flowrate through each element was determined using the venturi shown downstream of the injector. A Baratron pressure gage was used to measure the venturi upstream and throat pressures. The total injector flowrate (into a given manifold) was determined using the upstream venturi shown in Fig. 9 . A sectional view of the sampling head for determination of the flowmeter through the oxidizer orifices of an element is shown in Fig. 10 . The head fits over a triplet element and the

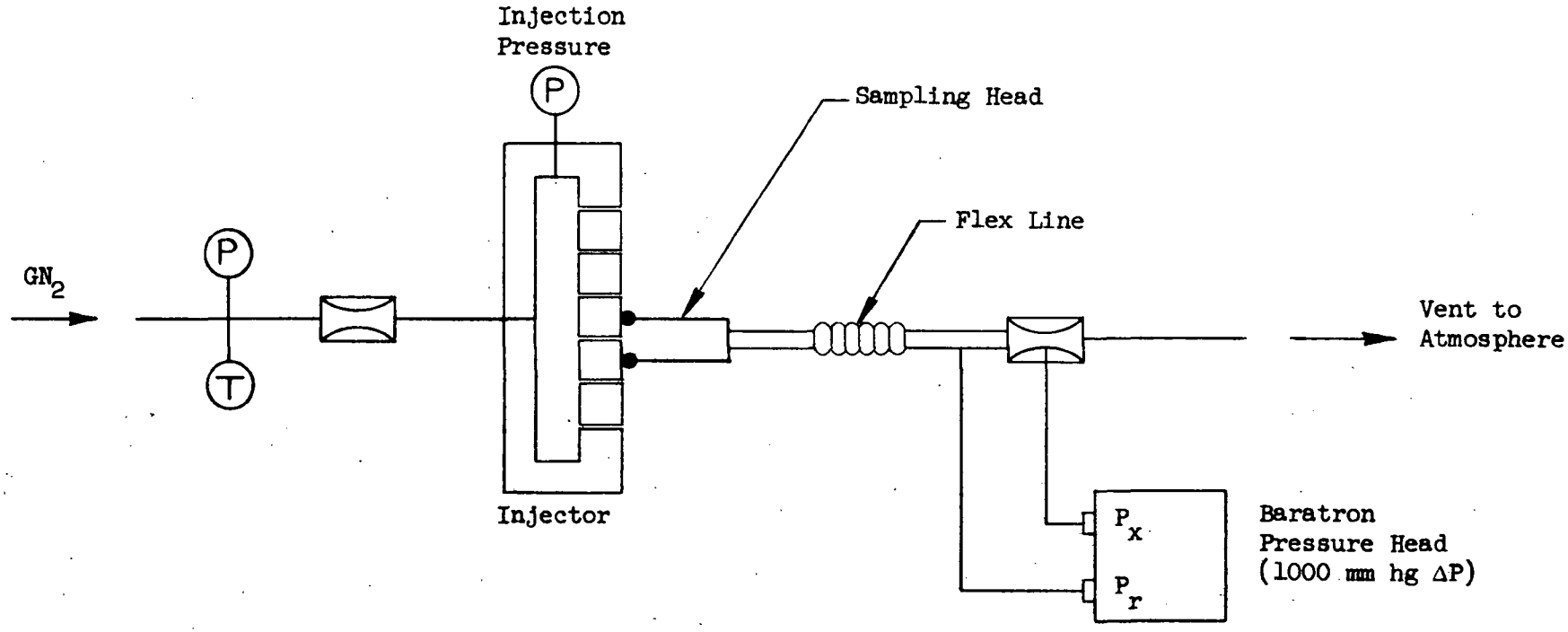

Figure 9. Schematic of Test Apparatus for Manifold Flow Distribution Measurements

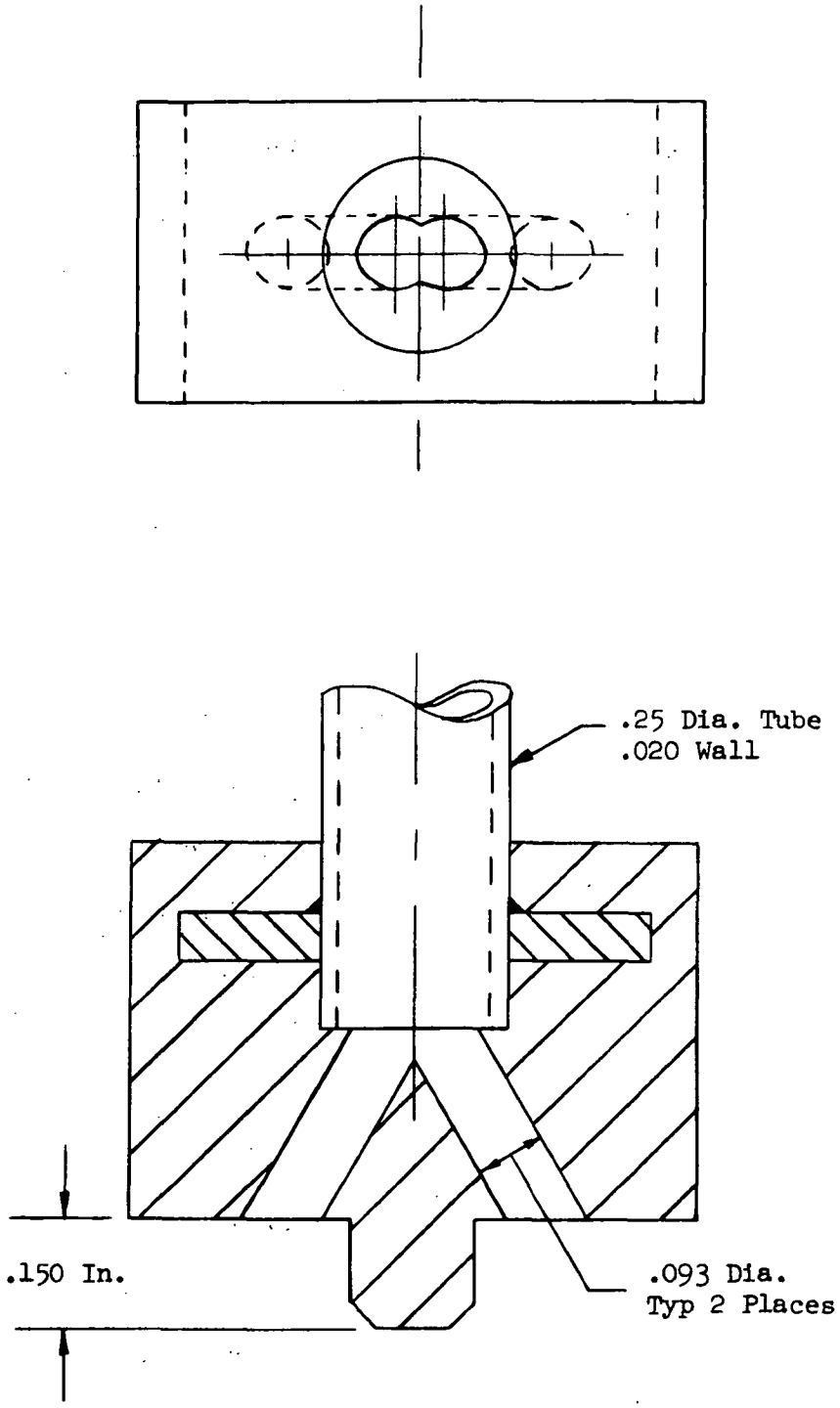

Figure 10. Injector Plug for Sampling
Two Impinging LOX Jets

central jet is plugged. The flow through the sample head is that coming through the two impinging oxidizer orifice jets. For the fuel orifice, a single tube incorporating a seal at the end which fits over the fuel orifice was used.

INJECTOR ELEMENT DESIGN

Successful cold flow modeling requires that the cold flow injector element be an exact duplicate of the hot fire element geometry. Therefore, the single element cold flow hardware was designed to match the hot fire element geometry, including orifice and free stream (L/D)'s and orifice inlet curvature. While the gas and liquid feed manifolds are not exact duplicates of the full scale injector, all feed velocities are similar to those of the hot fire injector. As an added measure to insure cold flow - hot fire similarity, the cold flow and hot fire hardware were fabricated from the same material using the same tooling.

Figure 11 shows the cold flow hardware assembly used for the mixing tests. In this case, the injector flows into the center of the mixing chamber and is surrounded by a uniform base bleed gas flow (GN_2) which prevents recirculation of the injected simulant gases. The same element hardware was used for the atomization tests. However, for the atomization tests, the mixing chamber is replaced by a 600-gallon pressurized vessel (Fig. 8) which collects the simulant (wax) droplets.

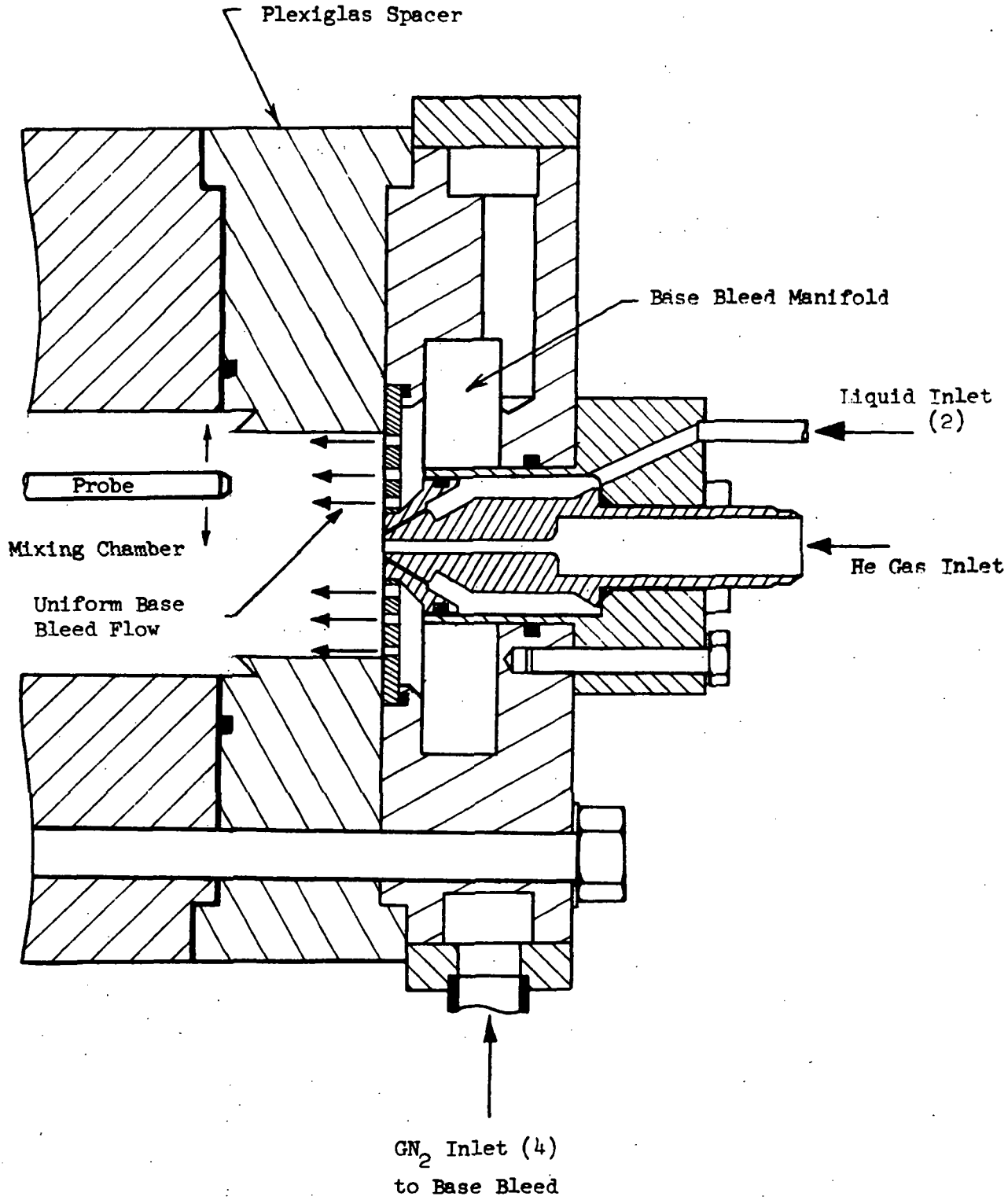

Figure 11. Cold Flow Injector Assembly (Mixing)

SINGLE ELEMENT COLD FLOW EXPERIMENTS

Selection of Cold Flow Modeling Technique

Mathematical analysis of gas/liquid impinging stream modeling criteria suggests, for fixed element geometry, that the gas dynamic parameter ($\rho_g V_g^2$), and the liquid/gas penetration parameter, (X_p/D_g) should control element spray formation processes. The liquid/gas penetration parameter may be physically interpreted as an index of the ability of the injected liquid stream to penetrate the gas (fuel) stream and is defined as follows:

$$\frac{X_p}{D_g} = 1.25 \left(\frac{MR}{D_L/D_g}\right) \left(\frac{\rho_g}{\rho_L}\right)^{1/2} \cos \theta$$

where θ = angle between injector face and the liquid jet

D = orifice diameter

ρ = density

MR = O/F mixture ratio

Since mixing and atomization processes are inherently related, the same set of variables is thought to control both mixing and atomization (dropsize).

Experimental tests have demonstrated that the variables X_p/D_g, ρ_g, and V_g can be used to characterize impinging type elements. In addition, atomization tests using gaseous nitrogen and helium have shown that the parameter ($\rho_g V_g^2$) does correlate mass median dropsize data in terms of both ρ_g and V_g (experimental range: $2.5 \leq \rho_g V_g^2 \leq 18$ psi). However, prior to this

program, no gas/liquid impinging elements had been cold flowed with the gas dynamic parameter in the range of 60 to 260 psi which was planned for the Task IV hot fire testing. Furthermore, the dependence of mixing on ($\rho_g V_g^2$) had not yet been confirmed due to insufficient test data. Therefore, as a conservative approach to modeling, it was evident that all of the cold flow variables (X_p/D_g), ρ_g, and V_g should be equal to their respective hot-fire values. Where it is not possible to experimentally match all of these variables, cold flow modeling can be accomplished using the parameters (X_p/D_g) and (ρ_g/V_g^2), but this latter method of modeling should be used only where the deviation of ρ_g and V_g from the hot-fire values is not great.

Since, in this program, the hot-fire values of V_g and ($\rho_g V_g^2$) are much greater than those that can be attained using GN_2 (due to sonic velocity limitations) the injector characterization program was conducted using gaseous helium as the fuel (GH_2) simulant. The back pressure was selected so that the cold flow simulation tests matched the hot-fire values of (X_p/D_g), ρ_g and V_g for the mixture ratio range of 5:1 to 8:1. However, since the hot-fire gas velocity for the 3:1 mixture ratio case exceeds the subsonic range of helium, cold flow simulation for this mixture ratio was accomplished by matching hot-fire and cold flow (X_p/D_g) and ($\rho_g V_g^2$).

Experiments

The single-element hot-fire test conditions are presented in Table 6. Also presented in this table are the test conditions of the atomization and mixing tests that were conducted. Note that the two major modeling

TABLE 6 . SINGLE-ELEMENT COLD-FLOW TEST MATRIX

HOT-FIRE ELEMENT FLOW CONDITIONS (OXYGEN/HYDROGEN)

MR	P_c psia	$\rho_g V_g^2$ psi	X_p/D_g	V_g fps	V_L fps	ρ_g lbm/ft^3	$\dot{w}_g$/element lbm/sec	$\dot{w}_L$/element lbm/sec
3	250	253	0.248	3450	90	0.099	0.048	0.144
5	250	121	0.400	2460	100	0.093	0.032	0.160
8	250	55.3	0.625	1700	106	0.088	0.021	0.171

ATOMIZATION COLD FLOW TEST CONDITIONS (SHELL WAX 270/HELIUM)

2.13	184	259	0.246	2970	107	0.136	0.057	0.121
4.07	149	117	0.403	2330	119	0.100	0.033	0.134
6.81	144	53.9	0.635	1690	127	0.087	0.021	0.143

COLD-FLOW MIXING TEST CONDITIONS (WATER/HELIUM)

2.29	187	252	0.249	2700	93	0.160	0.061	0.140
4.89	110	118	0.400	2450	103	0.091	0.032	0.154
7.76	116	55.0	0.622	1710	109	0.087	0.021	0.164

variables, $\rho_g V_g^2$ and X_p/D_g, are nearly identical for both the expected hot-fire conditions and the cold flow tests. The results of the single-element tests are discussed below.

Atomization Test Results. Each of the atomization tests was run for a duration of approximately 15 seconds of steady-state flow. Wax samples were analyzed using the standard sieving technique. The data are presented in non-dimensional form in Fig. 12. The data show that the distribution normalized by $\bar{D}$ is essentially invariant, so that $\bar{D}$ alone is a good index of the dropsize distribution. This normalized dropsize distribution curve is similar to the data presented in Ref. 2 for large thrust-per-element gas/liquid triplet injectors. Figure 13 shows the variation of mass median dropsize, $\bar{D}$, with element mixture ratio. The overall range in $\bar{D}$ was from about 100 μ to 225 μ.

The dropsize data of Fig. 13 are replotted in Fig. 14 where $\bar{D}$ is shown as a function of the gas dynamic parameter, $\rho_g V_g^2$. Mehegan, et al, found (Ref. 2) that the mass median dropsize for impinging type elements ($1.5 < \rho_g V_g^2 < 17$ psi) was inversely proportional to a power of $\rho_g V_g^2$. Although the penetration parameter, X_p/D_g, is also a variable for the data shown in Fig. 14, additional data presented in Ref. 2 show that the mass median dropsize is insensitive to X_p/D_g over the range 0.2 to 0.7. Since the subject tests fall within this range of penetration, Fig. 14 shows that the inverse power relationship also holds for the range $50 \leq \rho_g V_g^2 \leq 260$ psi.

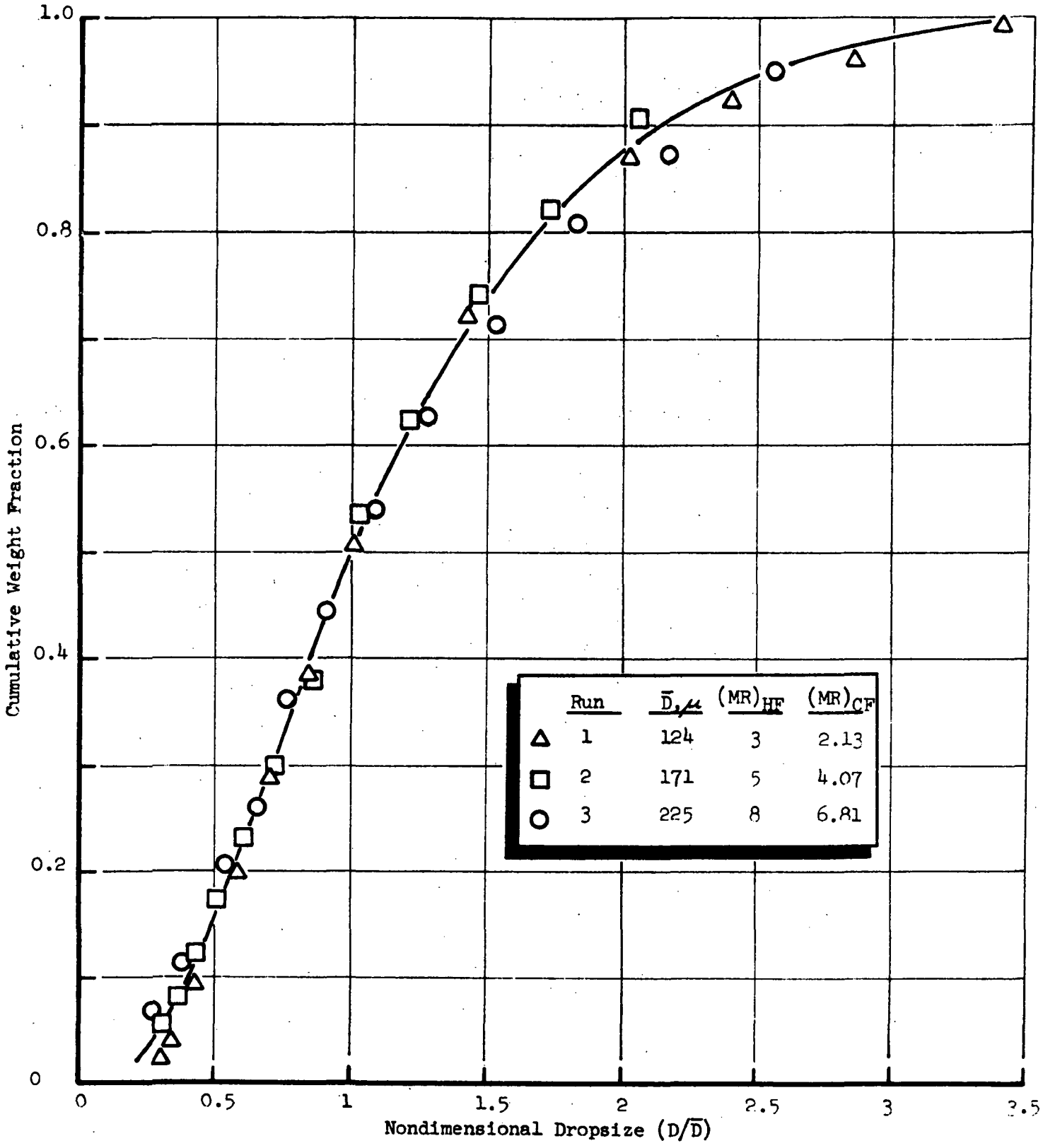

Figure 12. Atomization Test Results: Dropsize Distribution Curve

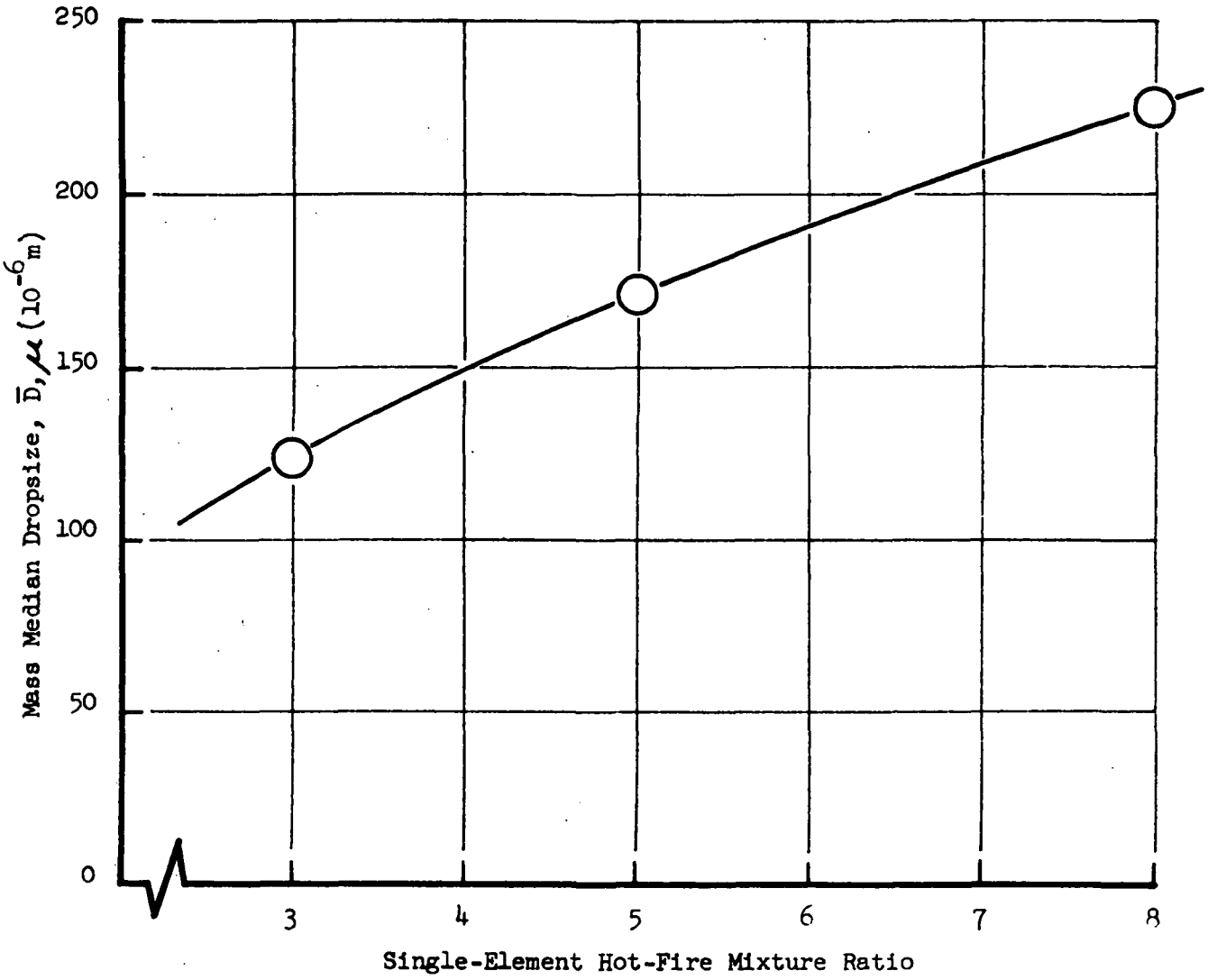

Figure 13. Mass Median Dropsize, $\bar{D}$, as a Function of Single-Element Mixture Ratio

Run No.	$\bar{D}, \mu$	$\rho_g V_g^2$, psi	X_p/D_g	$(MR)_{HF}$	$(MR)_{CF}$
1	124	259	0.25	3	2.13
2	171	117	0.40	5	4.07
3	225	53.9	0.64	8	6.81

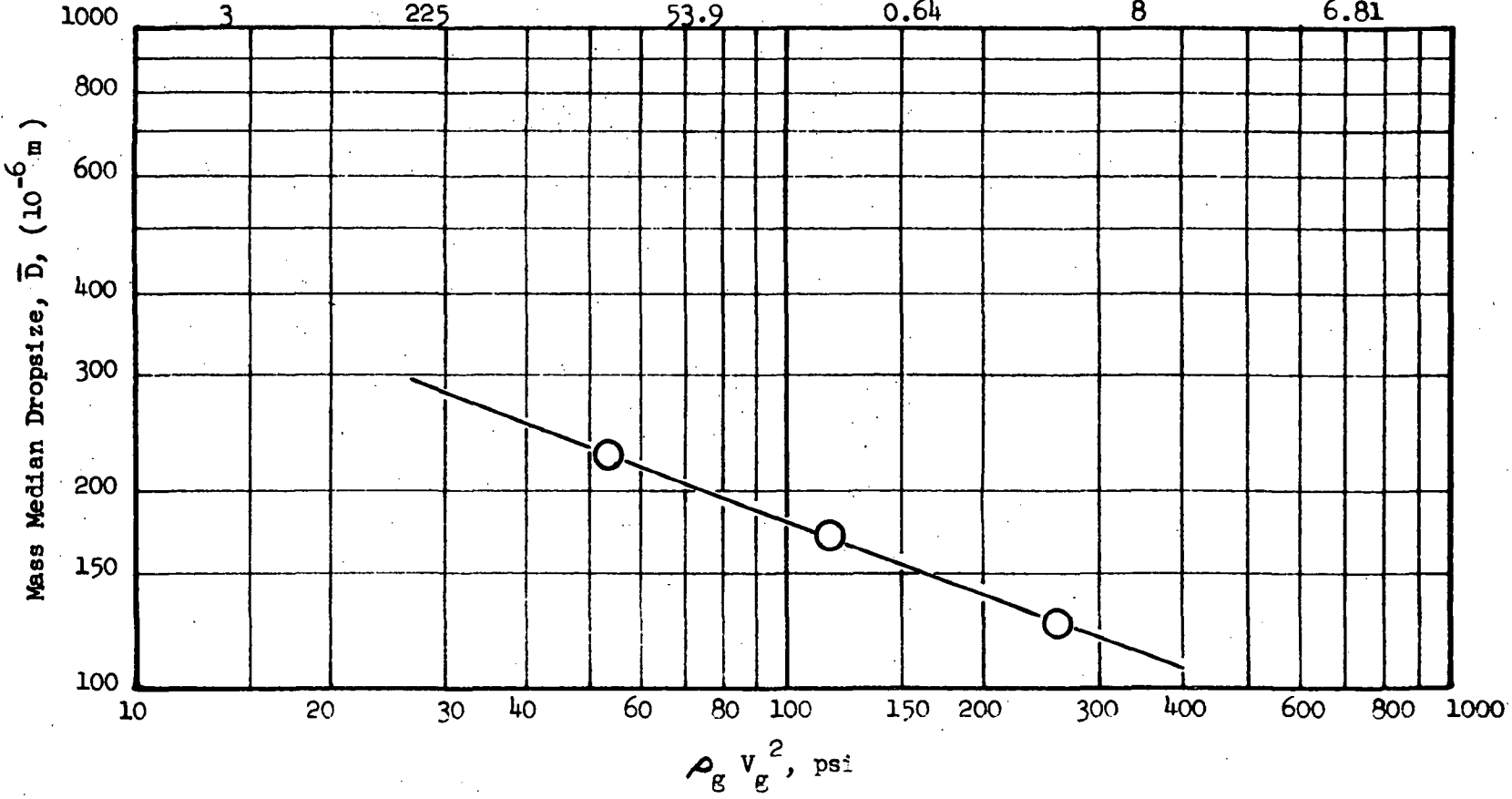

Figure 14. Mass Median Dropsize ($\bar{D}$) versus Gas Dynamic Parameter ($\rho_g V_g^2$)

Mixing Test Results. Four mixing tests were conducted. All three of the test conditions listed in Table 6 were run at a collection distance of 2-inches (Runs 5, 6 and 7) and the low mixture ratio case conditions were repeated using a collection distance of 5 inches (Run 4). Measurement at two distances is required for development of the GLISP program* since knowledge of variation of spray patterns with axial distance is required.

Mixing data can be presented in several useful forms. Normalized mass flux profiles (local mass flux/total injected flowrate) are particularly valuable when comparing data from several tests in which the injected mixture was varied. This is because the total volume under each profile (extended to three dimensions) is equal to unity. Therefore, changes in the location of gas and liquid flux concentrations can be easily seen by direct comparison of normalized mass flux profiles.

Figures 15 through 18 present the normalized profiles for the four tests conducted. On each of these figures, the four separate graphs are cross-sections taken at 11, 33, 56, and 70 degrees from the diameter containing the two oxidizer orifices. Note that the intersection of the gas and liquid curves corresponds to locations where the local mixture ratio is equal to the injected ratio; where the liquid mass flux curve is higher the mixture ratio is above

*Data from the mixing tests were reduced to a form which may be used for the development of the Gas Liquid Injection Spray Pattern (GLISP) program, which is part of the overall DER program.

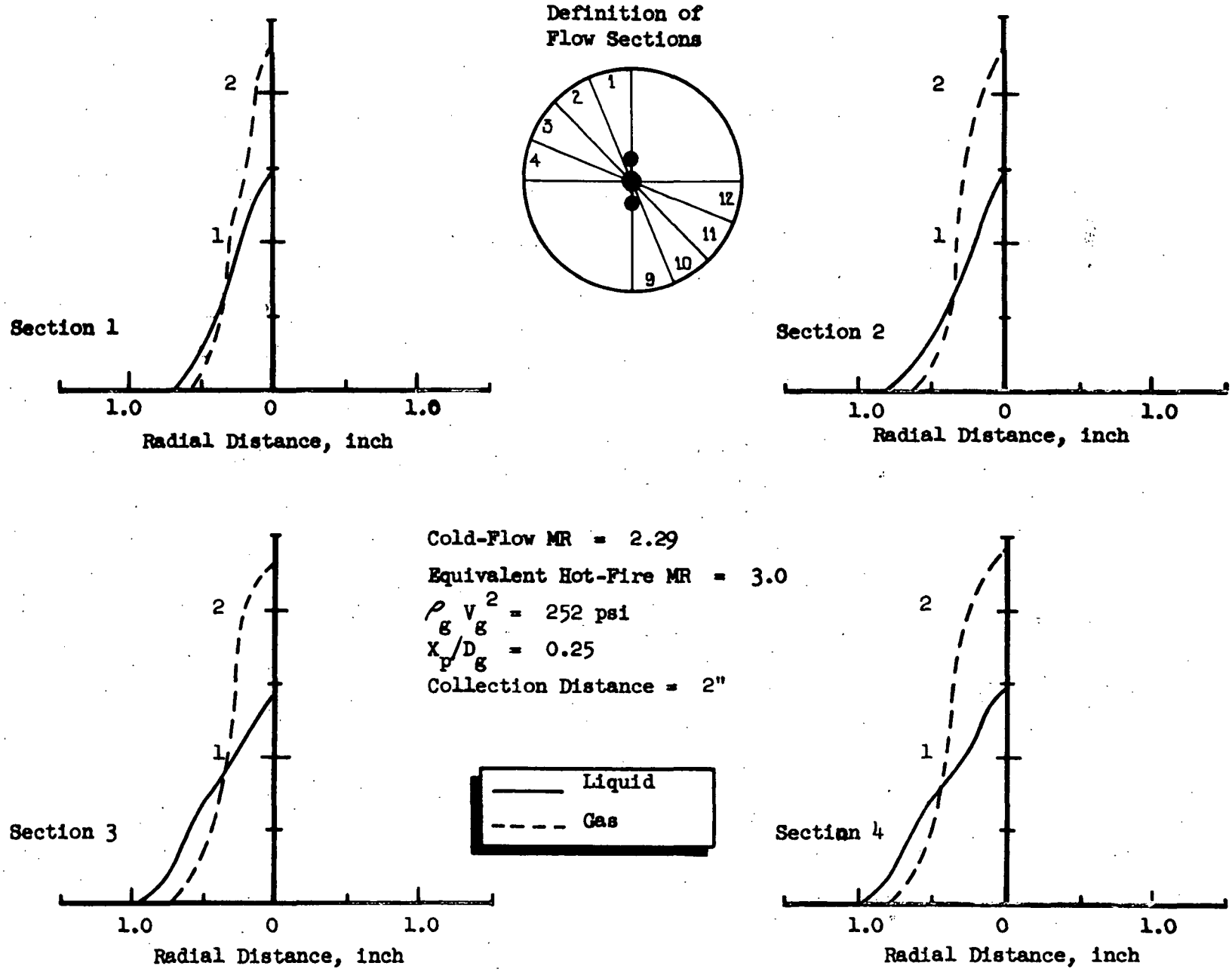

Figure 15. Normalized Mass Flux Profiles for Run #7: High Gas Dynamic Parameter, Low Liquid Penetration, 2" Collection Distance

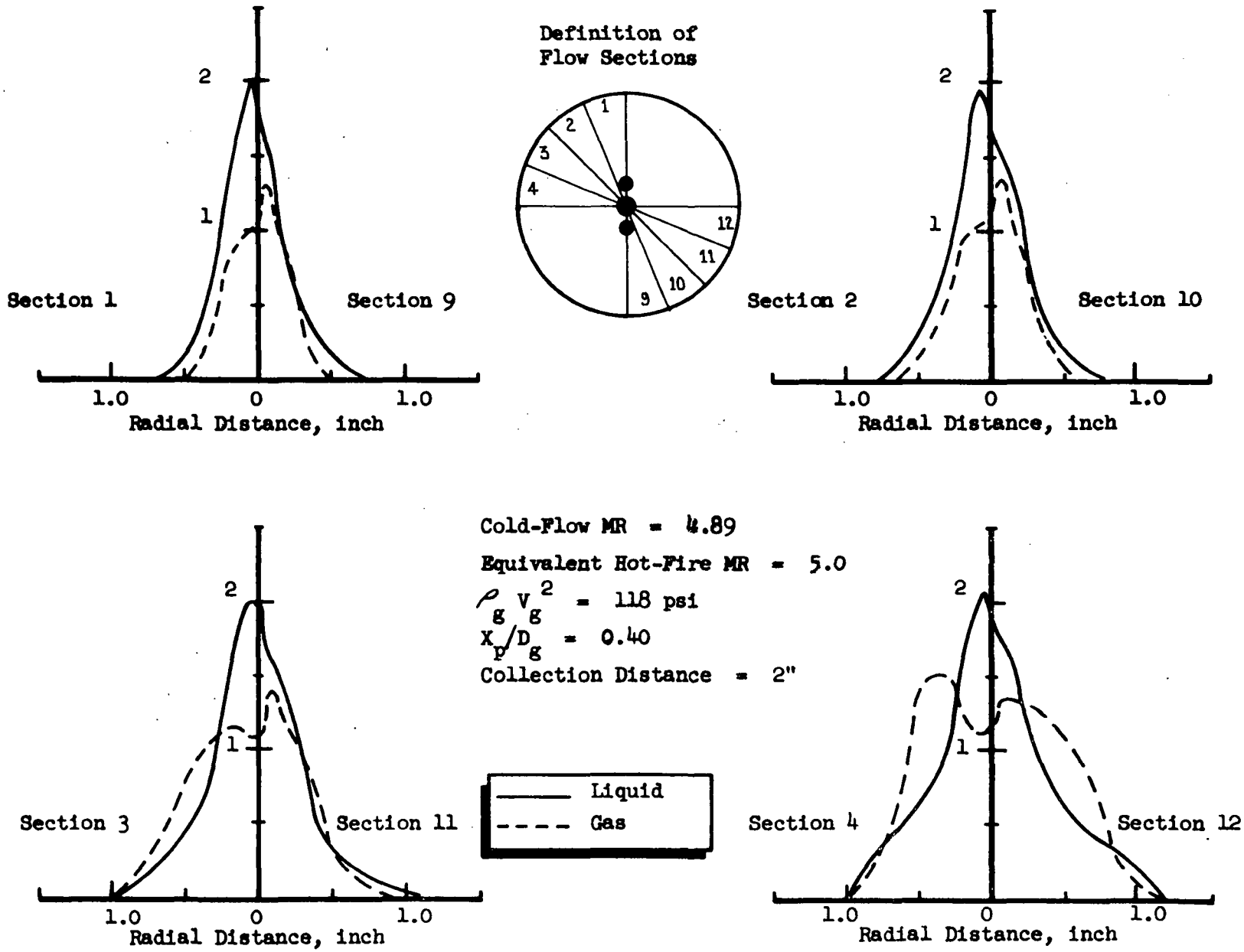

Figure 16. Normalized Mass Flux Profiles for Run #5: Medium Gas Dynamic Parameter, Medium Liquid Penetration, 2" Collection Distance

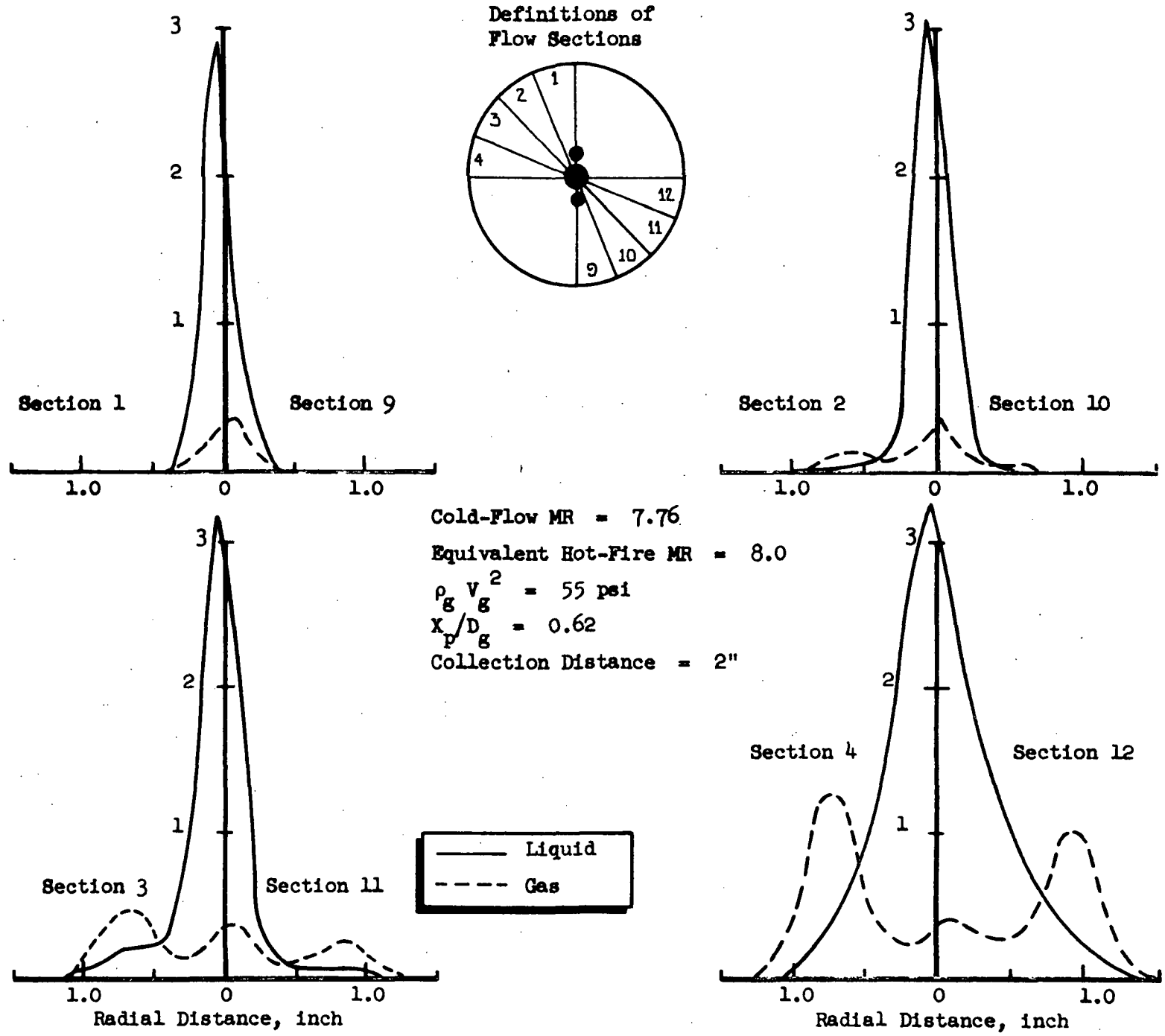

Figure 17. Normalized Mass Flux Profiles for Run #6: Low Gas Dynamic Parameter, High Liquid Penetration, 2" Collection Distance

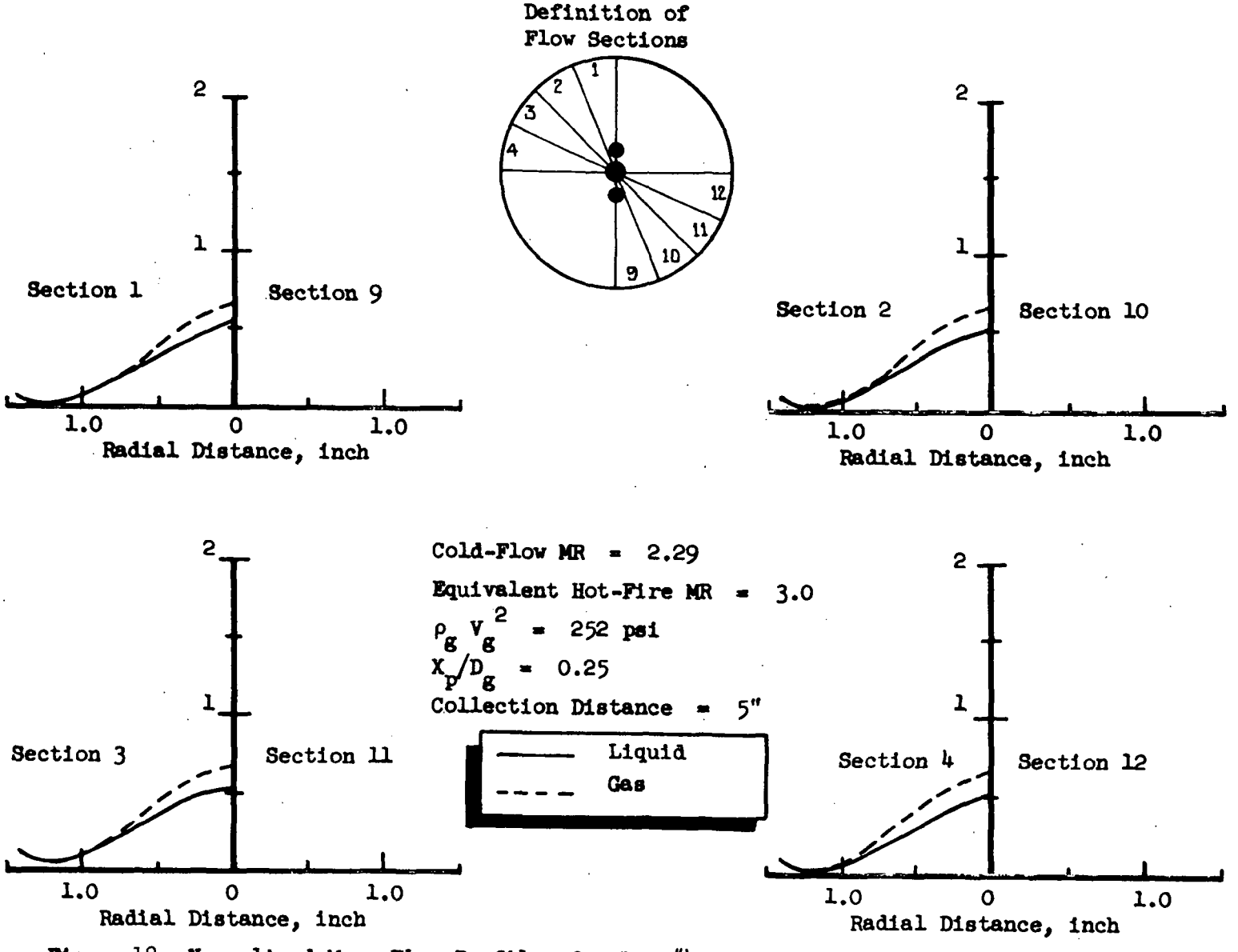

Figure 18. Normalized Mass Flux Profiles for Run #4: High Gas Dynamic Parameter, Low Liquid Penetration, 5" Collection Distance

that injected and vice versa. For example, in Fig. 15 where the liquid penetration parameter is low, the center portion of the flowfield is a region of low (below injected) mixture ratio. Beyond about 0.4 inch (radial position), the mixture ratio is above the injected value (liquid curve above gas curve).

Comparing Figures 15, 16, and 17, the effects of increasing penetration parameter (increasing X_p/D_g) and decreasing gas dynamic parameter ($\rho_g V_g^2$) can be seen. As would be expected, the increase in liquid penetration (with corresponding decrease in gas dynamic pressure) results in a splitting of the gas stream close to the injector as the gas flows around the liquid jets. In all cases the location of maximum normalized liquid flux is along the injector axis. However, the effect of increasing the liquid penetration parameter (X_p/D_g) is shown by the increasing value of this maximum and by the fact that the liquid flux profiles (at high penetration) begin to look like those of a liquid like-doublet injector element (i.e., elliptical).

Since optimum mixing occurs when the normalized gas and liquid profiles are equal, a comparison of Fig. 15 through 17 shows that the best single element mixing probably occurs between the hot-fire mixture ratios of 3 and 5. This conclusion is verified by Fig. 19, in which the mixing efficiency (η_{mix}) and mixing parameter, (E_m) have been plotted for the four tests. Also shown in this figure is the increase in both η_{mix} and E_m with increasing collection distance at the mixture ratio equals 3 condition. Figures 15 and 18 show that

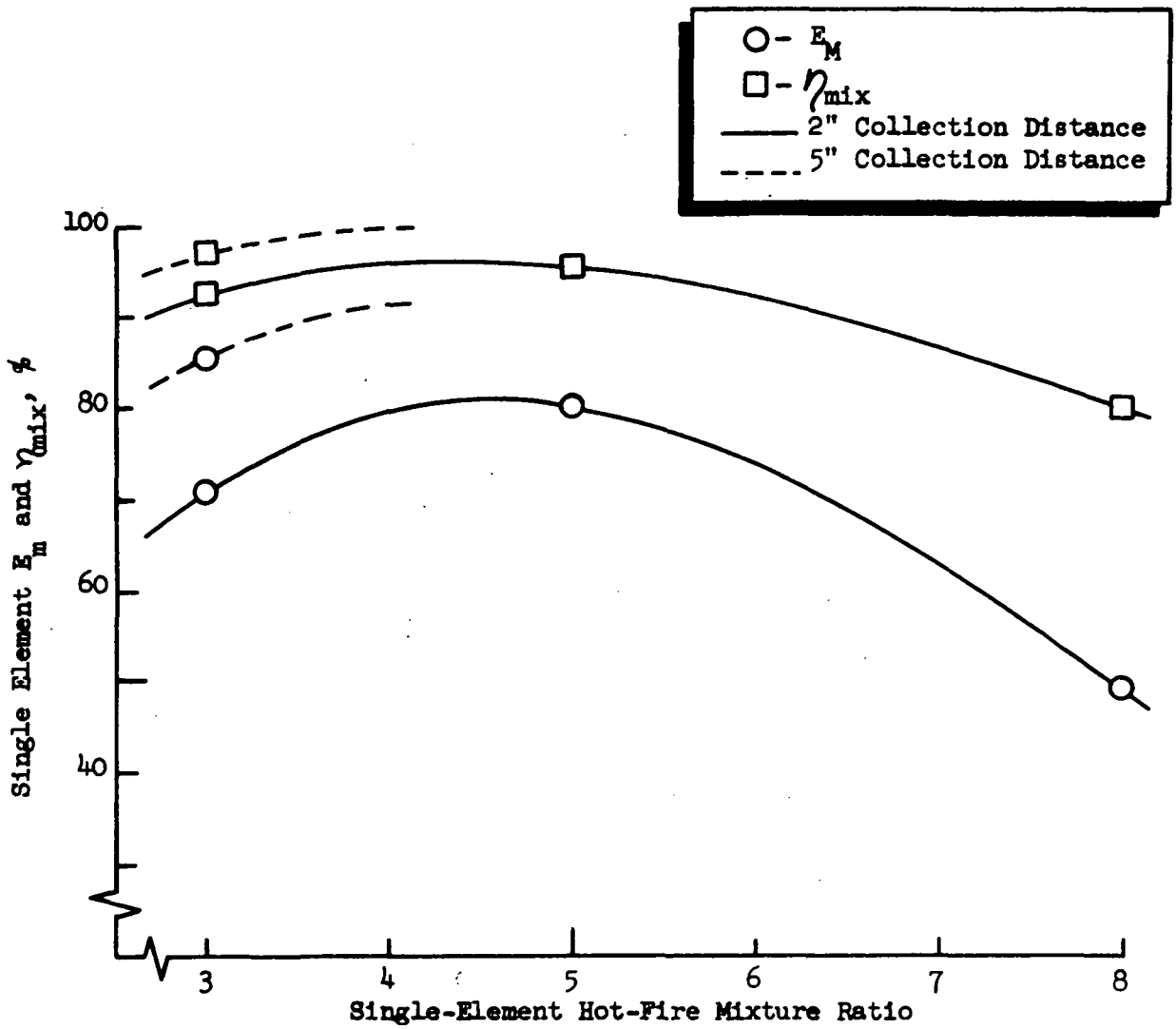

Figure 19. Single-Element Mixing Index (E_M) and Mixing Efficiency (η_{mix}) as a Function of Hot Fire Mixture Ratio

the reason for improvement is that the gas flowfield has expanded more rapidly than the liquid spray, partially counteracting the initial high concentration of gas near the center.

Another presentation of the data is given in Fig. 20 through 23 where lines of constant mixture ratio and total mass flux have been plotted at the collection plane.

Comments on the Single-Element Cold-Flow Test Results. The single-element cold-flow testing results have shown that over the range of anticipated hot fire test conditions the mixing and atomization of the propellants will vary significantly. All of the observed trends were expected and can be explained by considering the variation of the physical parameters liquid penetration (X_p/D_g) and gas momentum flux ($\rho_g V_g^2$).

Because the single-element, cold-flow data were run to model a specific hot-fire test matrix, all of the data has been presented as a function of single-element hot-fire mixture ratio. For the purpose of physical understanding of the flowfield,the same data can be replotted as a function of the two modeling parameters ($\rho_g V_g^2$ and X_p/D_g).

FULL SCALE INJECTOR MANIFOLD TESTS

Measurements were made of the flows through each orifice to determine the maximum flow variation between elements. It was desirable that the injector be designed such that all orifices flowed full and the overall pressure drops

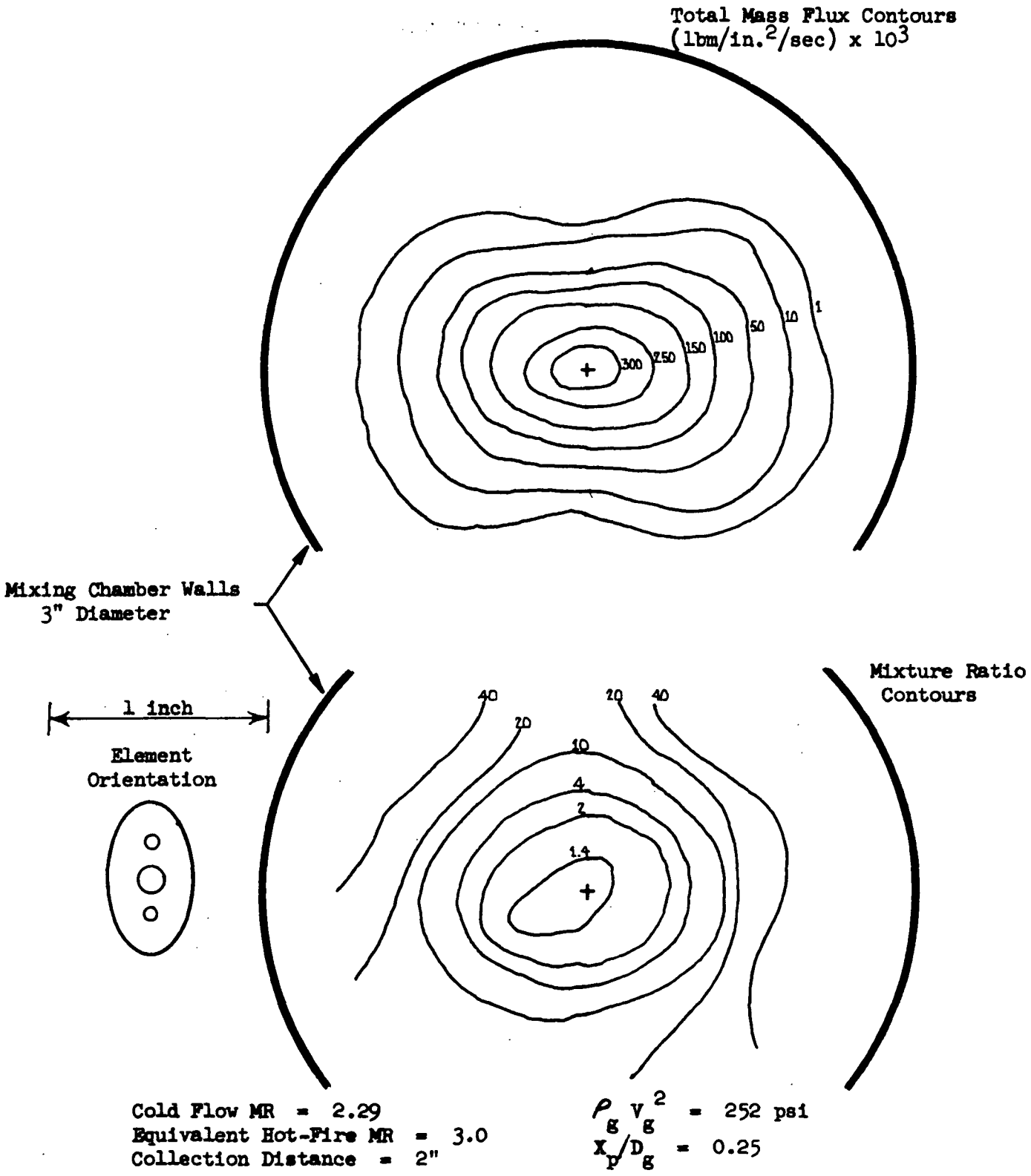

Figure 20. Total Mass Flux and Mixture Ratio Contours for Run #7: High Gas Dynamic Parameter, Low Liquid Penetration, 2" Collection Distance

ORIGINAL PAGE IS
OF POOR QUALITY

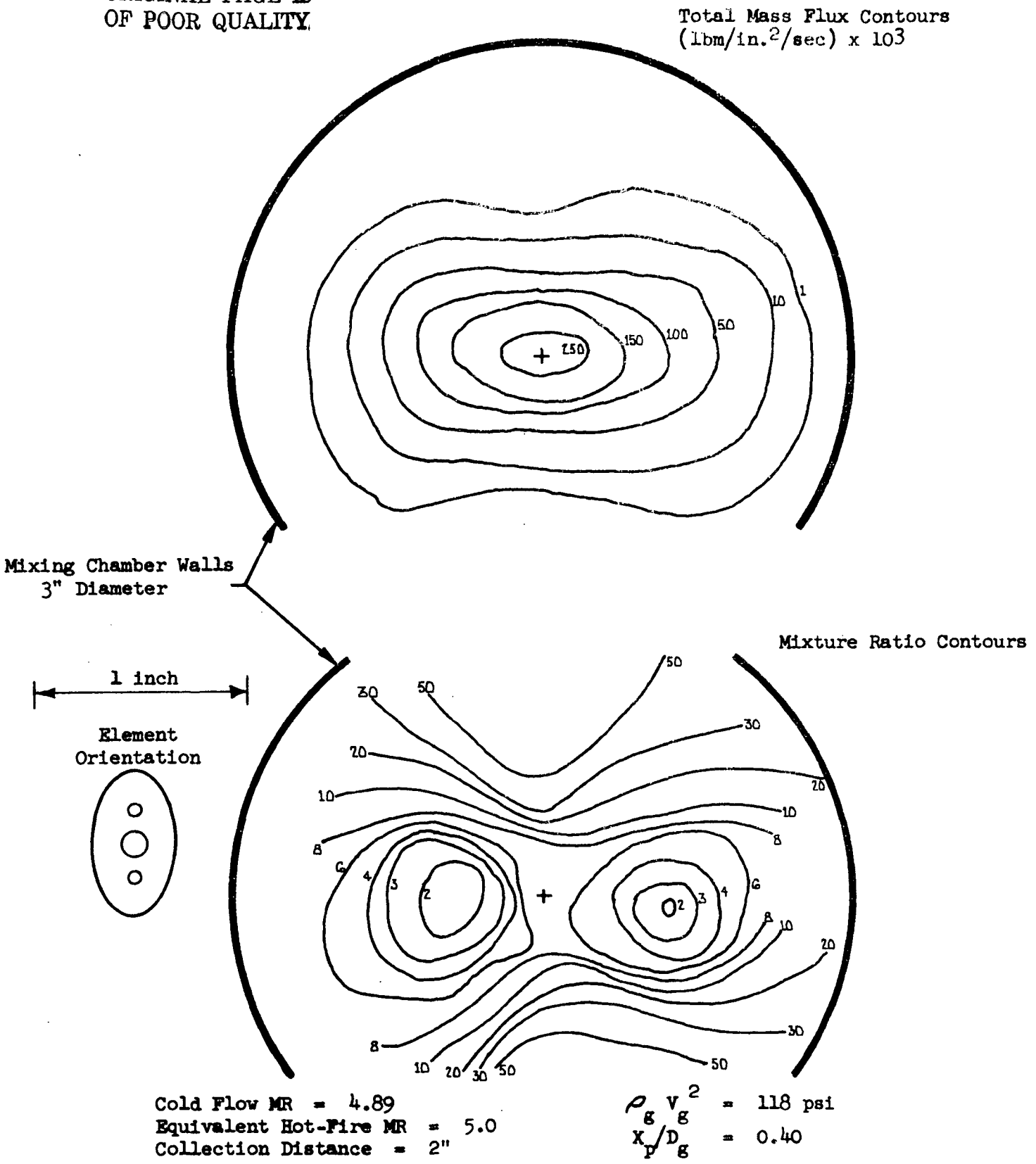

Figure 21. Total Mass Flux and Mixture Ratio Contours for Run #5: Medium Gas Dynamic Parameter, Medium Liquid Penetration, 2" Collection Distance

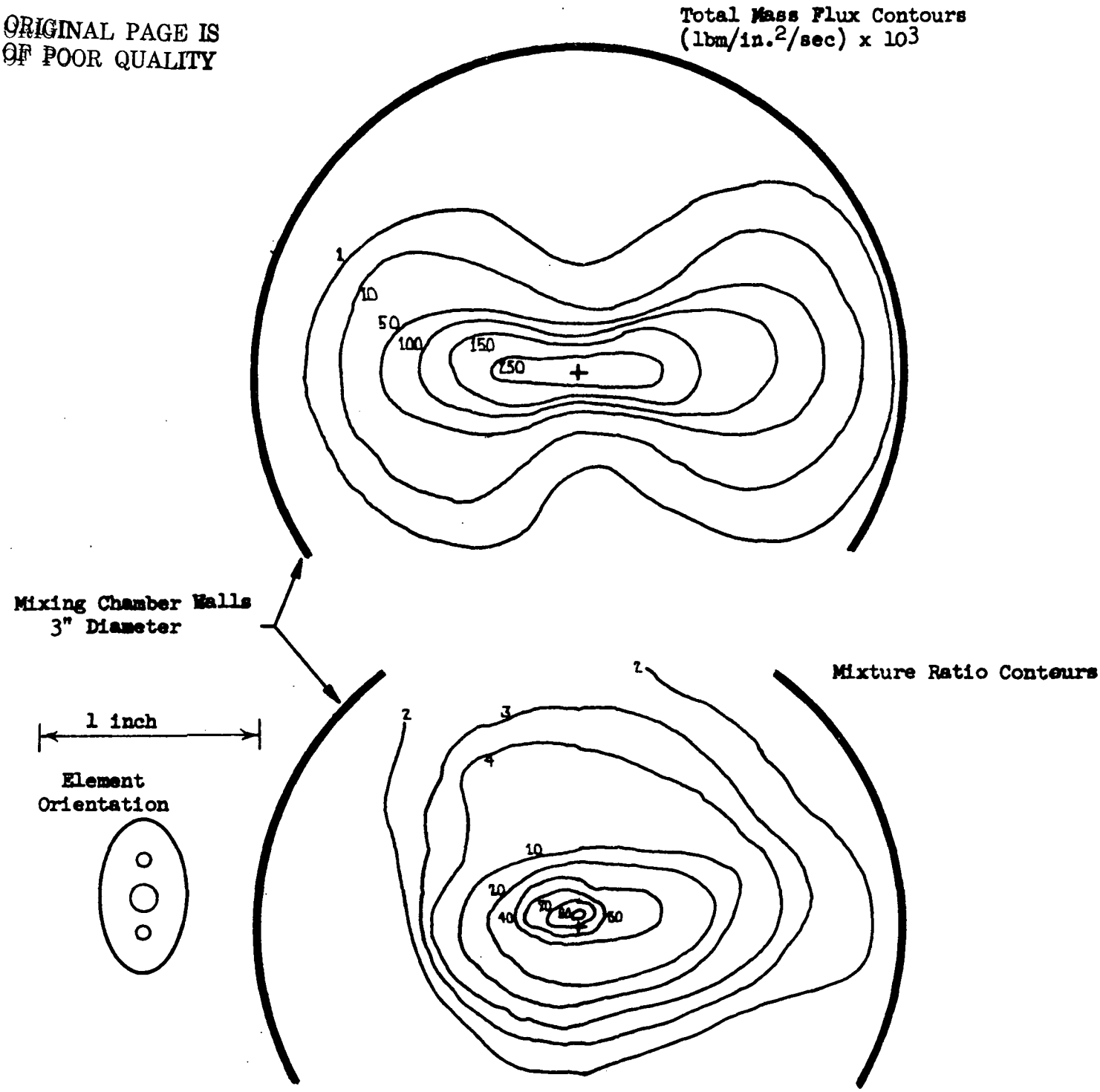

Figure 22. Total Mass Flux and Mixture Ratio Contours for Run #6: Low Gas Dynamic Parameter, High Liquid Penetration, 2" Collection Distance

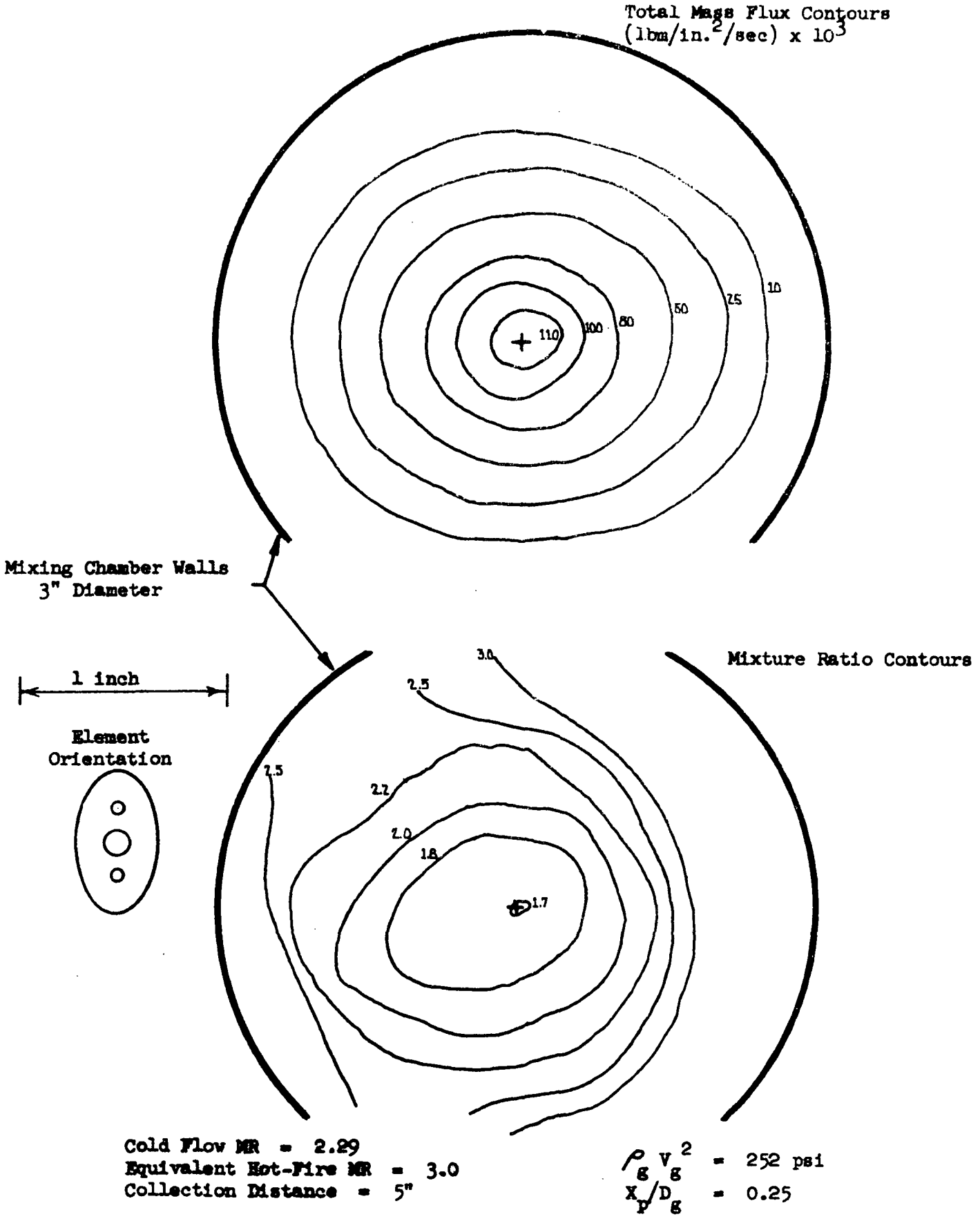

Figure 23. Total Mass Flux and Mixture Ratio Contours for Run #4: High Gas Dynamic Parameter, Low Liquid Penetration, 5" Collection Distance

(including manifold pressure drops) for each element be identical. This would ensure that the overall distributions in each zone would be equal to that specified by orifice area and manifold pressure.

The results of the tests are presented in Table 7 . The data are separated into zone and propellant. The element numbers start in the inner ring and are successively numbered as listed below.

Ring	Orifice Numbers
1*	1 through 8
2	9 through 24
3	25 through 48
4	1 through 48
5**	1 through 48

*1 is the inner ring containing 8 elements.
**5 is the BLC ring.

Note that the pressure difference between that upstream of the venturi and that at the venturi throat is listed. The injector manifold pressure was 2.72 psig, which results in a pressure ratio which is less than critical.

For constant total pressure upstream of the venturi the maximum deviation in flows are defined approximately by:

TABLE 7. SUMMARY OF MANIFOLD DISTRIBUTION MEASUREMENTS

Element No.	Main Fuel Manifold* (core) ΔP, mm H_g	Outer Fuel Manifold** ΔP, mm H_g	BLC Manifold*** ΔP, mm H_g	Oxidizer Core**** Manifold ΔP, mm H_g	Outer Oxidizer Manifold ΔP, mm H_g
1	81.3	66.4	76.0	103.2	99.5
2	92.0	65.0	78.4	101.8	98.5
3	82.0	69.2	74.1	102.5	94.0
4	98.0	67.1	76.4	101.3	94.0
5	74.0	69.2	79.7	102.1	94.4
6	89.0	66.4	75.5	100.1	94.8
7	76.0	69.7	72.2	101.2	99.8
8	88.0	69.9	82.1	100.3	107.6
9	72.0	65.6	77.6	100.0	116.2
10	71.0	67.6	83.1	104.3	102.3
11	79.1	70.1	79.3	102.8	108.4
12	82.1	71.5	109.0	101.3	100.5
13	71.5	71.0	60.2	99.0	100.0
14	70.5	72.0	80.2	102.0	103.0
15	76.3	64.0	90.3	104.0	100.2
16	78.4	72.0	86.5	101.5	103.3
17	72.3	69.5	95.5	100.8	108.4
18	70.1	70.0	82.2	103.0	94.5
19	72.5	71.0	85.3	107.7	105.3
20	73.4	70.0	84.3	101.5	99.5
21	65.5	65.6	70.1	101.2	103.5
22	70.5	67.0	94.2	104.3	101.4
23	79.3	69.5	85.2	101.0	101.2
24	80.3	67.5	114.2	100.0	100.0
25	66.3	67.2	99.8	100.7	87.0
26	69.0	68.2	98.9	101.2	101.4
27	66.4	67.5	74.4	100.0	100.6
28	67.3	69.8	96.5	99.5	104.0
29	66.3	70.1	97.5	104.2	100.0
30	67.2	69.5	70.0	102.8	104.1
31	69.0	68.2	80.0	102.5	99.5
32	67.4	70.0	100.0	106.3	105.2
33	67.2	70.5	98.2	104.1	104.2
34	69.2	70.5	86.4	102.1	99.5
35	72.4	70.5	96.5	101.4	103.5
36	67.4	70.5	72.3	105.0	101.4
37	64.3	69.5	79.3	106.8	106.4
38	68.4	69.4	82.4	101.1	99.5
39	67.6	69.9	84.5	103.3	92.4
40	66.4	69.5	72.4	101.1	101.2
41	67.6	68.4	92.4	109.5	109.5
42	66.5	69.0	81.4	104.0	102.4
43	66.5	69.8	90.3	103.2	99.5
44	66.4	69.0	90.0	100.5	100.0
45	65.0	68.0	88.5	103.3	101.0
46	68.3	69.6	99.0	102.6	100.1
47	69.4	68.5	82.5	106.8	90.0
48	66.4	69.0	99.6	102.1	93.1

*Inj. Press. - 12.4 psig
**Inj. Press. - 13.2 psig
***Inj. Press. - 15.6 psig
****Inj. Press. - 13.6 psig

$$\frac{\dot{w}_{min}}{\dot{w}_{max}} \equiv \sqrt{\frac{\Delta P_{min}}{\Delta P_{max}}} \qquad (1)$$

The percent deviation from the maximum value is defined as:

$$\% \text{ Dev} \equiv 1 - \sqrt{\frac{\Delta P_{min}}{\Delta P_{max}}} \qquad (2)$$

Using Eq. (2) the maximum flow deviation for each manifold is listed below

Manifold	% Dev
Outer oxidizer	11
Core oxidizer	4
Outer fuel	3
Core fuel	18
BLC	16

It should be noted that the average deviation is much less than the values listed above. Those represent only the maximum value measured. Comparing all the average deviations for all manifolds, the overall average deviation is about 5 percent. This value is acceptable.

B

TASK III. EXHAUST GAS SAMPLING SYSTEM DEVELOPMENT

SAMPLING SYSTEM DESIGN

The exhaust gas sampling and analysis system consists of exhaust gas sampling probes, sample collection banks, and the analysis unit. The function of the probe is to collect a sample of the combustion gas in a supersonic rocket exhaust environment. The sample collection bank stores the samples for later analysis and has both heating and cooling provisions to allow the gas sample to be held at any desired temperature, a capability which is needed during analysis. The analysis unit consists of pressure gauges and a gas chromatograph.

Probe Design

Three probes of the same type were designed by the Greyrad Corporation. A sketch of the design is shown in Fig. 24. The tip is able to reach any point in the nozzle exit plane. Two water cooling circuits are included, one for the centerbody and one for the cowl. The probe has sufficient strength to support itself in the exhaust stream when mounted by the terminal block.

The probe capabilities are:

1. Location: All three probes are capable of sampling any streamline from the nozzle centerline to a point 13.1 inches radially from the centerline.
2. Orientation: Each probe tip is capable of being oriented parallel to the local theoretical streamlines.
3. Traversing: The probes are not designed to be traversed during a test but may be moved, repositioned, and fastened manually between tests.

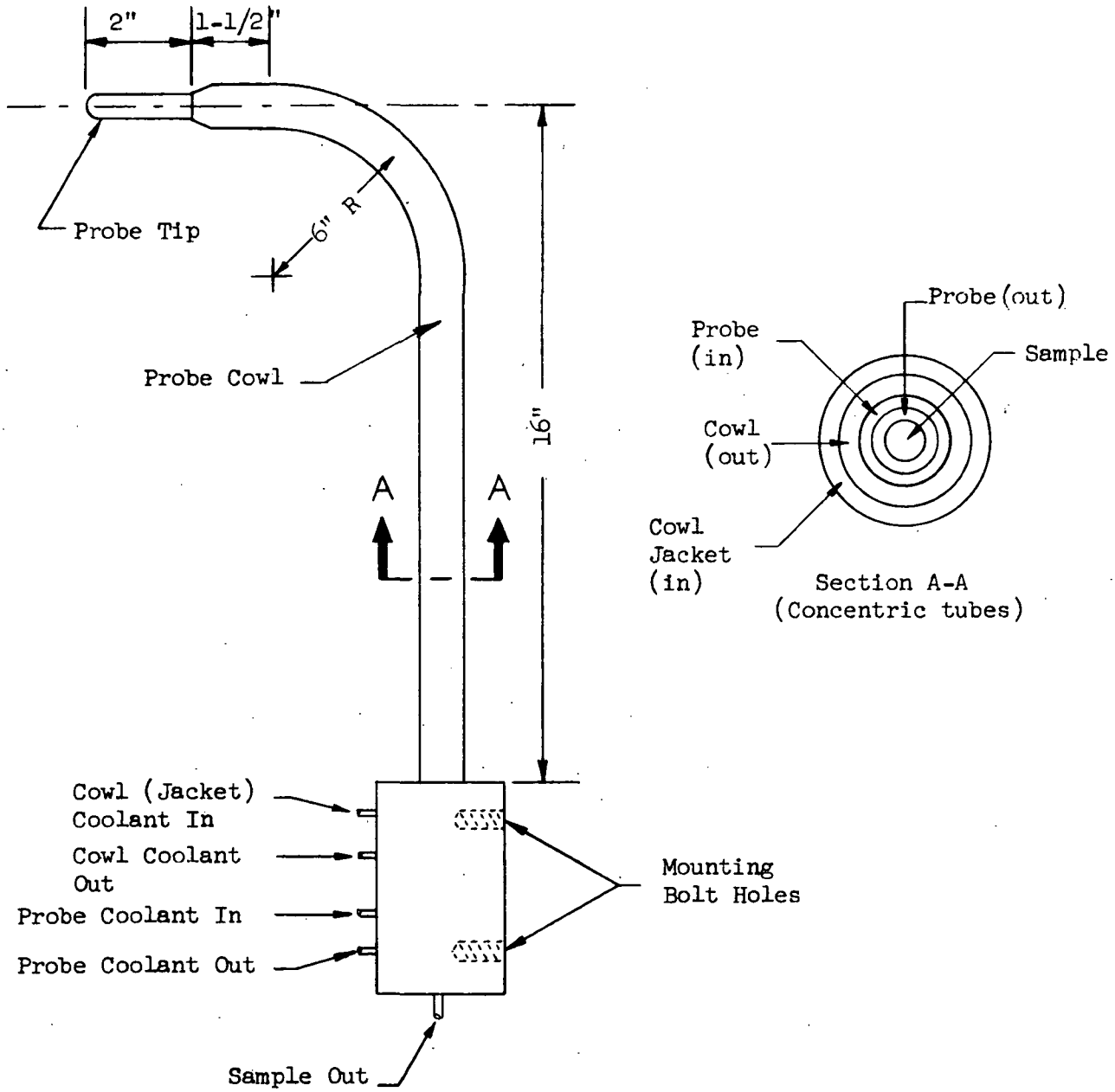

Figure 24. Selected Overall Probe Configuration

4. Recovery: At a chamber pressure of 250 psia and nozzle expansion ratio $\epsilon = 25$, the steady-state pressure recovery of the probes, when the gas collection system is filled, will be approximately 15 psia.

5. Response: A sample volume of 20 cubic inches will be filled in one second or less.

The size of the probe was determined by two considerations. First, an adequate size sample must be acquired in 1 second of sampling time. Second, the unit must be large enough to have space for the internal cooling passages. In this case, cooling and fabrication were the critical criteria.

The captured streamtube has a maximum diameter of approximately 0.28 inch. Because of the overall diameter of the probe the centerline of the captured streamtube can be within 0.35 inch of the wall. For the case of film cooling with 5% total flow, assuming that there is no mixing between the film and core (as a worst case), in the 25:1 area ratio case the film at the nozzle exit would occupy a zone approximately 0.5-inch thick. (For more realistic mixing assumptions, the zone will be much thicker.) Therefore, the probe allows meaningful sampling of the film/core interaction at the 25:1 area ratio. Mixing between the two mixture ratio zones within the core can be studied at either area ratio of 25:1 or 4:1.

The key heat transfer areas in the probe are the tip and shank, which must be protected from the impinging hot gas stream, and the gas sample extraction tube, which must cool the sample while preventing condensation of the water.

In the probe design, cold incoming coolant is fed up the outside of the shank, returning through the inner passage. Heated water is used to cool the sample while ensuring that its temperature cannot be reduced below the temperature of the coolant. The same heated water protects the probe leading edge.

Hot gas and coolant side heat transfer analyses were conducted to select the coolant conditions to ensure survivability of the probe's leading edge. From the results of the analysis the flow conditions summarized in Table 8 were selected. In addition to the inlet conditions, the resulting temperature at various locations on the probe is presented. It is seen that at these modest coolant flowrates and pressures, peak temperatures are at acceptable levels. Coolant bulk temperature rise is small in each case, on the order of 100 F. Cooling seems to pose no particular problems for the probe but it is clear from the heat flux levels that cooling is essential.

Since there are no heat transfer difficulties, the simplest method for assuring non-condensation of the combustion-generated water was to preheat the coolant so that its temperature is above that of the sample saturation temperature. Assuming that the maximum sample water content is 100%, and

TABLE 8

SAMPLING PROBE HEAT TRANSFER SUMMARY

	$\epsilon = 4:1$	$\epsilon = 25:1$
Assumed Probe Inlet Temperature, F	200	250
Assumed Probe Inlet Pressure, psig	500	500
Calculated Tip Temperature, F	1465	654
Calculated Tip Heat Flux, Btu/in.^{2}-sec	7.85	2.31
Calculated Tip Inner Passage Flowrate, lbm/sec	0.25	0.25
Calculated Cowl Temperature, F	1600	360
Calculated Cowl Flowrate, lbm/sec	0.7	0.35
Assumed Cowl Inlet Temperature, F	50-80	50-80
Assumed Cowl Inlet Pressure, psig	500	500

the maximum pressure achieved is 30 psia, the minimum wall temperature at the probe exit should be 250 F. Since there is no heat transfer difficulty, the coolant water was preheated to 250 F to completely avoid condensation problems. For the 4:1 expansion ratio, however, the water inlet cannot be 250 F due to excessive heat loads. For this condition the water can be preheated to only 200 F.

The support structure is shown in Fig. 25. It provides continuously-adjustable probe-tip location at any point between the centerline and the $\epsilon = 25$ nozzle exit boundary, and can keep the probe aligned with the theoretical (conical-flow) streamlines.

After receiving the probes from Greyrad they were flow checked to determine the Δp versus $\dot{w}$ characteristics. The results of these tests are presented in Fig. 26 . Note that probe #1 and #3 had similar characteristics while probe #2 yielded in a much higher pressure drop for the same flowrate ($\sim$40%). Subsequent testing at higher pressure ($\sim$ 1100 psi) resulted in a crack in the tip weld on probe #2. This can be repaired but there was no time to do so before the initial testing (Task IV). Therefore probes #1 and #3 were used in the hot-fire testing. In order to ensure that the probes would not experience heat transfer problems the actual flowrates selected for the initial test series were higher than these listed in the previous table. For the actual tests the nominal coolant flowrates were

$$\dot{w}_{tip} = 0.98 \text{ lb/sec}$$

$$\dot{w}_{cowl} = 2.1 \text{ lb/sec}$$

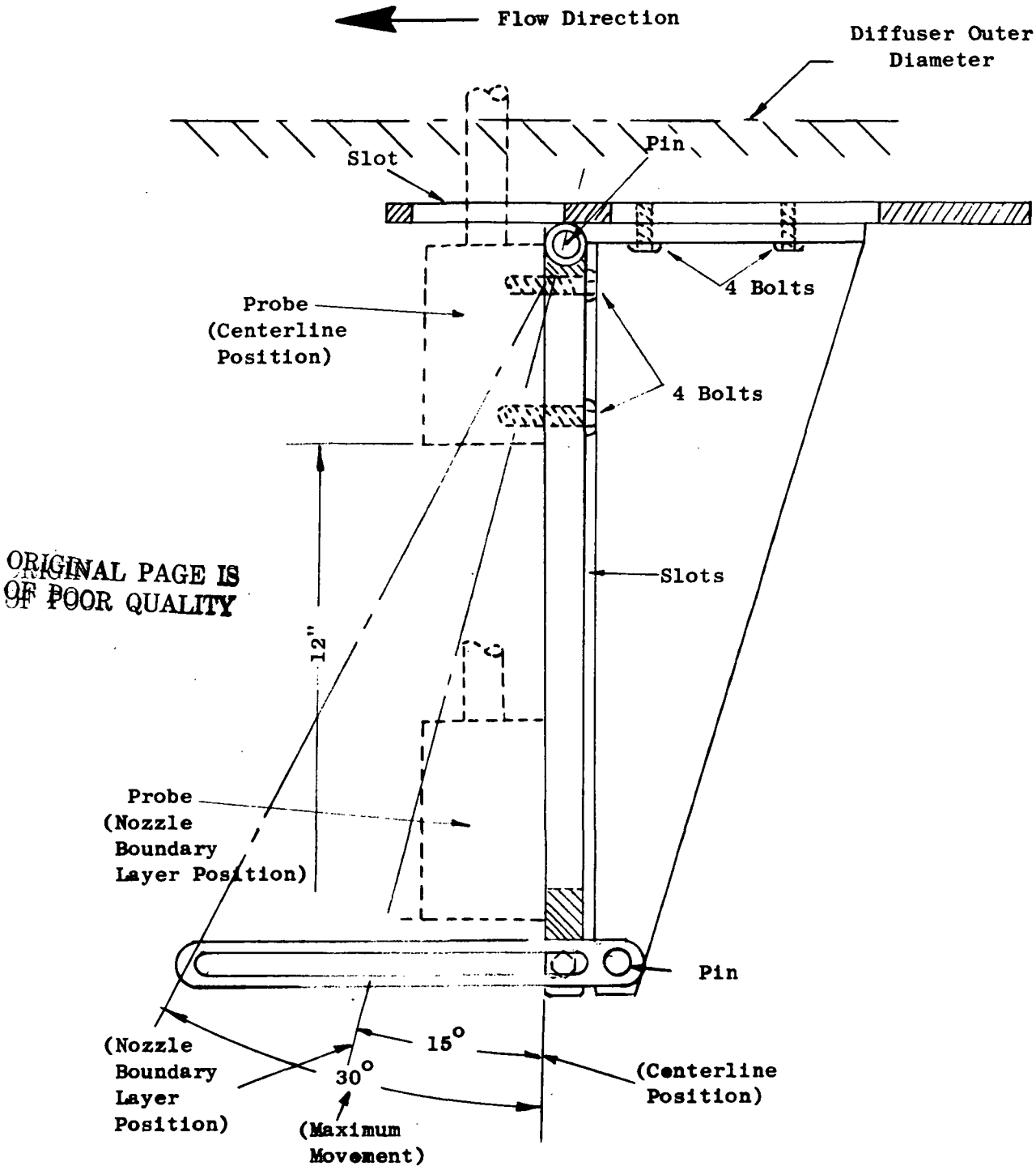

Figure 25. Probe Mounting Bracket

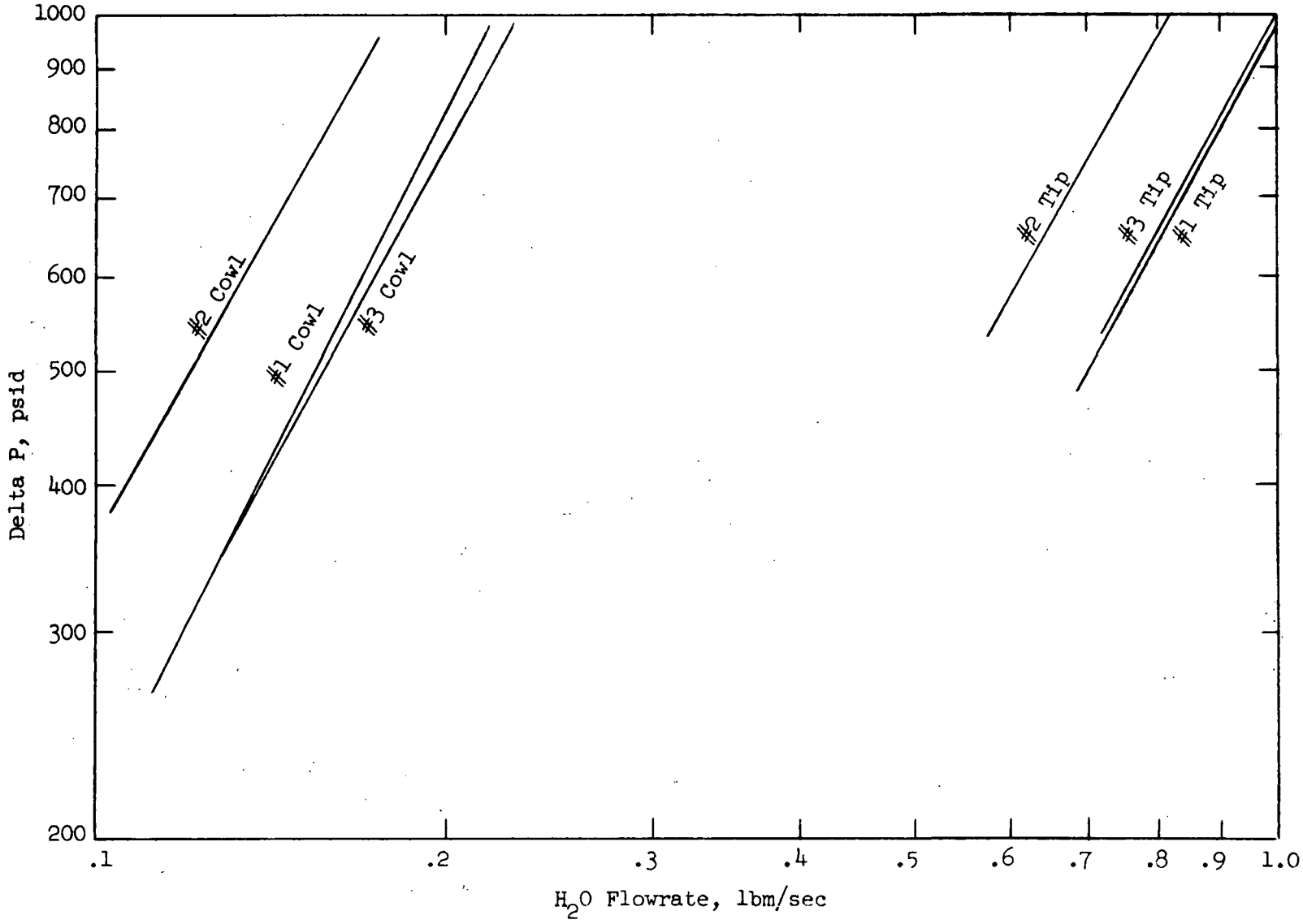

Figure 26. Flow Characteristics of the Greyrad Probes

Sample Block Design

The sample collection unit is shown in Fig. 27. Each of the three units is constructed from a solid block of aluminum and contains 10 sample cylinders. Heating capability is provided by six 2-kw heaters, which can raise the block temperature by 400 F in approximately 15 minutes. Cooling is provided by LN_2 flow through 6 passages and can cool the block 400 F in less than 10 minutes. The temperature range of 0 F to 400 F allows freezing or full vaporization of the water in the samples. A photograph showing an assembly view of the sample blocks is shown in Fig. 28.

Sample Procedure for Analysis of Hydrogen, Oxygen and Water Combustion Products

The analysis of hydrogen, oxygen and water is accomplished by a combination of P, V, T measurements and gas chromatography following a two-step procedure.

In the first step, the pressure of an individual sample is measured as it is drawn into a calibrated volume at a known, elevated temperature. Assuming ideal gas relationships, the total number of moles of gas in the sample vessel is calculated from $PV = nRT$.

Secondly, the sample vessel is cooled to a known temperature permitting condensation of water. The remaining gases are then expanded into the precalibrated analyzer system. A portion of the expanded sample is injected into a gas chromatograph for determination of the hydrogen/oxygen concentrations.

Given the system temperature, the concentrations of all three species may be calculated for the original sample, again using PVT relationships shown below:

1. Total moles of combustion gases, pressure measured at known elevated temperature:

$$n_{Total} = \frac{P_1 V_1}{RT_1} \tag{3}$$

2. Moles of hydrogen and/or oxygen are calculated from the calibrated gas chromatographic pressure value as determined (P_{H_2}) and the final system temperature (T_f):

$$n_{H_2} = \frac{P_{H_2} V_1}{RT_f} \qquad n_{O_2} = \frac{P_{O_2} V_1}{RT_f} \tag{4}$$

3. Water is calculated by difference:

$$n_{H_2O} = n_{Total} - (n_{H_2} + n_{O_2}) \tag{5}$$

The gas chromatographic analysis system shown in Fig. 29 was utilized for examination of gaseous propellant residuals in post-combustion samples. The system used a Beckman gas sampling valve and Heise gauge. A silica gel pre-column was installed to remove water in the sample. All system components, including the recorder, were mounted on a large cart for portability at the test site (CTL 4). In checkout tests instrumental sensitivity and separations for hydrogen, oxygen, and nitrogen were found to be adequate. It was found, however, that peak height measurements could not be used for quantification

FOLDOUT FRAME 1

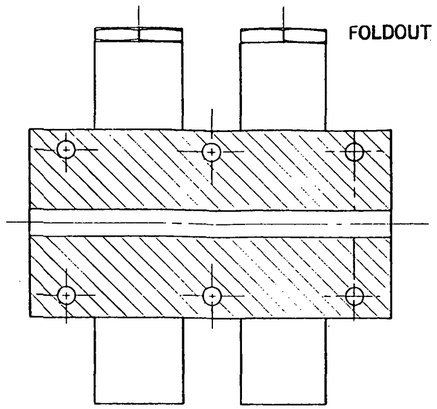

VIEW A-A

FOLDOUT FRAME 2

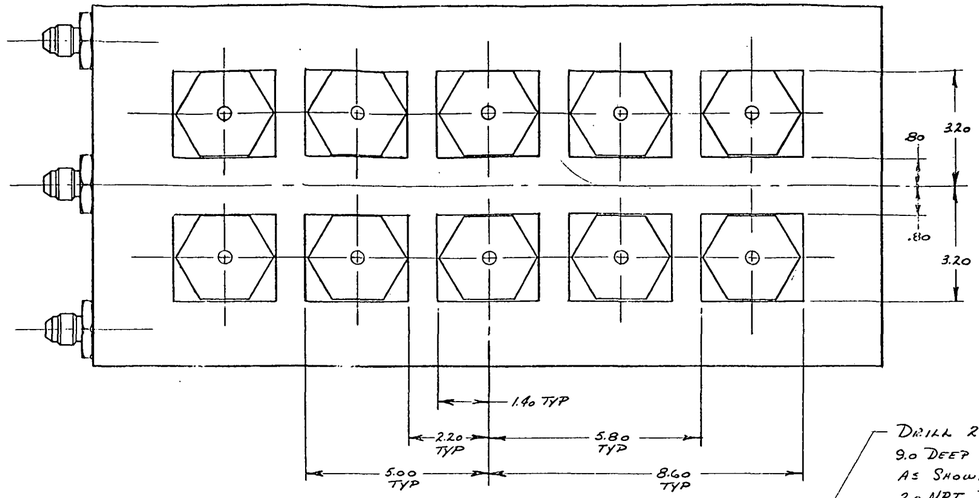

FOLDOUT FRAME 3

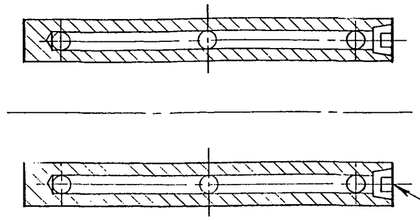

VIEW B-B

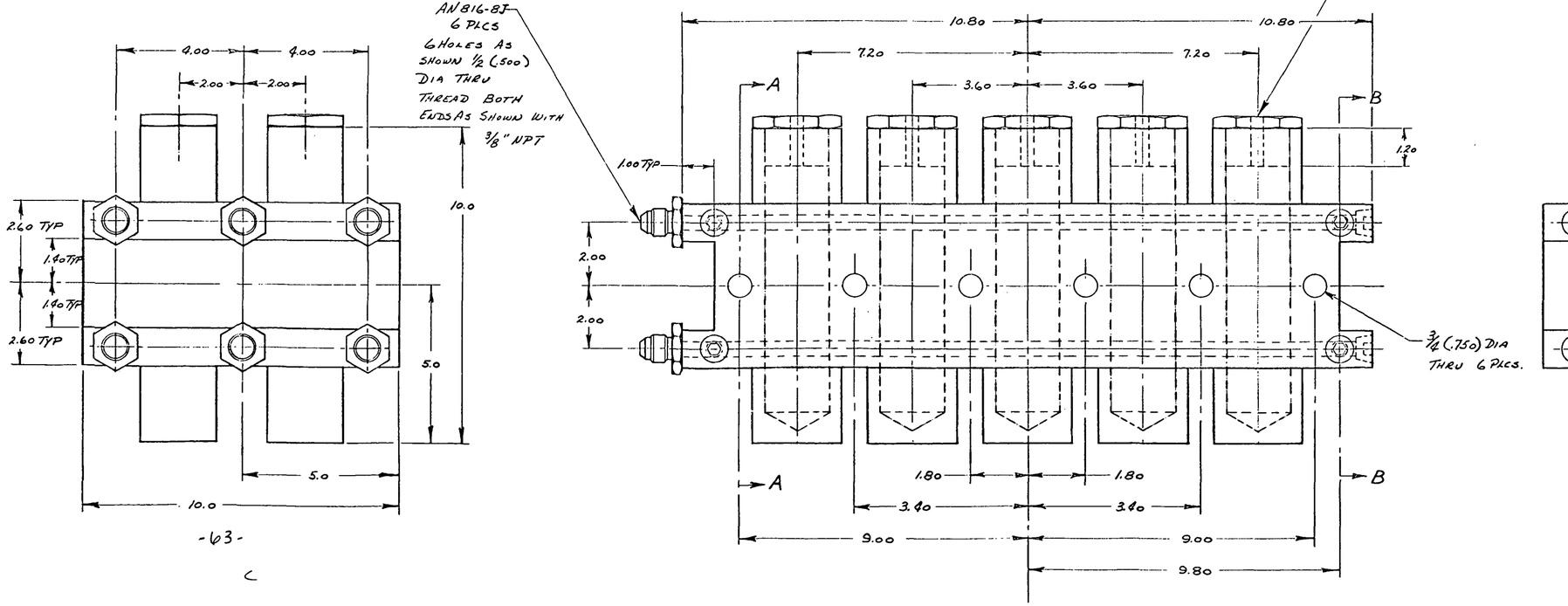

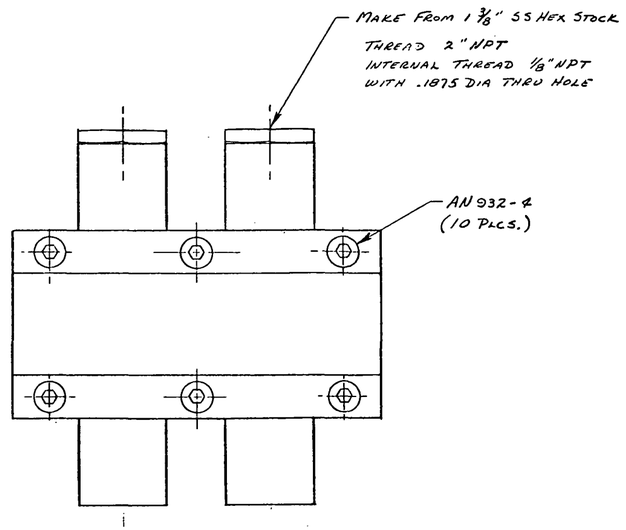

Figure 27. Sample Collection Unit Preliminary Design.

R-8903

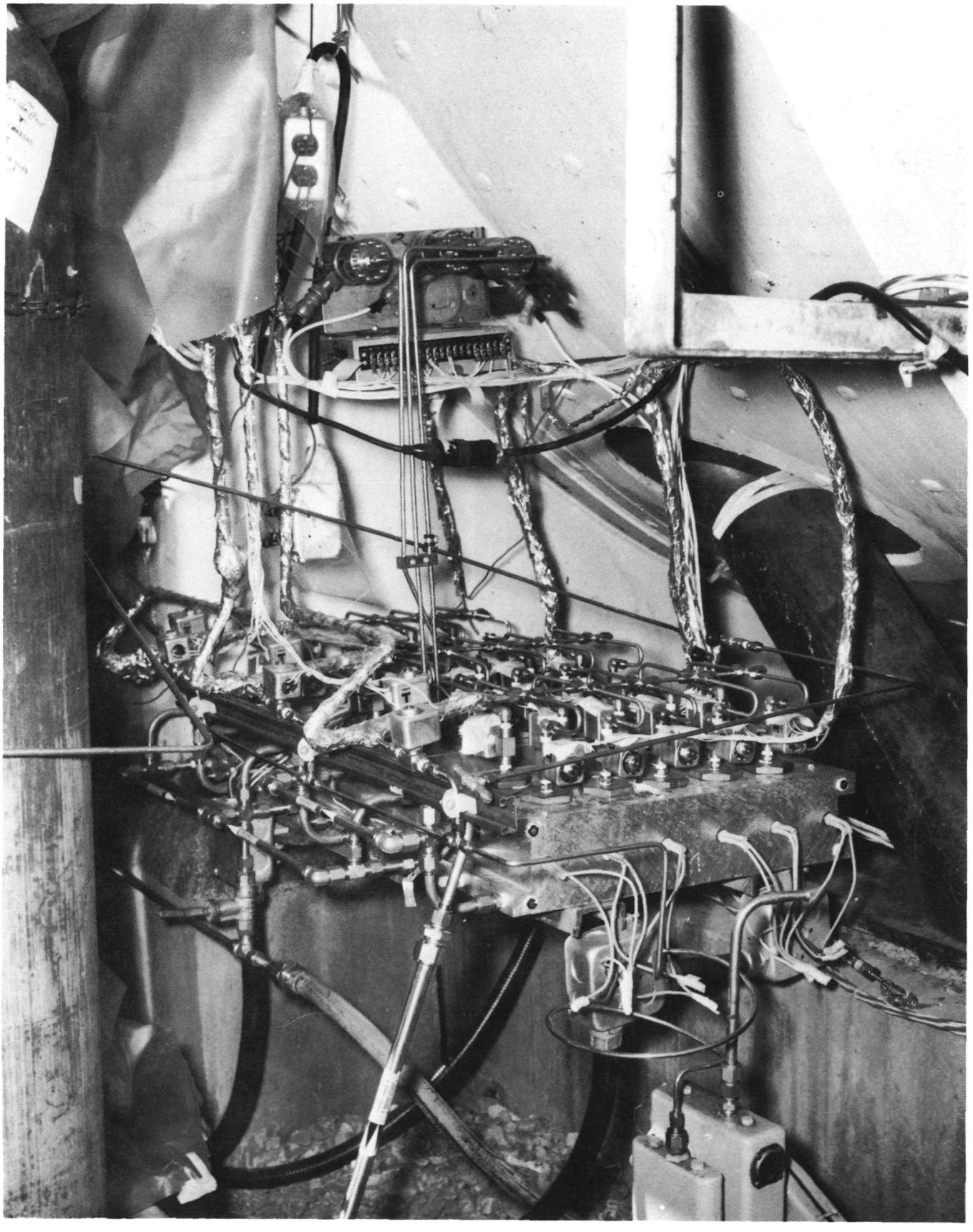

Figure 28. Sample Collection Unit

Preceding page blank

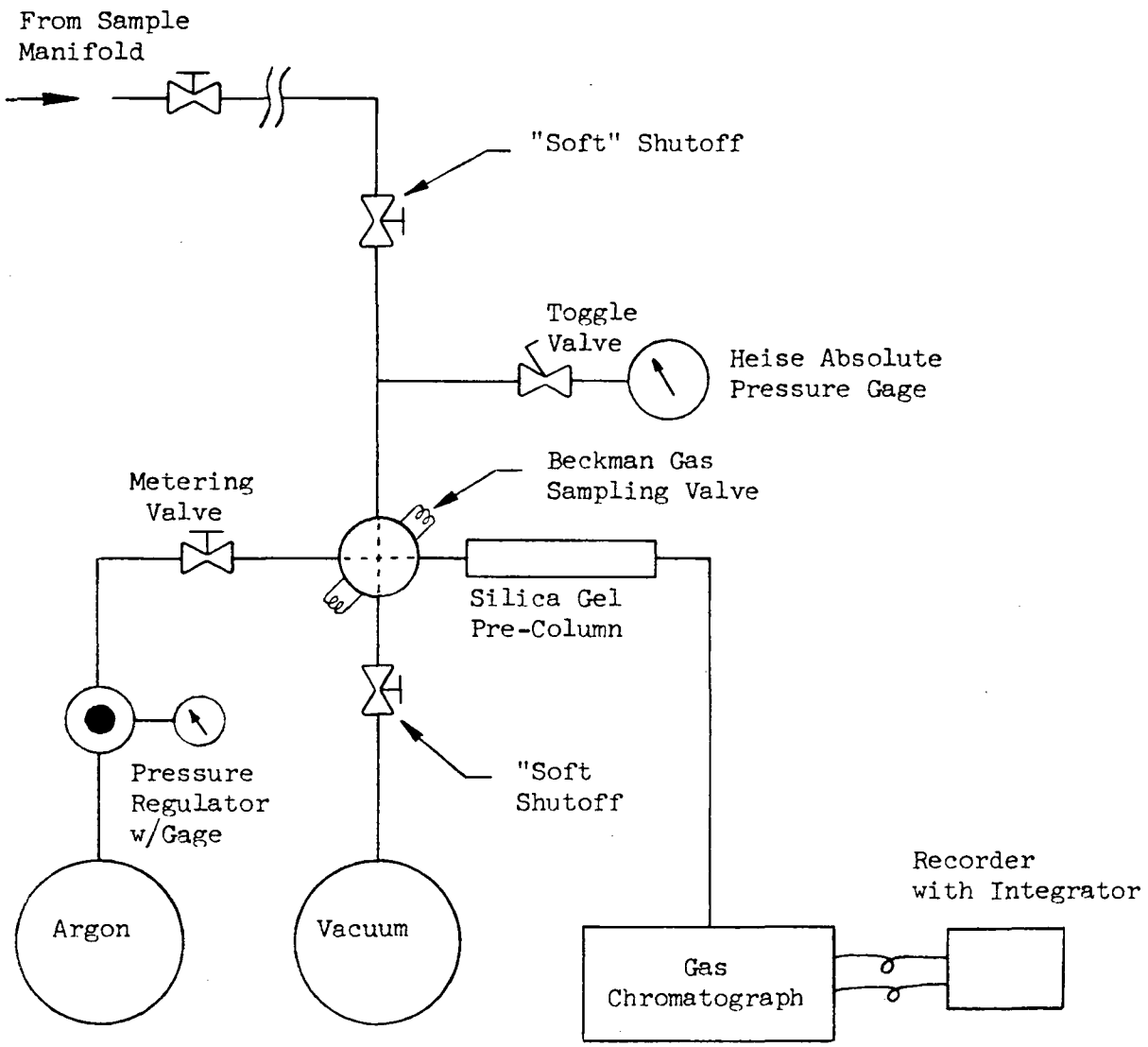

Figure 29. Schematic of Gas Chromatograph Analyzer for H_2 and O_2

because of spreading of the hydrogen peak at high concentrations, requiring use of slower integration methods. Response ratio calibrations were performed in the laboratory to minimize the final calibration requirements at the test site.

Calibration of Sample Blocks

The volumes of the 10 samplers in each block and the manifold associated with the samplers were determined manometrically using a calibrated volume and a vacuum system. The volumes obtained are shown in Tables 9 and 10 . Data on block #2 are omitted because they were not used in the subsequent tests. Difficulty in getting the sampler valves to seat properly was encountered. Typical valves were found to leak approximately 2 mm H_g pressure per minute from a sampler and 50-100 mm H_g/minute from a manifold at 1 atmosphere into an evacuated sampler. Because of this condition, certain steps not ordinarily performed with leak-free systems were taken during the on-site analysis and certain pre-analysis leak checkouts had to be eliminated.

TABLE 9

MEASURED VOLUMES OF SAMPLERS AND MANIFOLD OF BLOCK #1

SAMPLER NUMBER	VOLUME, cc
1-1	230
1-2	226
1-3	225
1-4	232
1-5	230
1-6	228
1-7	242
1-8	232
1-9	230
1-10	229
Manifold	83

TABLE 10

MEASURED VOLUMES OF SAMPLERS AND MANIFOLD OF BLOCK #3

SAMPLER NUMBER	VOLUME, cc
3-1	229
3-2*	224
3-3*	215
3-4	229
3-5	230
3-6	228
3-7	230
3-8	228
3-9	228
3-10	230
Manifold	70

*Valve leaks badly from manifold into sampler.

TASK IV. ENGINE PERFORMANCE TESTS

The engine characterization tests were planned to provide sufficient data for improved understanding of the physical processes occurring in rocket engines. This required testing in an altitude chamber sufficient for flow at 25:1 expansion ratio for a total pressure of 250 psia. The overall installation of the engine is shown in Fig. 30.

HOT-FIRE FACILITY (CTL IV - CELL 29B)

Propellant and Water Systems

The 29B test position consists of LOX, GO_2, and GH_2 propellant supply systems, altitude simulation systems, and instrumentation systems.

The test hardware is located in a 16-foot-diameter by 30-foot-long vacuum chamber and exhausts horizontally. A single-stage steam driven ejector system is piped to the capsule. The ejector system is capable of sustaining simulated altitude in excess of 23 kilometers in the vacuum chamber.

The propellant supply systems include temperature, pressure and flow control systems necessary for testing. The LOX tank and feed system is shown in Fig. 31. LOX is supplied to the injector from a 3000-psi, 600-gal uninsulated tank. Note that the LOX flows through the main line to a flowmeter, then divides into two branches. One branch feeds LOX to the core of the injector while the other provides propellant to the outer zone. Each branch is fitted with a flowmeter. In this way redundant measurements are made. The flowrates through

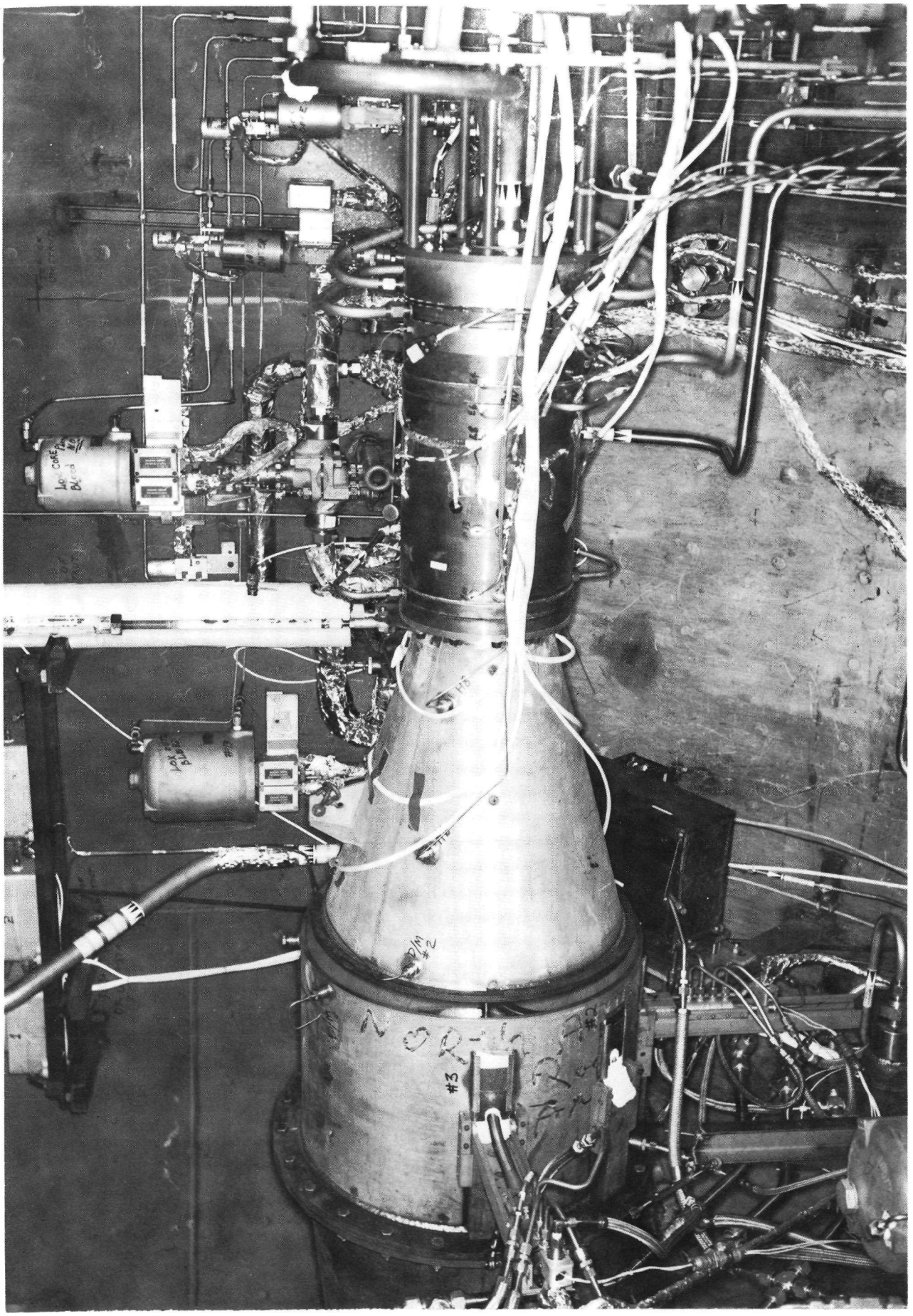

Figure 30. Engine Assembly

FOLDOUT FRAME 1

FOLDOUT FRAME 2

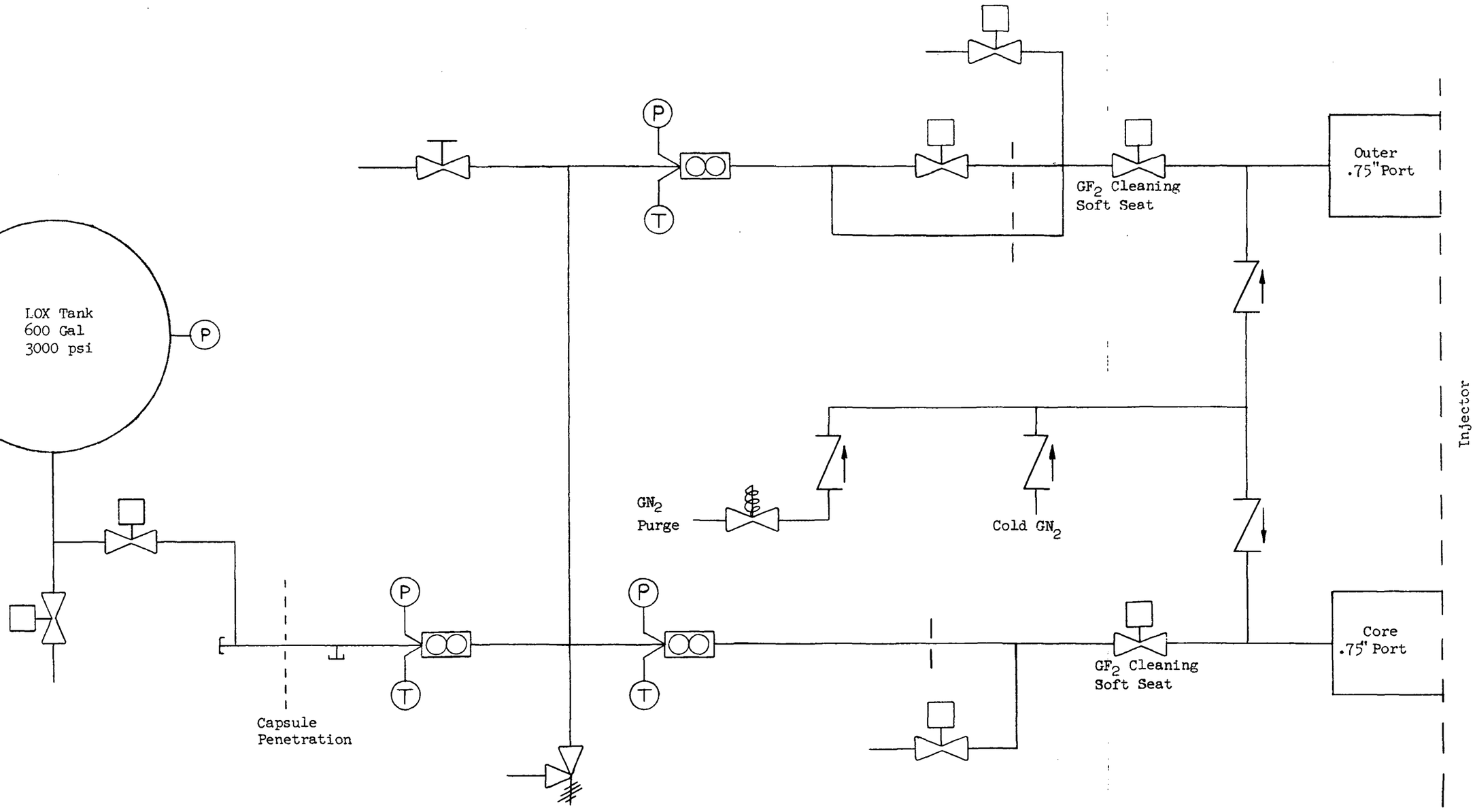

Figure 31. Stratified Injector LOX System

each branch are controlled with orifices as shown. The LOX core feed has a #7/16 (.4375 in. dia.) orifice upstream of the main valve. Two other orifices were a #29 (.136 dia) in the outer zone through line and a #25/64 (.3906 dia.) in the outer zone bypass line (with the shutoff valve). The nitrogen purge, as part of this system, is plumbed downstream of all main valves. This system provides both liquid and gaseous nitrogen. The liquid nitrogen is utilized to temperature condition the hardware before the firing to ensure that the LOX will not boil before injection into the combustion chamber.

The GH_2 is supplied from a 470-ft^3, 3000-psi storage vessel as shown in Fig. 32. For this system, the total propellant flow is divided into three zones; feeding (1) the BLC, (2) the core, and (3) the outer zone of the injector. The initial temperature of the hydrogen gas is ambient.

The chamber is water-cooled between tests and water is required to cool the probes. The entire water system is shown in Fig. 33 . Note that two tanks are used. The tank that supplies water to the cowl passages of the probes comes from a 360-gal, 2000-psi tank flowing ambient water. This tank also supplies water for cooling the chamber between runs. The other system is also a 360-gal, 2000-psi tank; however, this tank is heated by means of the heater shown in the sketch to about 250 F. Heated water from this tank supplies water to the probe center body annuli.

FOLDOUT FRAME 1

FOLDOUT FRAME 2

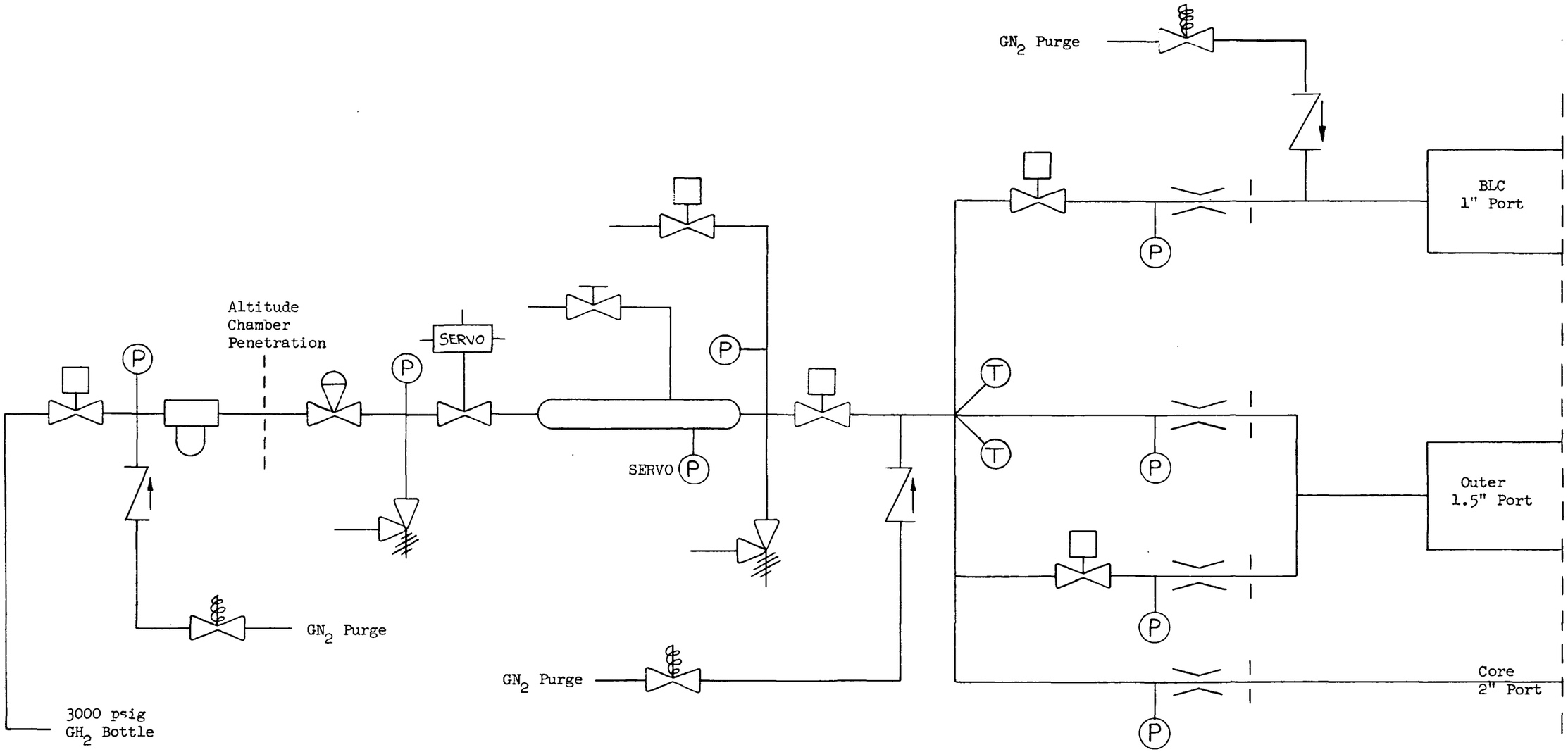

Figure 32. Stratified Injector GH_2 System

FOLDOUT FRAME 1

FOLDOUT FRAME 2

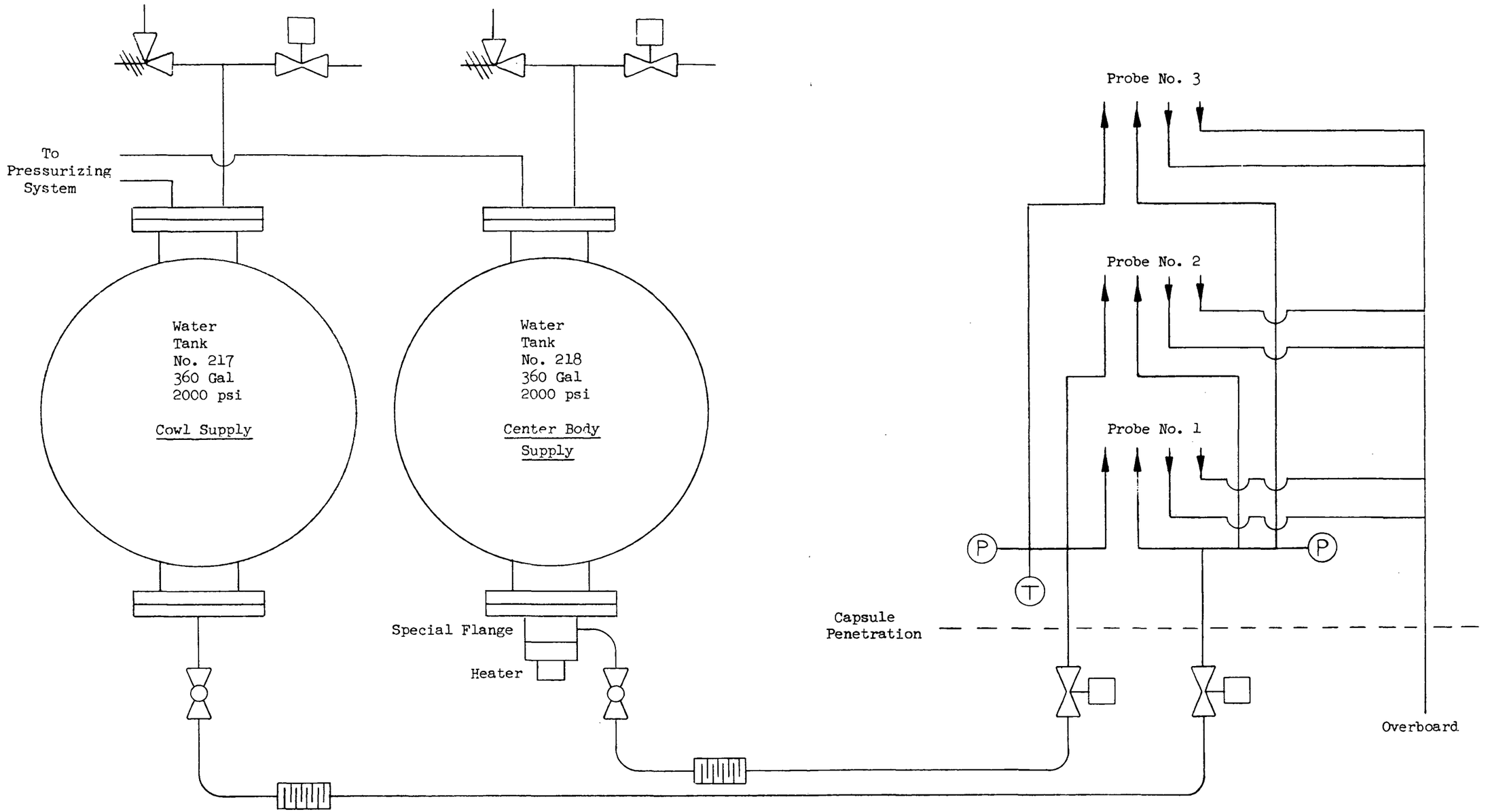

Figure 33. Stratified Injector Exhaust Sampling Probe Water System

Finally, the propellants were ignited with gaseous fluorine. The GF_2 system is shown in Fig. 34 . One fluorine K bottle was used and it is plumbed directly to the LOX system downstream of the LOX main valves. The pressure at the bottle is ~250 psia and the nominal flowrate is 0.17 lb/sec.

The overall instrumentation for all systems is shown on their respective schematics. The instrumentation within the blockhouse is listed in Table 11.

Sampling System

The probes are supplied with high pressure water in the manner illustrated in Fig. 35 . The heated water supply is approximately 250 F at the probe inlet and operated at maximum system capability. This pressure requirement is a result of choked flow areas in the probe tip flow passages. The cowl water supply pressure is 800 - 840 psi. Design water flow is 1.65 lb/sec and 1.38 lb/sec for the cowl and tip, respectively, through each probe.

The sample blocks utilized to capture the probe samples are also illustrated in Fig. 35 . The sequencing required during test operation is as follows:

1. Probe line heaters and block heaters on - off at 350 F; 300 F steady-state anticipated.
2. All samples valves and B&C identified valves open - evacuate system by vacuum pumping - open all valves.
3. Pressurize water system and establish flow.
4. Hyperflow start to stable operation.
5. Open B 1 - 3 and S 1 - 1, S 2 - 1, and S 3 - 1

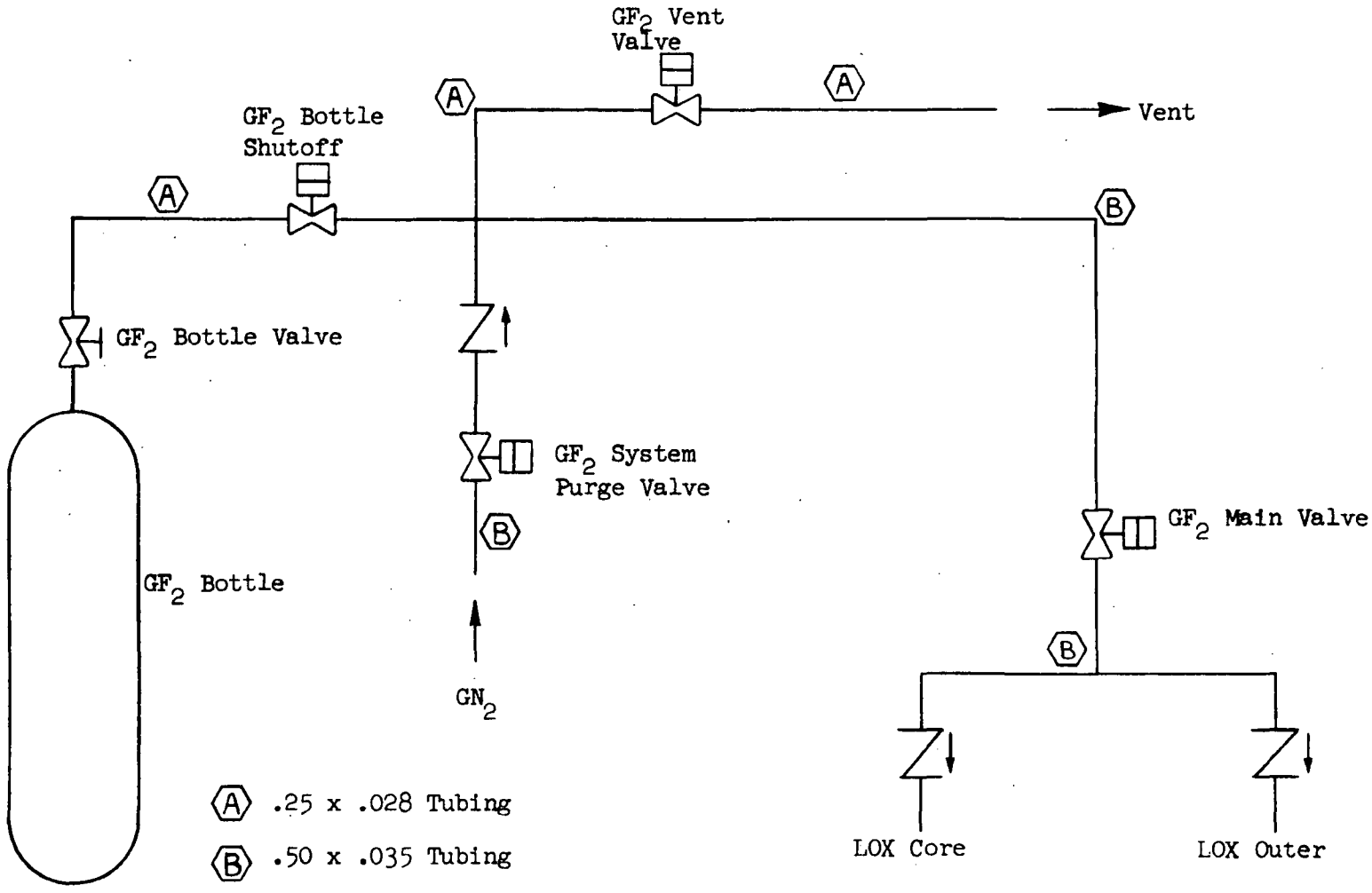

Figure 34. Stratified Injector GF_2 System

TABLE 11

INSTRUMENTATION CAPABILITIES AT CELL 29A

Location	Instrumentation
Instrumentation inside of altitude can	56 channels for pressure, thrust, RTD, flow 6 channels for accelerometers 34 channels iron/constantan only 12 channels iron/constantan or chromel/alumel 3 channels 2 psia pressure systems
Instrumentation outside of altitude can	12 channels for pressure, thrust, RTD, flow 20 channels iron/constantan or chromel/alumel
Recording capabilities	100 channels digital system with sample rate up to 40 KC 36 channels direct write oscillograph frequency response 240 cps 15% 8 channels Brush recording, 80 mm full scale frequency response of 30 cps. 200 cps at reduced amplitude 8 channels Brush recording, 40 mm full scale frequency response of 55 cps. 200 cps at reduced amplitude 54 channels direct inking graphic recorders frequency response of 1 cps 40 channels 28 VDC event; Signal recordings frequency response 10 cps 24 channels 28 VDC event; Signal recordings on 8 channels of direct write oscillograph 48 channels 28 VDC event; Signal recordings on digital system 42 channels of high frequency analog recording up to 20 KC

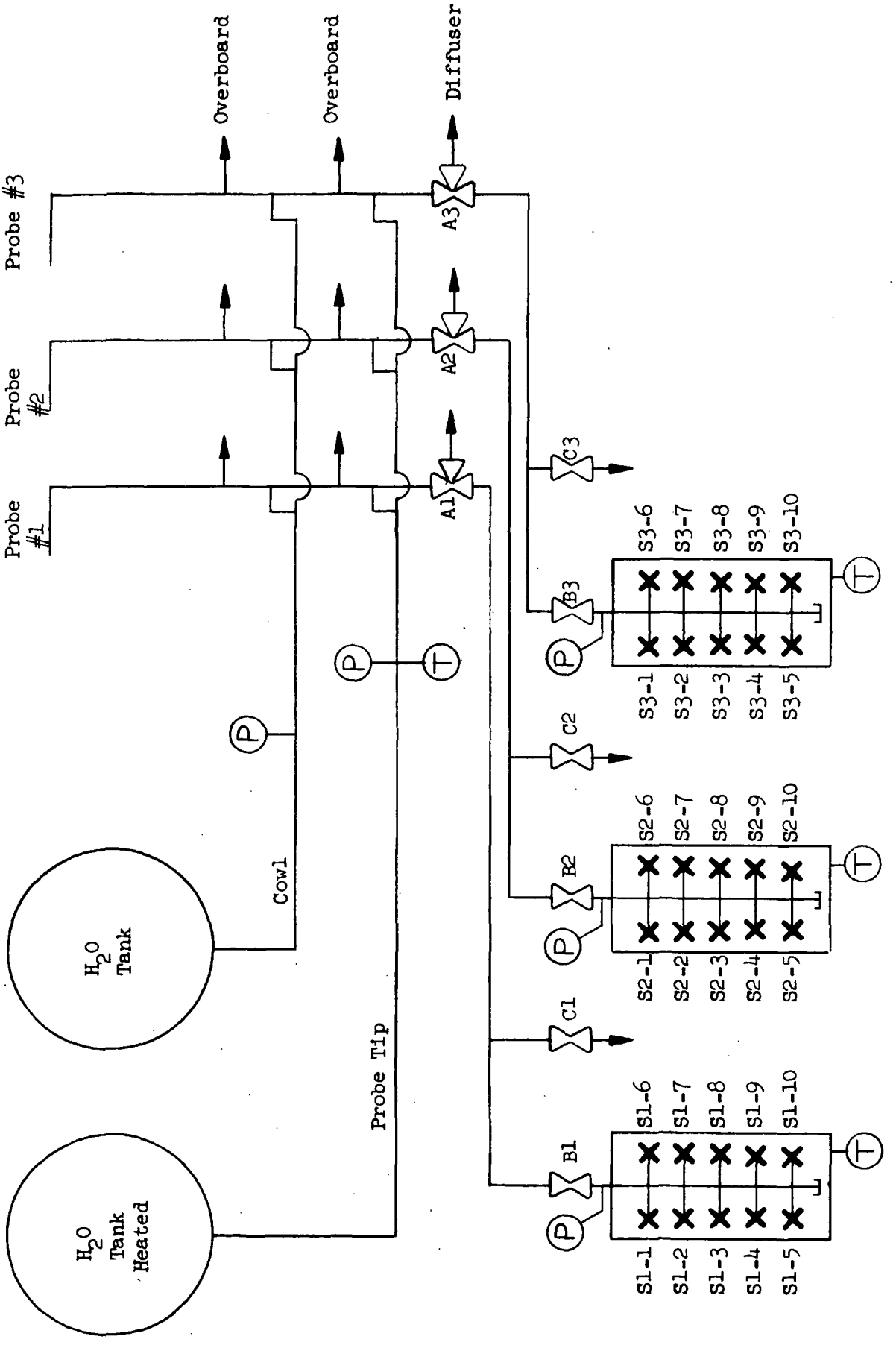

Figure 35. Sample Flow System Schematic

6. Engine start + 850 msecs close A1 - A3

7. Engine start + 1850 msecs open A1 - A3 and S1 - 1, S2 - 1 and S3 - 1

8. Open C1 - C3 and S1 - 2, and S3 - 2

9. Repeat #6, 7, and 8, increasing sample number until test series is complete.

The sample blocks use six heaters each. It takes approximately 15 minutes to heat each block to 350 F. Control of this heating circuit is in the control block house. DIGR readout to monitor the respective temperatures in each block is also available in the blockhouse. A firex water supply to cool the sample blocks for posttest analysis was also used. This supply is controlled manually at the sample site and was used to condense the water from the sample specimens.

Valve Sequence

Using the line lengths and sizes for the individual systems per the schematics, the individual line volumes differ by a factor of 5. The fuel side line volume is much larger. Converting this to fill times, the fuel side primes in approximately 15 msec while the oxidizer side requires about 330 msecs. Therefore, the operational sequence is:

1. Probe water supply on - both coolants

2. Engine start

3. LOX purge on (pressure check off)

4. +100 msec GH_2 main open

5. +130 msec GF_2 main open

6. +200 msec LOX main open - GF_2 main closed

7. +600 msec P_c verification (75 psi)

8. +850 msec record gas samples to +1850 msec

9. +2000 msec engine cut. - all purges on$\sim$5 secs

10. Engine coolant water supply on

This operation is repeated throughout the test series until all scheduled tests are completed.

TESTING

A total of 15 tests was obtained during four hyperflows. While a maximum 8-10 tests are possible during each hyperflow, system malfunctions during the initial three hyperflows resulted in fewer tests. The maximum hyperflow duration is 10-14 minutes. This maximum duration limitation is due to propellant tank capacities. The test sequence is summarized in Table 12 .

The first two hyperflows are designated as checkout tests and no useful data were obtained. Two facility problems were encountered:(1) the GH_2 main valve

TABLE 12

TEST SEQUENCE SUMMARY

Test Series	Run No.	Remarks
Series #1 Checkout (2 Hyperflows)	538 539 540 541	GH_2 main valve malfunctioned and water in probe passages froze during chilldown
Series #2 Checkout (1 Hyperflow)	542 543 544	Data obtained Water in coolant passages froze Data obtained
Series #3 Checkout (1 Hyperflow)	545 546 547 548 549 550 551 552	All tests yielded data

did not open, and (2) the water in the probe passages froze during chilldown. The valve malfunction was due to a faulty solenoid valve. The probe water freezing problem was overcome by continuously flowing water through the probes during the chilldown operation. The third hyperflow is designated as series #2. Only three runs were obtained during this series due to the excessive time required to unfreeze the water in the coolant passages between runs 542 and 544. Data were not obtained for run 543 because the run was terminated before mainstage was achieved. Test series #3 included 8 tests and all yielded satisfactory data. All tests were run at approximately 225 psia chamber pressure using the nozzle area ratio 25:1.

Performance

Typical time histories of several key parameters are presented in Figs. 36 through 38. Figure 36 shows that the total LOX flowrate was just achieving steady-state at test termination. Consequently, both the chamber pressure and the thrust are also varying during the entire run, as shown on Figs. 37 and 38. Here again the chamber pressure and thrust have just about achieved steady state by the termination of the test. The time histories suggest that all tests were stable. I_{sp} and C* performance were calculated for each test based on flowrate, chamber pressure and thrust near the end of each run. A summary of the performance data for all tests is contained in Table 13. Note that the efficiencies are about 97%, which suggests that the chamber is sufficiently long for near complete (or complete) vaporization of the LOX. In addition to performance, this table lists other pertinent data for each test. The overall ranges in BLC and mixture ratio achieved were within the ranges desired.

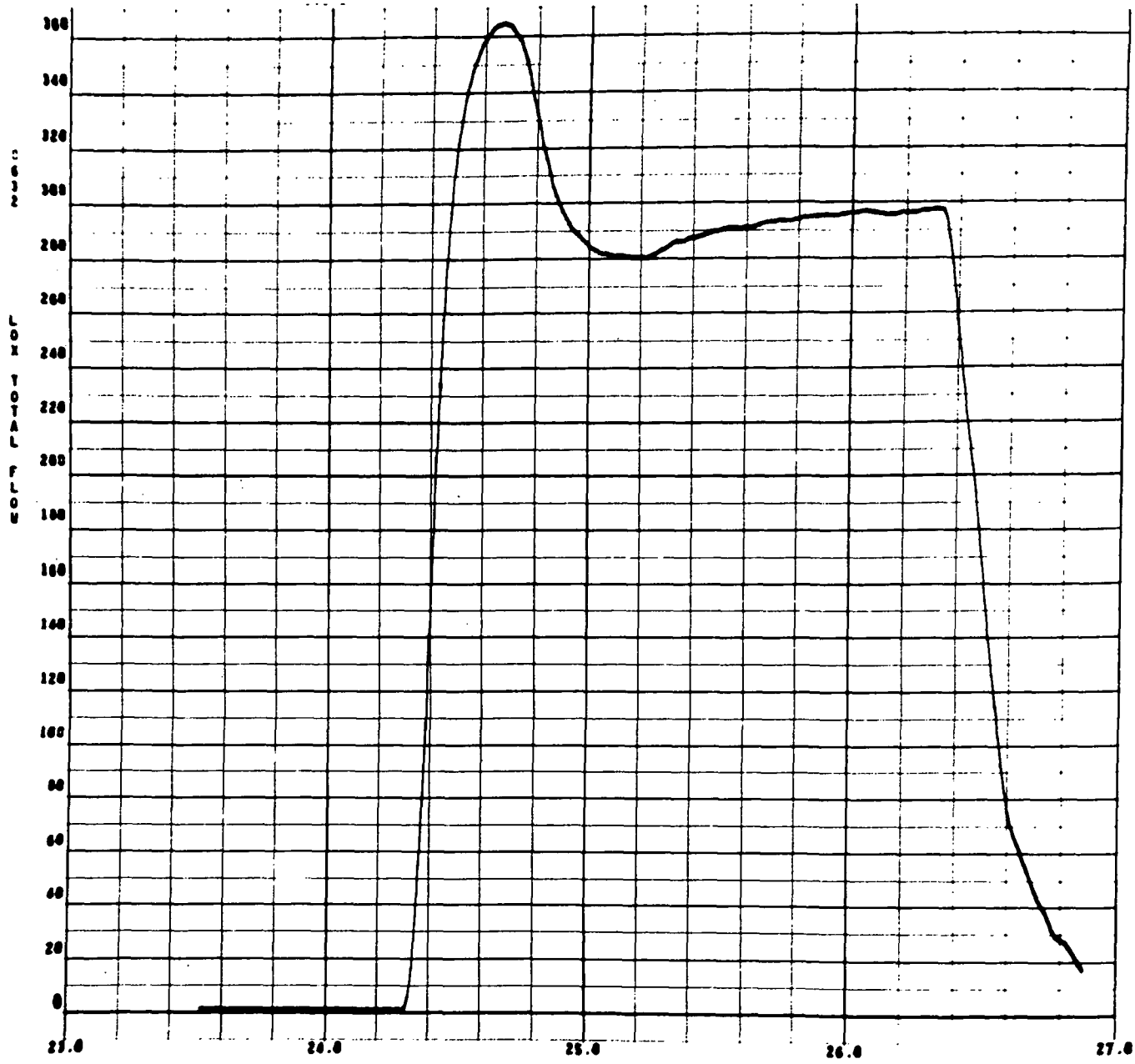

Figure 36. Total LOX Flowrate -Time History for Run 547

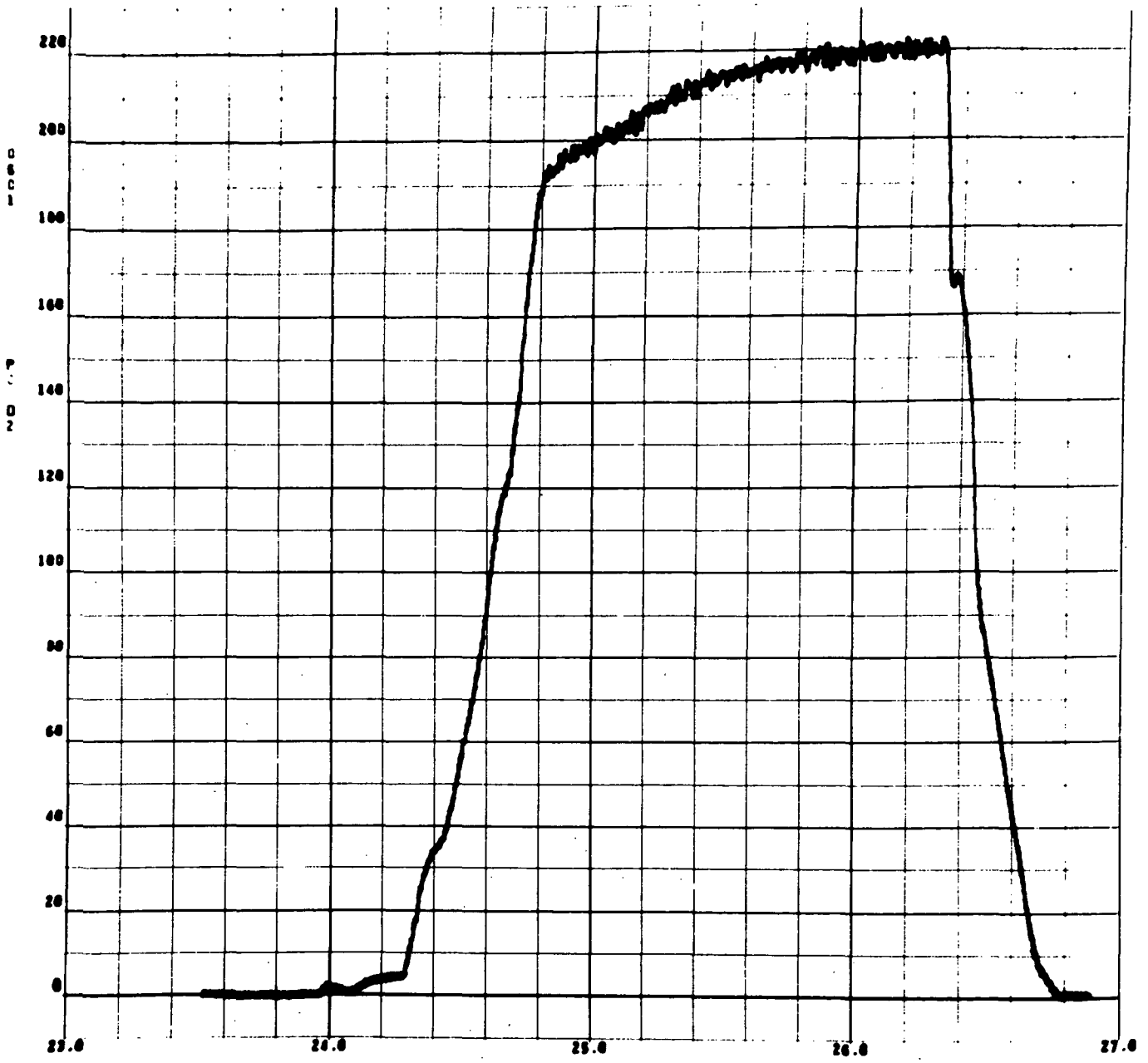

Time, Sec

Figure 37 . Chamber Pressure-Time History for Run 547

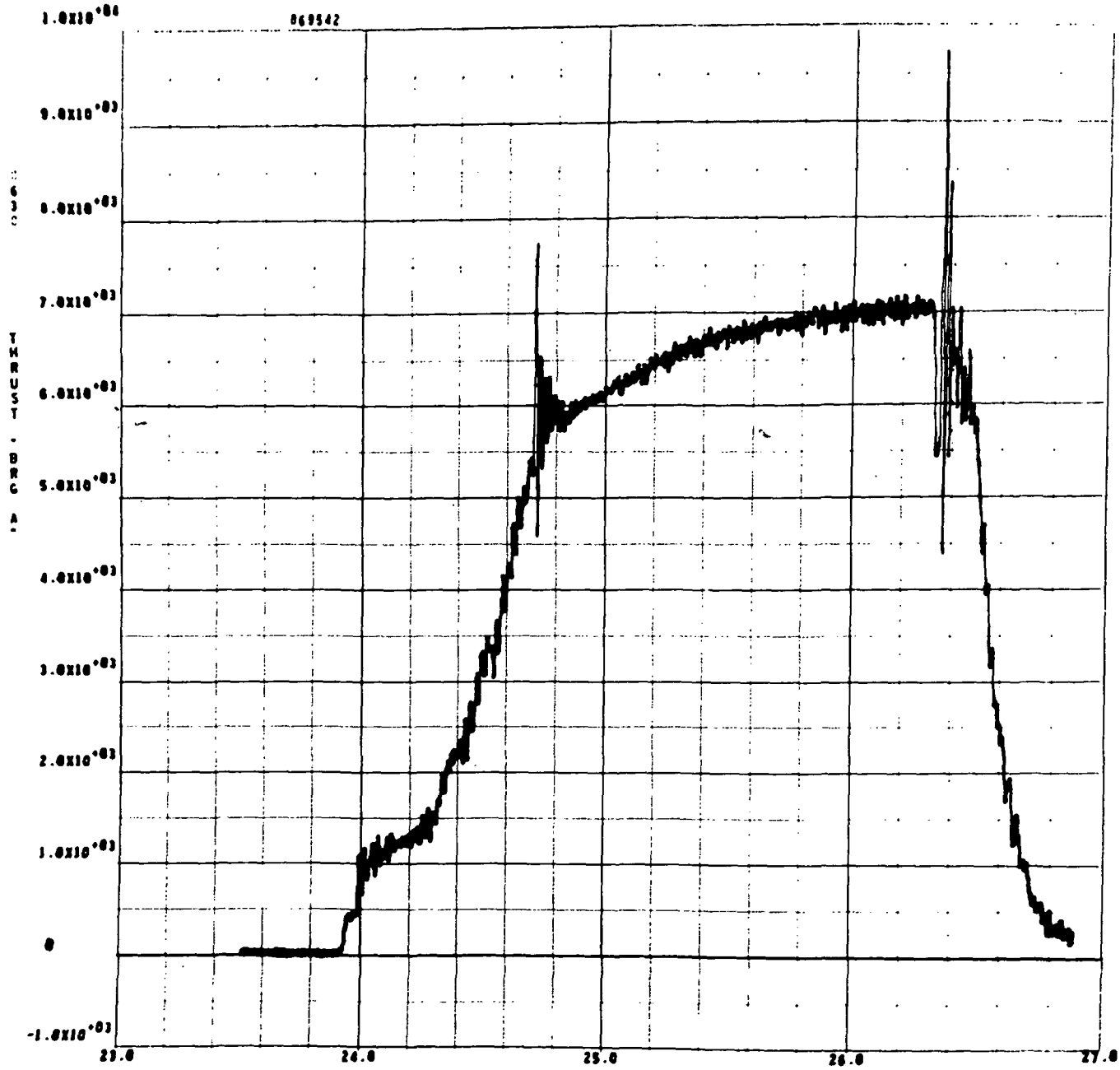

Time, Sec.

Figure 38. Thrust-Time History for Run 547

ORIGINAL PAGE IS
OF POOR QUALITY

C-3

TABLE 13. SUMMARY OF TEST RESULTS

LOX/GH2 STRATIFIED INJECTOR D A REDUCTION 5P049

TEST NUMBER 869- 542
TEST DATE 1103/70/ 0
IBM DATE 11/10/71
TEST CELL CTL4-29B

		SITE PERFORMANCE
LOCAL AMBIENT PRESSURE	(PSIA)	13.886
ENVIRONMENTAL PRESSURE	(PSIA)	1.051
THRUST (SITE)	(LB)	7218.6
THRUST (VACUUM)	(LB)	7701.8
CHAMBER PRESSURE 7,8 AVG	(PSIA)	231.66
MIXTURE RATIO (OVERALL)	(O/F)	5.482
MIXTURE RATIO (CORE)	(O/F)	7.976
MIXTURE RATIO (OUTER RING)	(O/F)	4.711
SPECIFIC IMPULSE	(SEC)	407.6
C-STAR (NOZ STAG)	(FT/SEC)	7320.
C-SUB-F (NOZ STAG)		1.6790
C-SUB-F VACUUM (NOZ STAG)		1.7914
THEORETICAL C-STAR (NOZ STAG)	(FT/SEC)	7617.
THEORETICAL C-SUB-F (NOZ STAG)		1.8710
THEORETICAL SPECIFIC IMPULSE	(SEC)	442.9
C-STAR EFFICIENCY		0.9610
C-SUB-F EFFICIENCY		0.9574
ISP EFFICIENCY		0.9202
FUEL WEIGHT FLOWRATE (TOTAL)	(LB/SEC)	2.915
BLC WEIGHT FLOWRATE	(LB/SEC)	0.281
RELATIVE OXID F/M AGREEMENT	(%)	-1.31
PERCENT BLC OF FUEL	(%)	9.651
OXID WEIGHT FLOWRATE	(LB/SEC)	15.981
TOTAL WEIGHT FLOWRATE	(LB/SEC)	18.897
THROAT AREA	(SQ IN)	17.92
EXIT AREA	(SQ IN)	459.85
LOX OUTER DELTA P	(PSID)	112.46
LOX CORE DELTA P	(PSID)	204.61
GH2 OUTER DELTA P	(PSID)	91.17
GH2 CORE DELTA P	(PSID)	49.61
GH2 BLC DELTA P	(PSID)	86.11

R-8903
86

ORIGINAL PAGE IS
OF POOR QUALITY

TABLE 13 (Continued)

LOX/GH2 STRATIFIED INJECTOR DATA REDUCTION

TEST NUMBER 869- 544
TEST DATE 1103/70/ 0
IBM DATE 11/10/71
TEST CELL CTL4-298

		SITE PERFORMANCE
LOCAL AMBIENT PRESSURE	(PSIA)	13.886
ENVIRONMENTAL PRESSURE	(PSIA)	0.891
THRUST (SITE)	(LB)	7391.5
THRUST (VACUUM)	(LB)	7801.2
CHAMBER PRESSURE 7,8 AVG	(PSIA)	232.44
MIXTURE RATIO (OVERALL)	(O/F)	5.778
MIXTURE RATIO (CORE)	(O/F)	6.941
MIXTURE RATIO (OUTER RING)	(O/F)	6.165
SPECIFIC IMPULSE	(SEC)	413.3
C-STAR (NOZ STAG)	(FT/SEC)	7366.
C-SUB-F (NOZ STAG)		1.7105
C-SUB-F VACUUM (NOZ STAG)		1.8053
THEORETICAL C-STAR (NOZ STAG)	(FT/SEC)	7539.
THEORETICAL C-SUB-F (NOZ STAG)		1.8830
THEORETICAL SPECIFIC IMPULSE	(SEC)	441.2
C-STAR EFFICIENCY		0.9771
C-SUB-F EFFICIENCY		0.9587
ISP EFFICIENCY		0.9368
FUEL WEIGHT FLOWRATE (TOTAL)	(LB/SEC)	2.785
BLD WEIGHT FLOWRATE	(LB/SEC)	0.333
RELATIVE OXID F/M AGREEMENT	(%)	-1.13
PERCENT BLC OF FUEL	(%)	11.968
OXID WEIGHT FLOWRATE	(LB/SEC)	16.091
TOTAL WEIGHT FLOWRATE	(LB/SEC)	18.875
THROAT AREA	(SQ IN)	17.95
EXIT AREA	(SQ IN)	459.85
LOX OUTER DELTA P	(PSID)	360.56
LOX CORE DELTA P	(PSID)	470.51
GH2 OUTER DELTA P	(PSID)	304.61
GH2 CORE DELTA P	(PSID)	307.88
GH2 BLC DELTA P	(PSID)	359.51

TABLE 13 (Continued)

LOX/GH2 STRATIFIED INJECTOR D. A REDUCTION 5R049

TEST NUMBER 869-545
TEST DATE 1103/70/0
IBM DATE 11/10/71
TEST CELL CTL4-29B

		SITE PERFORMANCE
LOCAL AMBIENT PRESSURE	(PSIA)	13.886
ENVIRONMENTAL PRESSURE	(PSIA)	1.161
THRUST (SITE)	(LB)	6574.8
THRUST (VACUUM)	(LB)	7108.7
CHAMBER PRESSURE 7,8 AVG	(PSIA)	216.65
MIXTURE RATIO (OVERALL)	(O/F)	5.089
MIXTURE RATIO (CORE)	(O/F)	7.702
MIXTURE RATIO (OUTER RING)	(O/F)	4.196
SPECIFIC IMPULSE	(SEC)	404.2
C-STAR (NOZ STAG)	(FT/SEC)	7366.
C-SUB-F (NOZ STAG)		1.6331
C-SUB-F VACUUM (NOZ STAG)		1.7658
THEORETICAL C-STAR (NOZ STAG)	(FT/SEC)	7712.
THEORETICAL C-SUB-F (NOZ STAG)		1.8547
THEORETICAL SPECIFIC IMPULSE	(SEC)	444.6
C-STAR EFFICIENCY		0.9551
C-SUB-F EFFICIENCY		0.9520
ISP EFFICIENCY		0.9093
FUEL WEIGHT FLOWRATE (TOTAL)	(LB/SEC)	2.888
BLC WEIGHT FLOWRATE	(LB/SEC)	0.290
RELATIVE OXID F/M AGREEMENT	(%)	-1.47
PERCENT BLC OF FUEL	(%)	10.025
OXID WEIGHT FLOWRATE	(LB/SEC)	14.697
TOTAL WEIGHT FLOWRATE	(LB/SEC)	17.586
THROAT AREA	(SQ IN)	17.94
EXIT AREA	(SQ IN)	459.85
LOX OUTER DELTA P	(PSID)	88.77
LOX CORE DELTA P	(PSID)	158.86
GH2 OUTER DELTA P	(PSID)	95.01
GH2 CORE DELTA P	(PSID)	52.02
GH2 BLC DELTA P	(PSID)	91.60

TABLE 13 (Continued)

LOX/GH2 STRATIFIED INJECTOR DATA REDUCTION 5RC49

TEST NUMBER 869- 546
TEST DATE 1103/70/ 0
IBM DATE 11/10/71
TEST CELL CTL4-29B

		SITE PERFORMANCE
LOCAL AMBIENT PRESSURE	(PSIA)	13.886
ENVIRONMENTAL PRESSURE	(PSIA)	0.909
THRUST (SITE)	(LB)	6697.9
THRUST (VACUUM)	(LB)	7116.0
CHAMBER PRESSURE 7,8 AVG	(PSIA)	217.20
MIXTURE RATIO (OVERALL)	(O/F)	5.064
MIXTURE RATIO (CORE)	(O/F)	6.896
MIXTURE RATIO (OUTER RING)	(O/F)	3.756
SPECIFIC IMPULSE	(SEC)	408.4
C-STAR (NOZ STAG)	(FT/SEC)	7461.
C-SUB-F (NOZ STAG)		1.6577
C-SUB-F VACUUM (NOZ STAG)		1.7612
THEORETICAL C-STAR (NOZ STAG)	(FT/SEC)	7718.
THEORETICAL C-SUB-F (NOZ STAG)		1.8535
THEORETICAL SPECIFIC IMPULSE	(SEC)	444.6
C-STAR EFFICIENCY		0.9666
C-SUB-F EFFICIENCY		0.9502
ISP EFFICIENCY		0.9185
FUEL WEIGHT FLOWRATE (TOTAL)	(LB/SEC)	2.874
BLC WEIGHT FLOWRATE	(LB/SEC)	0.0
RELATIVE OXID F/M AGREEMENT	(%)	-2.17
PERCENT BLC OF FUEL	(%)	0.0
OXID WEIGHT FLOWRATE	(LB/SEC)	14.551
TOTAL WEIGHT FLOWRATE	(LB/SEC)	17.425
THROAT AREA	(SQ IN)	17.96
EXIT AREA	(SQ IN)	459.85
LOX OUTER DELTA P	(PSID)	97.03
LOX CORE DELTA P	(PSID)	173.22
GH2 OUTER DELTA P	(PSID)	118.40
GH2 CORE DELTA P	(PSID)	62.82
GH2 BLC DELTA P	(PSID)	2.06

TABLE 13. (Continued)

LOX/GH2 STRATIFIED INJECTOR DATA REDUCTION 5RL49.

TEST NUMBER 869- 548
TEST DATE 1103/70/ 0
IBM DATE 11/10/71
TEST CELL CTL4-29B

		SITE PERFORMANCE
LOCAL AMBIENT PRESSURE	(PSIA)	13.886
ENVIRONMENTAL PRESSURE	(PSIA)	1.010
THRUST (SITE)	(LB)	6475.8
THRUST (VACUUM)	(LB)	8940.1
CHAMBER PRESSURE 7,8 AVG	(PSIA)	211.63
MIXTURE RATIO (OVERALL)	(O/F)	4.854
MIXTURE RATIO (CORE)	(O/F)	7.281
MIXTURE RATIO (OUTER RING)	(O/F)	4.042
SPECIFIC IMPULSE	(SEC)	403.9
C-STAR (NOZ STAG)	(FT/SEC)	7375.
C-SUB-F (NOZ STAG)		1.6441
C-SUB-F VACUUM (NOZ STAG)		1.7620
THEORETICAL C-STAR (NOZ STAG)	(FT/SEC)	7766.
THEORETICAL C-SUB-F (NOZ STAG)		1.8448
THEORETICAL SPECIFIC IMPULSE	(SEC)	445.3
C-STAR EFFICIENCY		0.9497
C-SUB-F EFFICIENCY		0.9551
ISP EFFICIENCY		0.9071
FUEL WEIGHT FLOWRATE (TOTAL)	(LB/SEC)	2.935
RLC WEIGHT FLOWRATE	(LB/SEC)	0.288
RELATIVE OXID F/M AGREEMENT	(%)	-2.46
PERCENT RLC OF FUEL	(%)	9.821
OXID WEIGHT FLOWRATE	(LB/SEC)	14.248
TOTAL WEIGHT FLOWRATE	(LB/SEC)	17.183
THROAT AREA	(SQ IN)	17.97
EXIT AREA	(SQ IN)	459.85
LOX OUTER DELTA P	(PSID)	119.81
LOX CORE DELTA P	(PSID)	261.19
GH2 OUTER DELTA P	(PSID)	105.37
GH2 CORE DELTA P	(PSID)	54.76
GH2 RLC DELTA P	(PSID)	107.57

TABLE 13 (Continued)

LOX/GH2 STRATIFIED INJECTOR DATA REDUCTION 5R049

TEST NUMBER 869- 549
TEST DATE 1103/70/ 0
IBM DATE 11/10/71
TEST CELL CTL4-29B

		SITE PERFORMANCE
LOCAL AMBIENT PRESSURE	(PSIA)	13.886
ENVIRONMENTAL PRESSURE	(PSIA)	0.988
THRUST (SITE)	(LB)	6548.6
THRUST (VACUUM)	(LB)	7003.0
CHAMBER PRESSURE 7,8 AVG	(PSIA)	216.42
MIXTURE RATIO (OVERALL)	(O/F)	5.171
MIXTURE RATIO (CORE)	(O/F)	6.161
MIXTURE RATIO (OUTER RING)	(O/F)	5.586
SPECIFIC IMPULSE	(SEC)	402.0
C-STAR (NOZ STAG)	(FT/SEC)	7457.
C-SUB-F (NOZ STAG)		1.6756
C-SUB-F VACUUM (NOZ STAG)		1.7383
THEORETICAL C-STAR (NOZ STAG)	(FT/SEC)	7692.
THEORETICAL C-SUB-F (NOZ STAG)		1.8580
THEORETICAL SPECIFIC IMPULSE	(SEC)	444.2
C-STAR EFFICIENCY		0.9694
C-SUB-F EFFICIENCY		0.9356
ISP EFFICIENCY		0.9070
FUEL WEIGHT FLOWRATE (TOTAL)	(LB/SEC)	2.817
BLC WEIGHT FLOWRATE	(LB/SEC)	0.341
RELATIVE OXID F/M AGREEMENT	(%)	-2.52
PERCENT BLC OF FUEL	(%)	12.089
OXID WEIGHT FLOWRATE	(LB/SEC)	14.565
TOTAL WEIGHT FLOWRATE	(LB/SEC)	17.382
THROAT AREA	(SQ IN)	17.97
EXIT AREA	(SQ IN)	459.85
LOX OUTER DELTA P	(PSID)	136.77
LOX CORE DELTA P	(PSID)	340.73
GH2 OUTER DELTA P	(PSID)	68.45
GH2 CORE DELTA P	(PSID)	72.74
GH2 BLC DELTA P	(PSID)	136.89

TABLE 13 (Continued)

LOX/GH2 STRATIFIED INJECTOR OF A REDUCTION SEL 49

TEST NUMBER 869-550
TEST DATE 1103/70/ 0
IBM DATE 11/10/71
TEST CELL CTL4-29B

		SITE PERFORMANCE
LOCAL AMBIENT PRESSURE	(PSIA)	13.886
ENVIRONMENTAL PRESSURE	(PSIA)	1.458
THRUST (SITE)	(LB)	6246.1
THRUST (VACUUM)	(LB)	6916.5
CHAMBER PRESSURE 7,8 AVG	(PSIA)	207.29
MIXTURE RATIO (OVERALL)	(O/F)	4.682
MIXTURE RATIO (CORE)	(O/F)	6.886
MIXTURE RATIO (OUTER RING)	(O/F)	3.972
SPECIFIC IMPULSE	(SEC)	414.6
C-STAR (NOZ STAG)	(FT/SEC)	7444.
C-SUB-F (NOZ STAG)		1.6185
C-SUB-F VACUUM (NOZ STAG)		1.7922
THEORETICAL C-STAR (NOZ STAG)	(FT/SEC)	7802.
THEORETICAL C-SUB-F (NOZ STAG)		1.8276
THEORETICAL SPECIFIC IMPULSE	(SEC)	445.6
C-STAR EFFICIENCY		0.9541
C-SUB-F EFFICIENCY		0.9753
ISP EFFICIENCY		0.9305
FUEL WEIGHT FLOWRATE (TOTAL)	(LB/SEC)	2.936
BLC WEIGHT FLOWRATE	(LB/SEC)	0.285
RELATIVE OXID F/M AGREEMENT	(%)	-2.24
PERCENT BLC OF FUEL	(%)	9.711
OXID WEIGHT FLOWRATE	(LB/SEC)	13.745
TOTAL WEIGHT FLOWRATE	(LB/SEC)	16.681
THROAT AREA	(SQ IN)	17.97
EXIT AREA	(SQ IN)	459.85
LOX OUTER DELTA P	(PSID)	138.83
LOX CORE DELTA P	(PSID)	311.40
GH2 OUTER DELTA P	(PSID)	108.02
GH2 CORE DELTA P	(PSID)	56.32
GH2 BLC DELTA P	(PSID)	107.09

TEST NUMBER 869- 551
TEST DATE 1103/70/ 0
IBM DATE 11/10/71
TEST CELL CTL4-29B

		SITE PERFORMANCE
LOCAL AMBIENT PRESSURE	(PSIA)	13.886
ENVIRONMENTAL PRESSURE	(PSIA)	0.941
THRUST (SITE)	(LB)	7019.4
THRUST (VACUUM)	(LB)	7452.0
CHAMBER PRESSURE 7,8 AVG	(PSIA)	229.18
MIXTURE RATIO (OVERALL)	(O/F)	5.394
MIXTURE RATIO (CORE)	(O/F)	7.831
MIXTURE RATIO (OUTER RING)	(O/F)	4.651
SPECIFIC IMPULSE	(SEC)	396.4
C-STAR (NOZ STAG)	(FT/SEC)	7302.
C-SUB-F (NOZ STAG)		1.6454
C-SUB-F VACUUM (NOZ STAG)		1.7469
THEORETICAL C-STAR (NOZ STAG)	(FT/SEC)	7639.
THEORETICAL C-SUB-F (NOZ STAG)		1.8671
THEORETICAL SPECIFIC IMPULSE	(SEC)	443.3
C-STAR EFFICIENCY		0.9559
C-SUB-F EFFICIENCY		0.9356
ISP EFFICIENCY		0.8943 ✓
FUEL WEIGHT FLOWRATE (TOTAL)	(LB/SEC)	2.940
BLC WEIGHT FLOWRATE	(LB/SEC)	0.285
RELATIVE OXID F/M AGREEMENT	(%)	-1.67
PERCENT BLC OF FUEL	(%)	9.702
OXID WEIGHT FLOWRATE	(LB/SEC)	15.857
TOTAL WEIGHT FLOWRATE	(LB/SEC)	18.797
THROAT AREA	(SQ IN)	17.97
EXIT AREA	(SQ IN)	459.85
LOX OUTER DELTA P	(PSID)	124.73
LOX CORE DELTA P	(PSID)	162.42
GH2 OUTER DELTA P	(PSID)	99.16
GH2 CORE DELTA P	(PSID)	51.98
GH2 BLC DELTA P	(PSID)	96.84

TABLE 13 (Continued)

LOX/GH2 STRATIFIED INJECTOR DATA REDUCTION 5R049

TEST NUMBER P69- 552
TEST DATE 1103/70/ 0
IBM DATE 11/10/71
TEST CELL CTL4-29B

		SITE PERFORMANCE
LOCAL AMBIENT PRESSURE	(PSIA)	13.886
ENVIRONMENTAL PRESSURE	(PSIA)	1.007
THRUST (SITE)	(LB)	4806.2
THRUST (VACUUM)	(LB)	5269.0
CHAMBER PRESSURE 7,8 AVG	(PSIA)	224.10
MIXTURE RATIO (OVERALL)	(O/F)	5.315
MIXTURE RATIO (CORE)	(O/F)	7.291
MIXTURE RATIO (OUTER RING)	(O/F)	3.918
SPECIFIC IMPULSE	(SEC)	290.0
C-STAR (NOZ STAG)	(FT/SEC)	7389.
C-SUB-F (NOZ STAG)		1.1521
C-SUB-F VACUUM (NOZ STAG)		1.2630
THEORETICAL C-STAR (NOZ STAG)	(FT/SEC)	7658.
THEORETICAL C-SUB-F (NOZ STAG)		1.8639
THEORETICAL SPECIFIC IMPULSE	(SEC)	443.6
C-STAR EFFICIENCY		0.9648
C-SUB-F EFFICIENCY		0.6776
ISP EFFICIENCY		0.6538
FUEL WEIGHT FLOWRATE (TOTAL)	(LB/SEC)	2.877
BLC WEIGHT FLOWRATE	(LB/SEC)	0.0
RELATIVE OXID F/M AGREEMENT	(%)	-1.77
PERCENT BLC OF FUEL	(%)	0.0
OXID WEIGHT FLOWRATE	(LB/SEC)	15.290
TOTAL WEIGHT FLOWRATE	(LB/SEC)	18.166
THROAT AREA	(SQ IN)	17.97
EXIT AREA	(SQ IN)	459.85
LOX OUTER DELTA P	(PSID)	118.94
LOX CORE DELTA P	(PSID)	165.14
GH2 OUTER DELTA P	(PSID)	118.25
GH2 CORE DELTA P	(PSID)	58.56
GH2 BLC DELTA P	(PSID)	0.16

R-8903
95

Pressure Profiles

A summary of the static pressures measured along the wall of the chamber and nozzle are listed in Table 14. Axial station locations for all of the measurements were presented in Table 3. A comparison of the static pressures measured for test 547 with those calculated from the Rocketdyne N-element model for full shifting equilibrium is presented in Fig. 39. Note that all of the data follow the full shiting equilibrium line very closely.

Heat Flux Profiles

Transient temperature histories were obtained during all runs at the axial locations shown on Table 15. The actual temperature-time histories for all runs are not included in this report due to size considerations (i.e., 30 temperatures per test = 300 additional pages). This information is available at Rocketdyne. Analysis of these results will yield the heat flux as a function of axial distance. The analysis requires a two-dimensional flat plate analysis which is not within the scope of this portion of the program.

In order to check the data, a simplified analysis was conducted to calculate the apparent heat flux for all measurements. The analysis assumes that the segment thicknesses are small enough so that the hot side temperature essentially follows the cold side (i.e., infinite conductivity).

TABLE 14. SUMMARY OF CHAMBER AND NOZZLE STATIC PRESSURES

Pressure Tap No.	Test No.										Expansion Ratio
	542	544	545	546	547	548	549	550	551	552	
1	243.1*	-	227.2	228.0	231.5	221.8	226.5	216.7	240.0	239.4	Not Applicable
2	242.0	-	226.7	-	232.9	224.5	226.3	217.1	240.7	235.1	
3	230.3	230.9	215.4	216.3	221.7	210.0	214.8	205.6	227.6	222.8	
4	232.0	232.8	217.5	218.6	224.2	212.6	217.4	208.4	230.6	226.0	
5	235.1	236.1	220.0	220.8	226.7	215.5	220.5	211.4	233.8	228.8	
6	232.1	233.1	217.1	217.9	223.8	212.7	217.7	208.8	231.1	226.1	
7	230.2	230.9	215.1	215.6	221.4	210.0	214.7	205.6	227.5	222.4	
8	233.2	234.0	218.2	218.8	224.5	213.3	218.1	209.0	230.9	225.8	
9	48.47	49.14	44.71	44.61	46.57	43.26	44.67	42.11	47.52	40.29	1.5
10	48.30	49.00	44.76	44.71	46.57	43.40	44.81	42.29	47.61	46.40	1.5
11	16.78	17.24	15.55	15.54	16.33	15.12	15.72	14.74	16.76	16.33	3.0
12	16.52	17.00	14.65	15.29	16.03	14.87	15.42	14.49	16.53	16.12	3.0
13	6.22	6.48	5.53	5.66	6.04	5.49	5.71	5.31	6.13	5.93	5.44
14	4.58	-	4.14	-	-	-	-	-	4.32	3.96	7.47
15	2.504	2.672	2.291	2.309	2.466	2.239	2.365	2.216	2.574	2.481	11.71
16	1.755	1.862	1.636	1.652	1.726	1.607	1.651	1.903	1.804	1.745	15.54
17	1.532	0.463	0.596	0.499	0.461	0.562	0.527	0.685	0.497	0.514	23.70
18	1.218	1.041	1.415	1.144	1.056	1.281	1.199	1.511	1.130	1.171	24.04

*psia

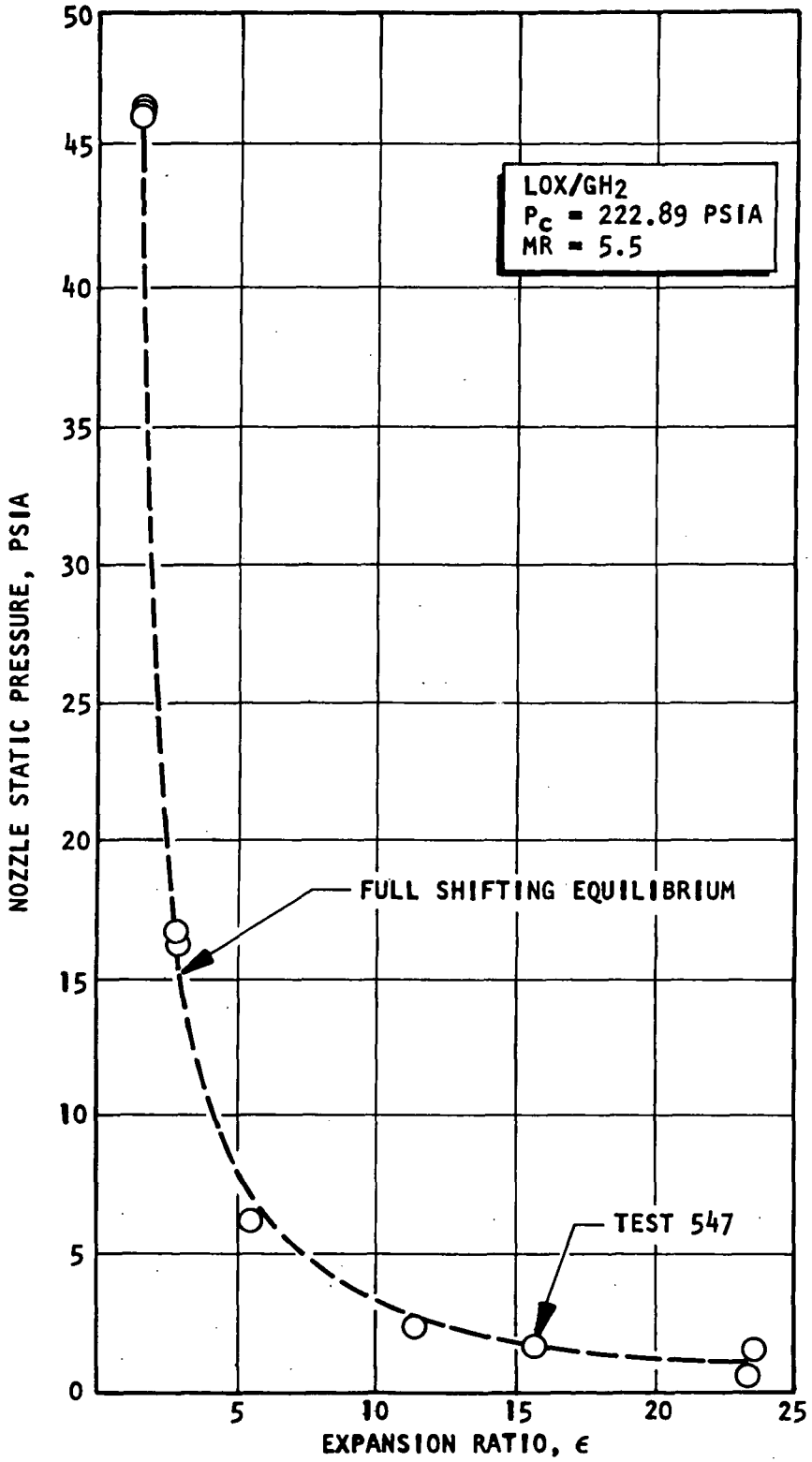

Figure 39. Nozzle Static Pressure as a Function of Expansion Ratio for Full Shifting Equilibrium

TABLE 15. SUMMARY OF Q/A MEASURED FOR ALL TESTS ASSUMING INFINITE CONDUCTIVITY

Temperature Segment No.	Test No. 542	544	545	546	547	548	549	550	551	552
1	11.4*	8.31	9.67	10.48	13.05	5.39	6.49	5.86	6.60	10.90
2	6.27	5.90	6.57	5.74	5.46	3.23	3.40	3.58	3.61	5.56
3	6.35	5.53	BAD	7.34	7.21	5.87	5.30	5.50	6.72	7.54
4	7.46	6.43	6.91	8.89	7.47	5.74	5.58	5.33	6.46	7.87
5	6.88	6.05	6.38	6.69	6.41	5.44	5.34	5.14	6.25	6.72
6	6.79	6.03	6.18	6.85	6.41	5.36	5.20	5.12	5.99	6.77
7	6.53	6.21	5.94	6.50	6.34	5.77	5.58	5.43	6.28	6.47
8	6.43	6.16	5.47	6.47	6.33	5.68	5.58	5.44	6.16	6.60
9	5.64	5.58	5.08	5.87	5.43	4.80	4.80	4.45	5.42	5.62
10	5.80	5.89	5.58	5.68	5.70	4.68	4.73	4.61	5.02	5.42
11	6.87	6.62	6.41	6.49	6.81	5.87	5.87	5.69	6.47	6.81
12	6.84	6.52	6.53	6.69	6.66	5.87	5.87	5.65	6.38	6.72
13	7.48	7.40	7.12	7.06	BAD	BAD	BAD	BAD	BAD	BAD
14	7.76	7.44	7.48	7.50	7.34	6.05	5.97	5.80	7.00	7.72
15	9.23	8.97	8.61	8.81	8.56	6.87	6.53	6.22	7.90	8.47
16	8.85	9.07	8.67	8.56	8.25	6.72	6.60	6.24	7.87	8.25
17	10.05	9.61	9.10	9.00	9.51	8.25	8.20	7.79	9.17	9.32
18	8.29	8.15	7.62	7.75	7.90	7.07	6.97	6.72	5.39	7.84
19	8.17	8.07	7.48	7.34	7.57	6.35	6.18	5.89	7.18	7.34
20	7.82	7.65	7.29	7.07	7.21	5.90	5.94	5.58	6.88	6.88
21	5.58	5.43	5.21	5.03	5.09	4.40	4.04	3.82	4.74	5.03
22	5.46	5.09	5.11	5.17	4.84	3.95	3.96	3.76	4.56	4.89
23	5.30	3.40	3.04	2.94	2.89	2.39	2.29	2.26	2.73	2.94
24	3.35	3.05	2.82	2.80	2.73	2.22	2.22	2.16	2.35	2.79
25	BAD	BAD	BAD	BAD	BAD	BAD	BAD	BAD	BAD	BAD
26	0.311	0.364	0.384	0.349	0.277	0.232	0.214	0.132	BAD	BAD
27	0.095	0.149	0.126	0.143	0.145	0.131	0.127	BAD	0.121	0.121
28	0.144	0.172	0.171	0.166	0.154	BAD	BAD	BAD	BAD	BAD
29	0.106	0.164	0.117	0.197	0.147	0.251	BAD	BAD	BAD	BAD

*BTU/in.^{2}-sec

The resulting heat balance on the segment provides the relationship shown below:

$$\left(\frac{Q}{A}\right) = \rho \ell C_p \, dT/d\Theta \qquad (6)$$

where $\frac{Q}{A}$ = heat flux

ρ = density of material (copper)

ℓ = thickness of heat path

C_p = specific heat at constant pressure of material

$dT/d\Theta$ = slope of temperature-time history

The accuracy of this approach depends on the magnitude of the Biot number, $h\ell/K$, where h is the hot gas heat transfer coefficient and K is the thermal conductivity of the material. Assuming that the heat transfer coefficient calculated from the Bartz equation is reasonably accurate, the Biot number was calculated for each heat flux segment. The results are presented in Fig. 40. Note that the segments in the throat region are much too thick resulting in a Biot number of ~ 0.26. Consequently, the magnitude of the calculations in the throat region are expected to be in considerable error ($\sim$20 to 30%). Trends in the data however, should be accurate.

The results of calculating Q/A from Eq. (6) for all tests are listed in Table 15 . The results from test 547 are plotted in Fig. 41 as a function of chamber length. Also shown on this figure is the heat flux profile predicted from the Bartz equation. Note that the trend in heat flux with nozzle dimension is as anticipated. All data show reasonable trends in Q/A versus chamber length. Consequently, no apparent error is seen in the data.

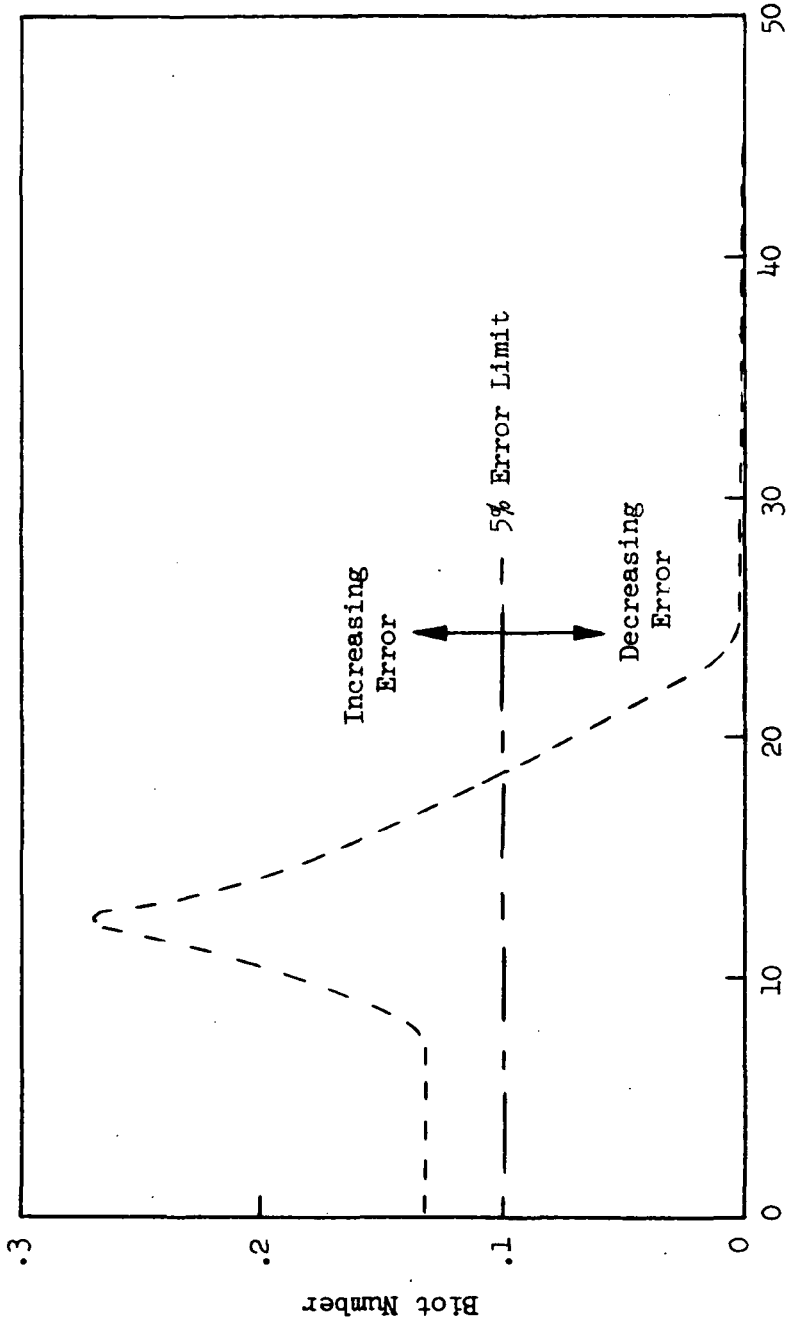

Figure 40. Biot Number as a Function of Chamber Length

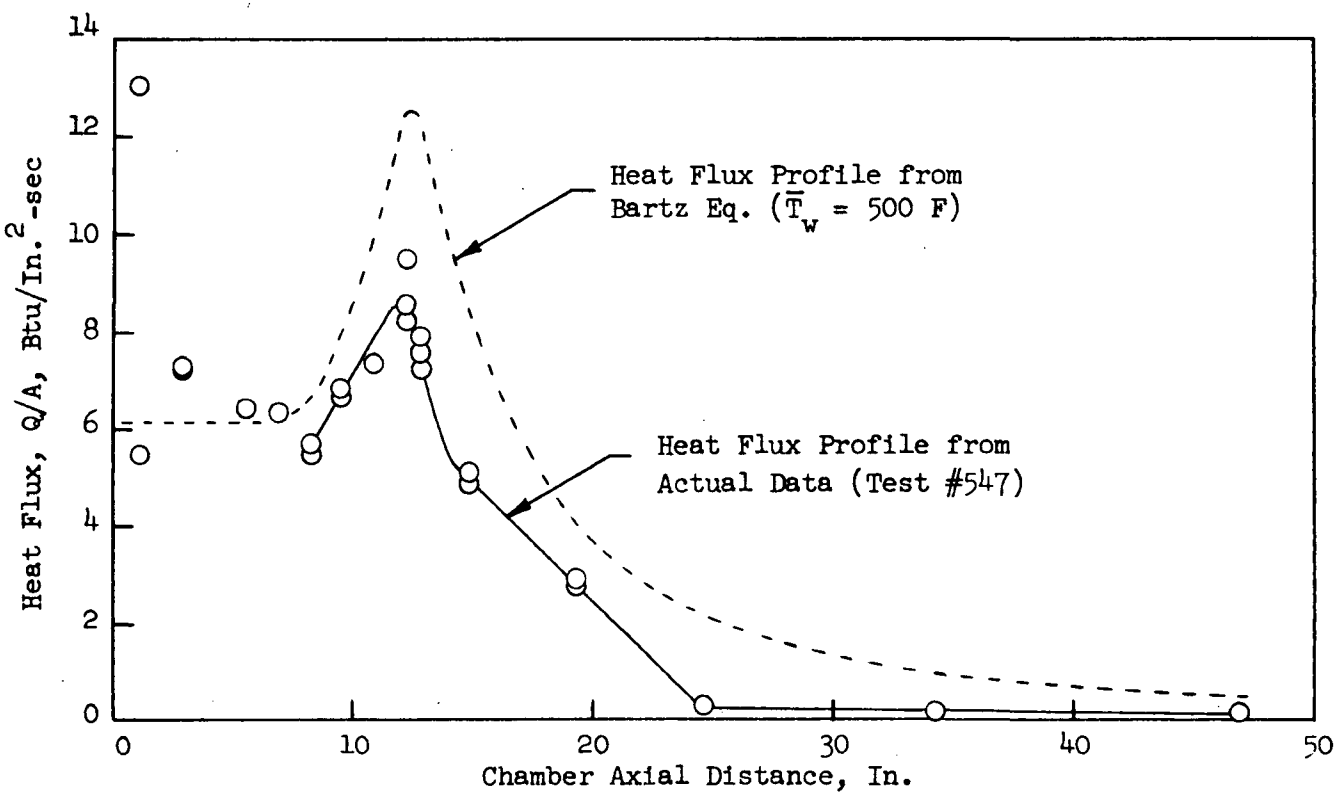

Figure 41. Comparison of Measured Heat Flux with that Predicted Using the Bartz Equation

Exhaust Gas Sampling

The two functional probes were positioned at an expansion ratio of 25:1 and were angled parallel to the theoretical stream line direction. One probe was positioned along the axial centerline of the nozzle to record the mixture ratio of the central zone. The second probe was positioned at the center of the outer zone between the inner core and BLC rings.

Ten of the test firings provided samples. The samples were obtained at temperatures sufficiently high ($\sim$300 F) to maintain the products in the gaseous state. There was a series of three tests (two of which provided samples) followed some 45 minutes later by a series of 8 tests. Between tests, the manifolds were evacuated and maintained at vacuum. After test completion, the manifolds were again evacuated and maintained at vacuum until the sampling inlet of the gas analyzer could be connected to the back of the manifold (a period of approximately 15-30 minutes).

The analysis for hydrogen, oxygen, and water was accomplished by a combination of PVT measurements and gas chromatography (GC). From the recorded pressure and temperature of each sample and the known volume of each sampler, the total moles of gas in each sample vessel were calculated. The samplers were cooled to condense all water and the remaining gases from each sample were expanded into the precalibrated analyzer system. A portion of the expanded gas was injected into the gas chromatograph for determination of hydrogen, oxygen, and/or air. Using PVT data, the total moles of hydrogen and/or oxygen in the sample were calculated. The presence of nitrogen indicated air leaks into the

sample and only excess oxygen was used in the calculations. Water was obtained by difference. Mixture ratios ($\frac{\text{mass oxygen}}{\text{mass hydrogen}}$) were then calculated for each of the samples.

The GC analyses were begun within 40 minutes after the test firings and completed within six hours. Calibrations using known quantities of air were performed three times; before, during, and after sample analyses.

Table 16 lists the experimentally obtained data and the results of the GC analyses. The following equations were used to calculate results

$$\text{Total moles Sample} = \frac{V_{\text{sampler,cc}}}{22.4 \text{ cc/mM}} \times \frac{P}{14.7} \times \frac{492}{T°R} \qquad (7)$$

Using the linear coefficient of heat expansion of aluminum of 23.6 in./in./c $\times 10^{-6}$, the volumes of the samplers were corrected from 76 to 300 F. This was a 1% increase in volume.

$$\text{mm } H_2 \text{ (or } O_2\text{) in Sample} = \text{mm } H_2 \text{ in GC} \times \frac{\text{Total V}}{V_{\text{sampler}}} \qquad (8)$$

mm H_2 in GC = Calculated mm H_2 obtained from the GC curves

Total V = $\text{Volume}_{\text{sampler}} + \text{Volume}_{\text{manifold}} + \text{Volume}_{\text{GC inlet and line}}$

$$\text{moles } H_2 \text{ (or } O_2\text{)} = \frac{V_{\text{sampler}(76°F)}}{22.4} \times \frac{\text{mm } H_2}{760} \times \frac{273}{T} \qquad (9)$$

TABLE 16

SUMMARY OF SAMPLING TEST DATA

Sample	Psia	Block T F	$V_{Block,cc}$ 76F	Total mMoles Gas	mMoles H_2	mMoles XS O_2	mMoles H_2O	% Air In Sample
3-1*	13.2	285	229	6.11	4.76	--	1.35	10
3-2	--	--	224					
3-3	12.1	266	215	5.40	1.89	0.015	3.49	32
3-4	13.3	318	229	5.90	4.68	0.015	1.20	7
3-5	14.5	314	230	6.49	5.37	--	1.12	14
3-6	16.1	309	228	7.20	5.30	--	1.90	11
3-7	15.0	306	230	6.79	3.77	--	3.02	4
3-8	16.0	303	228	7.21	1.82	--	5.39	32
3-9	14.1	300	228	6.38	6.04	--	0.34	8
3-10	16.2	296	230	7.43	0.30	--	7.13	20
1-1**	4.93	2.93	230	2.27	0.08	0.46	1.73	72
1-2	--	--	226	--				
1-3	4.29	275	225	1.98	0.09	0.71	1.18	66
1-4	5.53	332	232	2.44	0.06	1.34	1.04	42
1-5	7.95	328	230	3.50	lost sample		--	--
1-6	3.37	323	228	1.48	0.28	0.28	0.92	82
1-7	3.63	320	242	1.70	0.11	0.28	1.31	74
1-8	4.48	316	232	2.02	0.02	1.39	0.61	70
1-9	2.70	314	230	1.21	0.03	0.41	0.77	85
1-10	4.80	310	229	2.13	--	--	2.13	N.A.

*Probe located on centerline of nozzle
**Probe located on centerline of outer zone.

Using the results of Table 16, the mixture ratios were calculated and are shown in Table 17. When calculating the amount of gaseous oxygen found in the cooled samples, the following assumptions were made:

1. The total pressure in a sample recorded at test time was composed only of H_2, O_2, and H_2O. All air leakage into samples was posttest.
2. The presence of nitrogen represented air leakage from the manifold into the sampler and only oxygen in excess of air was used in the calculations.

It was found that samples from probe 3 contained from 4 to 32% air, while samples from probe 1 ranged from 42 to 85% air. This is shown in the last column of Table 17. This is logical since samples from probe 3 were three times as large as samples from probe 1 and all latter samples were significantly below atmospheric.

Additional error could have occurred because the calculations were performed without regard to the amount of sample loss that might have occurred whenever the manifold was evacuated. All of the problems are the result of leakage through the valves when a large ΔP occurs. This problem must be eliminated in order to obtain meaningful sample data.

Comparison of the results with the actual flowed mixture ratio from Table 17 shows that no correlation or trend exists. This result is thought not to be related to the gas chromatographic approach but rather to the presence of faulty valves.

TABLE 17

MIXTURE RATIOS (MR) OF EXHAUST SAMPLES

	H_2O			H_2		O_2				
Sample	mMole	wt. H mg	wt.O mg	mMole	wt.	mMole	wt.	wt. O_2	wt. H_2	MR
3-1	1.35	2.72	21.6	4.76	9.60	--	--	21.6	12.3	1.76
3-3	3.49	7.04	55.8	1.89	3.81	0.015	0.2	56.0	10.8	5.18
3-4	1.20	2.42	19.2	4.68	9.43	0.015	0.2	19.4	11.8	1.64
3-5	1.12	2.26	17.9	5.37	10.83	--	--	17.9	13.09	1.37
3-6	1.90	3.83	30.4	5.30	10.68	--	--	30.4	14.51	2.10
3-7	3.02	6.09	48.3	3.77	7.60	--	--	48.3	13.69	3.53
3-8	5.39	10.87	86.2	1.82	3.67	--	--	86.2	14.54	5.93
3-9	0.34	0.69	5.44	6.04	12.18	--	--	5.44	12.87	0.42
3-10	7.13	14.37	114.1	0.30	0.60	--	--	114.1	14.97	7.62
1-1	1.73	3.49	27.7	0.08	0.16	0.46	7.36	35.1	3.65	9.62
1-3	1.18	2.38	18.9	0.09	0.18	0.71	11.4	30.3	2.56	11.8
1-4	1.04	2.10	16.6	0.06	0.12	1.34	21.44	38.0	2.22	17.1
1-5	--	--		--		--	--	--		
1-6	0.92	1.85	14.7	0.28	0.56	0.28	4.48	19.2	2.41	7.97
1-7	1.31	2.64	21.0	0.11	0.22	0.28	4.48	25.5	2.86	8.92
1-8	0.61	1.23	9.76	0.02	0.04	1.39	22.2	32.2	1.27	25.2
1-9	0.77	1.55	12.3	0.03	0.06	0.41	6.56	18.9	1.61	11.7
1-10	2.13	4.29	34.1	0.0	0.00	0.0	0.0	34.1	4.29	7.95

$$MR = \frac{\text{Mass O}}{\text{Mass H}}$$

Consequently, efforts to demonstrate reproducibility, or to demonstrate that the sampling probe obtained a representative sample, were not possible. In addition, the magnitude of air leakage into the samplers and possible sample leakage out prevents any determination of the accuracy of the results.

CONCLUSIONS AND RECOMMENDATIONS

The experimental results of this initial phase of the program clearly demonstrate that all systems are functional and will provide accurate detailed data to characterize the major physical processes occurring in the rocket engine.

Although all systems functioned,it is recommended that several modifications and checkouts be conducted before additional testing commences. These are:

1. Install an additional static pressure tap between an expansion ratio of 1.5 and 3.0. This will aid in better definition of the pressure profile in the region where dp/dx is large.
2. Modify all of the heat flux segments with Biot numbers greater than 0.1 so that the data reduction can be greatly simplified.
3. Recalibrate the probe sampling system by introducing known samples at the probe inlet and proceding through the entire sampling collection and analysis procedure.
4. Install better valves on the sample blocks to prevent leakage.
5. Test duration should be increased sufficiently to ensure steady-state operation (~0.5 to 1.0 sec).

Several stand modifications are also necessary in order to operate the stand more efficiently.

REFERENCES

1. Wrubel, J. A., Study of Dual-Channel Infrared Spectroradiometer Systems, Interim Report: Phase III and IV, Rocketdyne, a Division of North American Rockwell, Canoga Park, Calif., (to be published).

2. Mehegan, P. F., D. T. Campbell, and C. H. Scheuerman, Investigation of Gas-Augmented Injectors, Final Report, Rocketdyne, a Division of North American Rockwell, Canoga Park, Calif..

3. Burick, R. J., Atomization and Mixing Characteristics of Gas/Liquid Coaxial Injector Elements, AIAA Paper 71-672, June 14, 1971.

U.S. DEPARTMENT OF COMMERCE
National Technical Information Service
5285 Port Royal Road
Springfield, Virginia 22151

Date: January 31, 1973

Reply to Attn of: 954.01

Subject: NASA Document Discrepancy Report 73-58

To: Mr. E. E. Baker
Deputy General Manager
Informatics TISCO
P.O. Box 33
College Park, Maryland 20740

Re: N72-33738

☐ 1. Page(s) are missing from microfiche and paper copy. Please provide a complete copy.

☒ 2. Portions of this document are illegible when reproduced. Please provide a reproducible copy. Pages 87 thru 95.

☐ 3. A microfiche reproduction is not legible. The case file was not received. Please provide at least an acceptable microfiche.

☐ 4. Incorrectly priced at _____. It should be _____ for _____ pages. However, price will remain as announced in STAR.

☒ 5. Case file returned herewith.

☐ 6. Other:

Sincerely,

BO W. THOTT
Chief, Input Section
Phone: 703-321-8517
FC/ps